Impact of increased phenol loading rate on the phenol removal of an anaerobic membrane bioreactor operated at high sodium concentration

By

Chang Gao

in partial fulfilment of the requirements for the degree of

Master of Science

in Civil Engineering at the Delft University of Technology

Student number:	4725735	TU Delft
Supervisors:	Prof. dr. ir. J. Van Lier	TU Delft
	Dr. ir. H. Spanjers	TU Delft
	Ir. Victor Servando Garcia Rea	TU Delft
Thesis committee:	Dr. ir. H. Spanjers	TU Delft
	Prof. dr. ir. J. Van Lier	TU Delft
	Dr. ir. Robbert Kleerebezem	TU Delft

Acknowledgements

One of the most important decisions I have made was to give up my work in Beijing and pursue further study in TU delft two years ago. Until now, I am still grateful for the decision I made at that time. I would like to express my sincere thanks to my supervisors Dr. Ir. Henri Spanjers and ir. Victor Servando Garcia Rea who accepted me as a member of Bio-Xtreme. Whenever I met problems or miss directions in my research, they were always there to help me with their immense knowledge. I felt so lucky to get suggestions from them, which always inspire me to improve in this process.

It was the first time for me to get in touch with modeling and it was such an exciting experience, although I really felt difficult at the beginning. Special thanks to Magela Odriozola and Javier Pavez who enlightened me every time when I came across difficulties in programming. They really gave me lots of nice advices. Thank you, Antonio, who helped me to carry out the identification of the parameters together and taught me so many things on the analysis of modeling results.

I also want to give thanks to my friends and every member in the Bio-Xtreme team, especially Amer and Kiyan, who taught me everything in the lab. I really spend a happy time in the red lab accompanied by you. I have really learned a lot from them, not only academic skills, but also politics and customs. Thank you for broadening my view to the world.

Finally, I want to express my gratitude for my parents and all my family for their financial support and selfless love. Thank you for your understanding and supporting to every decision I made. Last but not the least, I would like to give thanks to my husband, Zhaojie Sun, who is always by my side. Thank you for introducing me such wonderful university and giving me such beautiful memory.

Delft, May 2019

Chang Gao

Abstract

Certain industrial wastewaters have posed a big challenge to biological water treatment systems because of their high toxic organic compounds concentration (e.g. phenol) and high salinity. The maximum biomass specific phenol bioconversion rate (PhCR) of a mesophilic (35 °C) anaerobic membrane bioreactor (AnMBR) under high sodium concentration [18.6 g Na^+/L] condition was studied by an increase in the biomass specific phenol loading rate (PhLR) through hydraulic retention time (HRT) decrease. The maximum PhCR achieved in our research was 73 mg Ph-COD/gVSS-COD·d, with acetate as co-substrate [2g AC-COD/L]. This result was lower than that reported by the previous study of Bioxtreme (193 mg Ph-COD/gVSS-COD·d) at lower sodium concentration [8.0 g Na^+/L].

On the other hand, a simplified ADM1 model was used to model the conversion of acetate to methane in batch experiments, among which, the inhibition of substrate (acetate or phenol) on microbial growth rate was described by Haldane equation. The kinetic parameters for acetate degradation were $K_{s,AC}$=300 mg COD/L, $K_{I,AC}$=821mg COD/L, $k_{m,AC} \times I$ =0.246 mg COD/mg COD·h without phenol addition and $K_{s,AC}$=300 mg COD/L, $K_{I,AC}$=806 mg COD/L, $k_{m,AC} \times I$=0.236 mg COD/mgCOD·h with the addition of 714 mg Ph-COD/L (300 mg Ph/L) at sodium concentration of 18.6 g Na^+/L, while it was $K_{s,AC}=6.7 \times 10^{-9}$ mg COD/L, $K_{I,AC}$=5670 mg COD/L, $k_{m,AC} \times I$=0.043 mg COD/mgCOD·h at lower sodium concentration [8.0 g Na^+/L] without phenol addition.

The kinetic parameters estimated for the batch experiments were applied in a mathematical model describing a dynamic experiment carried out in the AnMBR1 and validated with different HRTs. In the model, the conversion from phenol to acetate was considered and the kinetic parameters estimated for phenol degradation were $K_{s,Ph}$=20 mg COD/L, $K_{I,Ph}$=300 mg COD/L, $k_{m,Ph} \times I$=0.008 mg COD/mgCOD·h. It was proved that the simplified ADM1 model could well predict the phenol and acetate concentrations in the reactor at different PhLRs.

This research has provided an experimental and modeling approach for the maximum PhCR determination and could contribute to the understanding of the inhibition effect of sodium and phenol on PhCR in the treatment process of saline phenolic wastewater.

Keywords: Anaerobic membrane bioreactor; phenolic wastewater treatment; high sodium concentration; maximum phenol bioconversion rate; ADM1 model; kinetics

Abbreviations

ADM1	Anaerobic digestion model No 1	
AE Sensor	Acoustic emission sensors	
AMPTS	Automatic methane potential test system	
AnMBR	Anaerobic membrane bioreactor	
CGWW	Coal gasification wastewater	
COD	Chemical oxygen demand	g/L
EPS	Extracellular polysaccharide	
EGSB	Expanded granular sludge bed	
FID	Flame ionization detector	
GAC	Granular activated carbon	
GC	Gas chromatography	
HRAR	High-rate anaerobic reactors	
HRT	Hydraulic retention time	d
I/S	Inoculum substrate ratio	
PhCR	Biomass specific phenol bioconversion rate	gPh/gVSS·d
PhLR	Biomass specific phenol loading rate	gPh/gVSS·d
PVDF	Polyvinylidene difluoride	
RPM	Revolutions per minute	
RUASB	Recirculated up-flow anaerobic sludge blanket	
SMA	Specific methanogenic activity	gCOD/gVSS·d
SMPs	Soluble microbial products	
sOCR	Biomass specific organic conversion rate	gCOD/gVSS·d
sOLR	Biomass specific organic loading rate	gCOD/gVSS·d
SRT	Sludge retention time	d
TCD	Thermal conductivity detector	
TMP	Transmembrane pressure	bar
TSS	Total suspended solid	g/L
UASB	Up-flow anaerobic sludge blanket	
UF	Ultrafiltration	
VFA	Volatile fatty acid	

$_{v}$OLR	Volumetric organic loading rate	gCOD/L·d
VSS	Volatile suspended solid	g/L

Table of contents

1 Introduction

1.1 Background knowledge

Industrial wastewater such as effluent chemical industry, agro-food industry, textile and leather industry as well as petroleum industry contain large amounts of salt (Castillo-Carvajal & Sanz-Martin et al., 2014). The salt concentration can vary considerably between different manufacturers. For example, in the produced water of oil and gas industries, it might range from a few g /L to 300 g/L depending on various production processes (Neff, 2002).

High salt concentration might reduce microbial activity, as well as the density and particle size of the biomass, which leads to a decrease of biological treatment efficiency (Ismail et al., 2013). For anaerobic water treatment, the inhibition could be more serious, because anaerobic bacteria are more sensitive to high salinity compared to aerobic bacteria (Riffat & Krongthamchat, 2006).

Besides salt, phenolic compounds are also a concern when treating industrial wastewater such as those coming from petrochemical industries, in which phenol can reach concentrations of 2.8~1220.0 mg/L (Busca et al., 2008) and contribute to 60% ~ 80% of the total COD (Ji et al., 2016). The phenolic substances are toxic and have adverse effects on both human and environment. (Ji et al., 2016).

Moreover, high phenol concentration also inhibits the SMA and leads to biomass decay and wash out (Muñoz-Sierra et al., 2019). At the same time, BOD_5/COD ratio of certain industrial wastewater (e.g. CGWW) can be about 0.3, which makes it unfavorable for biological treatment. Chemical pretreatment such as advanced oxidation is usually employed before biological treatment (Zhao & Liu, 2016).

With the development of anaerobic water treatment technology, especially the appearance of HRAR systems (e.g. UASB and EGSB), more and more anaerobic reactors have been applied to treat industrial wastewater (Van Lier, 2001). Besides economic advantage compared to the chemical treatment, anaerobic treatment also has the benefit of biogas production, less energy consumption, and less sludge production (Speece, 1983; Henze et al., 2008) in comparison with the aerobic water treatment systems. Among the anaerobic reactors developed, the AnMBR is considered to be a good option to treat industrial wastewater with high salinity and high phenol concentration, due to its capacity to achieve full retention of specific biomass promoting better adaptation of the microorganisms to the extreme conditions of the wastewater (Dereli, 2012).

However, to our knowledge, there are no studies that take into account the effect of the increased PhLR (by HRT decrease) on the PhCR of an AnMBR under high sodium conditions. From an engineering point of view, it is important to study PhCR because it could allow us

either to treat a higher flow of wastewater with the same reactor configuration or design a smaller reactor. In addition, it is also important from a scientific point of view because it could allow us to know the limit of the treatment capacity of the suspended biomass.

On the other hand, to our knowledge, there are no studies on acetate and phenol degradation kinetics under anaerobic and high sodium conditions. The kinetics are important on the understanding of anaerobic degradation process of phenol and can be used for a mathematical model.

This research focused on the PhCR [mg Ph-COD/gVSS·d] of a mesophilic (35 °C) AnMBR under high sodium concentration [18.6 g Na^+/L] at different HRT conditions. As it has been shown in the last BioXtreme studies (Fonseca, 2018), acetate was used as co-substrate in the experiment to promote phenol removal efficiency. A simplified ADM1 model was used to describe the conversion from acetate to methane in batch experiments, among which, the inhibition of acetate on microbial growth rate was described by Haldane equation. The kinetic parameters derived from the batch experiments were applied to the model for dynamic experiment (including phenol degradation) and validated under different HRTs.

1.2 Research questions and objective

This research contained two experimental setups: batch and continuous experiments. The main objective of the research is to determine the effect of increasing PhLR on PhCR of a mesophilic (35 °C) AnMBR at high sodium concentration [18.6 g Na^+/L]. The sub-objective of the batch experiment is to determine the effect of phenol and sodium concentration on acetate degradation and derive the kinetic parameters for the mathematical model of a short-term dynamic experiment. The sub-objective for the continuous experiment is to determine the maximum PhCR at high sodium concentration and predict the phenol and acetate concentration in the reactor.

The research questions are described as following.

- **Batch experiment**

Research questions:

Q1: Considering a Haldane kinetic, what are the values of the kinetic parameters that could predict the acetate degradation by the AnMBR biomass at a high Na^+ concentration (18.6 g Na^+/L)?

Q2: Is there any inhibition effect on acetate degradation caused by phenol addition?

Q3: How are those kinetic parameters compared to that of an AnMBR biomass under a lower Na^+ concentration (8.0 g Na^+/L)?

➢ **Continuous experiment**

Research question Q4: What is the maximum PhCR of a mesophilic AnMBR under high Na^+ concentration (18.6 g Na^+/L) condition?

The scheme of the research strategy is shown in Figure 1.1.

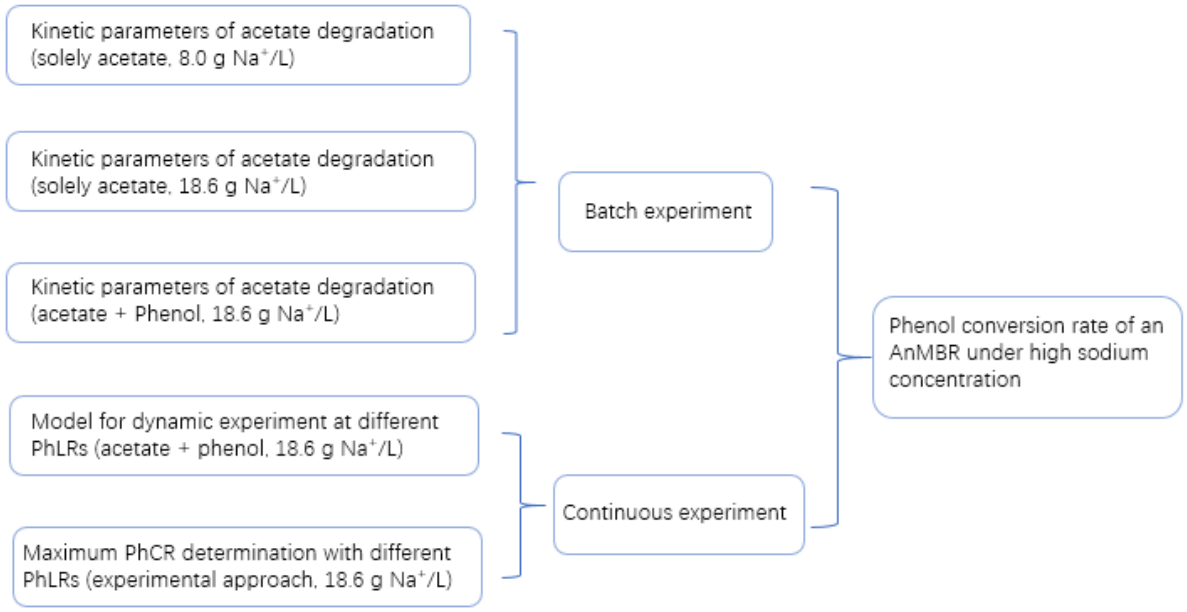

Figure 1.1 Scheme of the research strategy

1.3 Thesis layout

This master thesis includes 5 chapters.

Chapter 1 introduces the background of the research. The research gap, objective, and research questions are introduced

Chapter 2 discusses the literature review related to the research questions (Q1~Q4), including the effect of phenol and high sodium concentration on the performance of AnMBR (Q2 and Q3); anaerobic degradation process of phenol and kinetic modeling of anaerobic degradation (Q1); application of AnMBRs on industrial wastewater treatment (especially for saline and phenolic wastewater treatment) and effect of HRT and SRT on the performance of AnMBR (Q4).

Chapter 3 describes the research method and analysis.

Chapter 4 discusses the results of the experiment, mainly divided into the acetate decrease stage, transition stage and a short-term dynamic experimental stage.

Chapter 5 presents the conclusion of the thesis and gives further suggestions.

2 Literature review

2.1 Effect of salinity and phenol on industrial wastewater treatment performance

2.1.1 Effect of salinity on industrial wastewater treatment performance

High sodium concentration could cause cell disruptions by changing the ionic strength of the substrate (Kargi & Dincer, 1997) and cause differences on osmotic pressure across the biomass membranes. This might result in plasmolysis and reduced biological treatment efficiency (Yang, 2013; Lefebvre & Moletta, 2006) which could be even more serious with rapid sodium concentration changes (Kargi & Dincer, 1997). In order to balance the external osmotic pressure, microbes generally apply the "salt in" and the "compatible solute" strategy, which refers to increasing intracellular ion concentration and accumulating cytoplasm organic compatible solutes, respectively (Ismail et al., 2013).

This eventually affects the kinetics of the biological process. For example, salt could pose non-competitive inhibition to nitrification process, decreasing u_m and increasing K_S at the same time. With 5% salt dose, the nitrification rate could be decreased by nearly 20% (Dinçer & Kargi, 2002). It was reported by Quartaroli et al., (2017), that NaCl concentration higher than 125 g /L could completely inhibit ammonium removal in the aerobic batch reactors. Similar to nitrification process, high salinity also inhibits methanogenic process. Zhao et al. (2017) found that the hydrolysis and acidification process could be inhibited at high NaCl concentrations, while methanogenic process could be inhibited even at low NaCl concentrations. It was reported by De Vrieze (2016) that high sodium concentration could lead to a product shift from methane to carboxylate in the UASB, and dominant population shift to hydrogenotrophic Methanomicrobiales.

High sodium concentration might also reduce the bioavailability of trace metals (e.g. cobalt), which results in the decrease of methanogenic activity and biogas production (Feng et al., 2010). Muñoz-Sierra et al. (2017) studied the effect of different sodium concentrations on SMA. A maximum SMA at 6 g Na^+/ L and a fully inhibited SMA at 34 g Na^+/ L were observed when using biomass sludge coming from an AnMBR treating saline wastewater. Ismail et al. (2008) did not observe any difference in SMA and EPS when dealing with lower salinity (5 g Na^+/L and 15 g Na^+/L) with UASB. However, both research studies found significant decrease in the sludge particle size with high salinity, especially for the granular biomass. This might because high salinity leads to calcium leaching which hampers the biomass granulation process and pose negative effect on its mechanical strength and settlement. This will eventually result in biomass wash out and biomass density decrease (Gagliano et al., 2017). Another way that sodium can affect anaerobic treatment is by reducing the solubility of the organic matter dissolved in the water and lead to salt out effect, which negatively affect its bioavailability

(Castillo-Carvajal et al., 2014). Furthermore, high sodium concentration will also reduce the solubility of methane and CO_2, which leads to the pH increase.

Besides the effect of sodium, high chloride concentration will also inhibit the cell respiration (Lefebvre & Moletta, 2006) and aceticlastic methanogenesis (Ismail, 2013). This is due to its inhibitory effect on the synthesis of protein by preventing the combination of ribosomes and mRNA (Rath, 2016).

2.1.2 Strategy to cope with high salinity

The toxicity of the sodium depends on the antagonistic effects of different ions, the acclimation of the biomass to high sodium concentration and the substrate type. (Lefebvre & Moletta, 2006). Halotolerant and halophilic bacteria are usually employed for high-saline condition (Shi et al., 2012; Kargi & Dincer¸1998). Riffat & Krongthamchat (2007) applied halophilic bacteria to an anaerobic filter and achieved a COD removal efficiency of 80% when treating wastewater with sodium concentration lower than 37 g Na^+/L and OLR lower than 3 g/L·d. Adding substances, such as β-cyclodextrin and 2-hydroxypropyl could also be helpful to increase the organic solubility and decrease the salting out effect (Castillo-Carvajal et al., 2014) by balancing the osmotic pressure across the biomass membranes.

Besides of the addition of halo-bacteria, the application of digested co-substrate could also help to cope with high sodium conditions. This might be due to the digested co-substrate that could improve the bioavailability of the substrate and promote the hydrolysis of carbohydrates (Alhraishawi & Alani, 2018). Besides co-substrate, trace metals addition was also reported to be helpful for saline wastewater treatment. It was reported by Sudmalis et al. (2018) that adding calcium at 13 mg/L was effective for granules formation at 20 g Na^+/L. At the same time, the SMA could be recovered by 17% when dosing 0.5 mg/L of tungsten (Muñoz-Sierra et al., 2017).

Biomass acclimation was reported to be an effective method to reduce the negative effect of high sodium concentration. Muñoz-Sierra et al. (2018) used an AnMBR to treat phenolic wastewater at a concentration of 14 g Na^+/L, and achieved phenol removal efficiency of 99.9% after 180 days acclimation at a load of 1.73 mg Ph/gVSS· d.

2.1.3 The effect of PhLR on industrial wastewater treatment performance

Benzoate is an intermediate product in phenol conversion process at mesophilic temperature. Generally, the degradation of benzoate is considered to be the limiting step in phenol degradation, leading to the accumulation of benzoate and decrease of methane production when the conversion from phenol to methane is inhibited (Fedorak & Hrudey, 1984; Karlsson et al., 1999). It was reported by Hao et al. (2002) that higher initial phenol concentration in batch experiments would result in a more significant inhibition effect. With the consumption of phenol, the inhibition effect gradually decreased. The equations used to calculate PhLR and PhCR are shown in Equation 2.1.

$$PhLR = \frac{Q \cdot C_{in}}{V \cdot X}$$
$$PhCR = \frac{Q \cdot (C_{in} - C_{out})}{V \cdot X} \quad \text{(Equation 2.1)}$$

where Q is flow rate [L/h], C_{in} is phenol concentration in the influent [mg Ph-COD/L], C_{out} is phenol concentration in the permeate [mg Ph-COD/L], V is reactor working volume [L], and X is the biomass concentration[g VSS-COD/L]; PhLR and PhCR are biomass specific phenol loading rate and phenol conversion rate in mg Ph-COD/gVSS-COD·h.

From Equation 2.1 it can be seen that the increase of the PhLR might result from either the increase of the flow rate (shorten of the HRT) or the increase of the phenol concentration in the influent. Fang et al. (2004) studied the phenol degradation with UASB at ambient temperature and found that with a $_v$OLR higher than 6.0 g Ph-COD/L·d, a drastic deterioration of phenol removal efficiency occurred when phenol was used as the sole substrate. Similar results were reported by Lay & Cheng (1998) that PhLR higher than 1.40 g Ph-COD/gVSS·d will limit the methanogenic process of a RUASB.

2.1.4 Strategy to cope with the high PhLR

The phenol removal efficiency in batch experiments is affected by the initial acetate concentration, biomass concentration, pH, temperature and the addition of co-substrate (Arutchelvan et al., 2006). For continuous experiment with UASB, the acclimation of the biomass, effluent recirculation, as well as the supplement of co-substrates were proved to be effective for phenolic wastewater treatment (Veeresh et al., 2005).

It was suggested by Young & Rivera (1985) that long-term acclimation could significantly improve the phenol removal efficiency of the biomass. Besides, it would be better to use diluted phenol at the beginning and increase the concentration step by step to shorten the acclimation period. The step width is critical to the successful start-up of the reactor. It was proved by Suidan et al. (1998) that the system could be recovered with a step feeding increase from 0.38 g Ph/gVSS·d to 0.82 g Ph/gVSS·d at HRT of 30 days. However, a step increase to 0.97 g Ph/gVSS·d at the same condition resulted in a failure for the system.

Besides acclimation, co-substrate addition is another way to relieve the inhibition of high phenol concentration. The objective of adding co-substrate is to activate methanogens and lead them to acclimation. At the same time, it could also contribute to promote phenolic ring's hydrogenation, fission and fragmentation (Veeresh et al., 2005). It was reported by Tay et al. (2001) that adding glucose as co-substrate could mitigate the inhibition by high phenol concentration and accelerate phenol degradation. In addition, modern anaerobic reactors could also apply effluent recirculation to increase mass transfer between the microorganisms and the organic matter and promote the treatment efficiency. It was reported by Lay & Cheng (1998) that longer HRT (lower recirculation ratio) could lead to a decrease of microbial's substrate

affinity and a decrease of the treatment efficiency of the biomass of a RUASB, the maximum PhLR obtained from the research was 1.4 g Ph-COD/gVSS·d.

2.2 Anaerobic degradation of phenolic wastewater

2.2.1 General Anaerobic degradation process

Anaerobic digestion generally consists of four main processes: hydrolysis, acidogenesis, acetogenesis, and methanogenesis (Dahiya et al., 2015). Among them, the hydrolysis process determines the rate of the overall metabolic reaction. The scheme of the reaction is shown in Figure 2.1 (Henze et al., 2008).

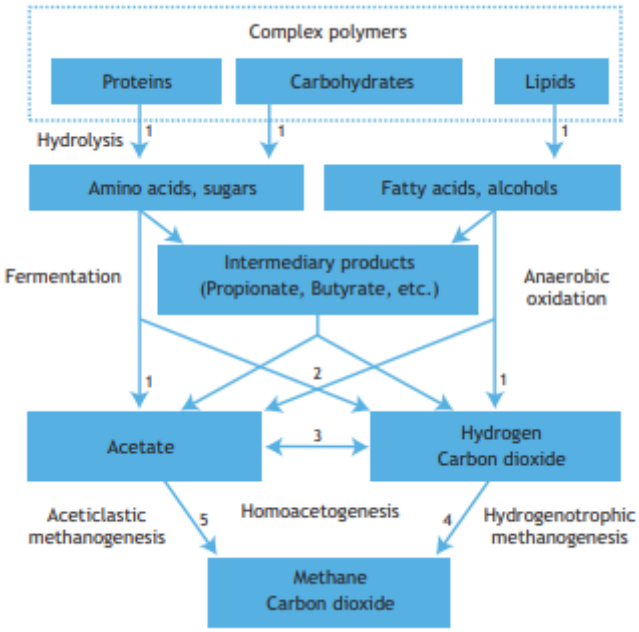

Figure 2.1 Anaerobic digestion process of the complex polymers. The bacteria groups unlabeled in the scheme: 1 Hydrolytic and fermentative bacteria. Syntrophic consortia involved: 2 Acetogenic bacteria, H_2 producer. In this process, VFA is converted to acetic acid and H_2 3 Homoacetogenic bacteria, H_2 consumer. In this process, acetic acid is generated via H_2 and CO_2 (taken from Gujer and Zehnder,1983).

Under standard conditions, the fermentative conversions are generally energetically unfavorable ($\triangle G_0' > 0$), so syntrophic consortium is usually needed to reduce the partial pressure of fermentative product (H_2) to lower than 10^{-3} atm and keep the fermentation proceeding. If the activity of H_2 consuming bacteria (e.g. homoacetogenic bacteria and methanogens) is lower than the activity of the acetogenic bacteria, the alkalinity in the reactor will be consumed, which will lead to a pH drop (Kleerebezem, 1999, Fonseca, 2018).

In the anaerobic degradation process, the methanogenesis could be considered to be the most important step. In this stage, the organic compounds (pollutants) are converted into methane and carbon dioxide, therefore removed from the medium. The two main pathways for methanogenic process are summarized in Table 2.1 (Henze, 2008), among which acetotrophic

methanogenesis contributes to about 70% COD removal, although it has lower maximum biomass growth rate than hydrogenotrophic methanogenesis. It was reported by Muñoz-Sierra et al., (2019) that, high sodium concentration could induce a shift from acetotrophic methanogenesis to hydrogenotrophic methanogenesis in an AnMBR and improve the enrichment of the salt-tolerant archaea Methanosaeta.

Table 2.1 Methanogenic reactions

Pathways	Reactions	$\Delta G_0'$ kJ/mol	μ_m 1/d	K_s mg COD/L
Acetotrophic methanogenesis	$CH_3COO^- + H_2O \rightarrow HCO_3^- + CH_4$	-31	0.12[a] 0.71[b]	30[a] 300[b]
Hydrogenotrophic methanogenesis	$CO_2 + 4H_2 \rightarrow CH_4 + 2H_2O$	-131	2.85	0.06

Note: a is Methanosarcina spec. and b is Methanosaeta spec (Henze et al., 2008).

As the H_2 is consumed in the hydrogenotrophic methanogenesis, partial pressure of H_2 could decrease to 10^{-4} atm so that the acetogenesis could proceed successfully. However, the methanogenesis could be easily impeded by toxic or inhibitory substances (e.g. phenol) in the wastewater or improper conditions such as low pH due to overloading. Inhibition causes VFA accumulation and reduces the capacity of degradation of the organic matter, in our case, phenol (Henze et al., 2008).

2.2.2 Anaerobic degradation process of phenol

Phenol degradation process is described by Young & Rivera (1985) as ring saturation - ring fission- organic acid intermediates – acetate. In this process, phenol plays a role as carbon and energy source (Karlsson et al., 1999). Knoll & Winter (1987) conducted a research on the degradation of phenol in sewage sludge with a stirred Biostat V reactor. When N_2/CO_2 was applied in the batch bottle, little intermediate product (e.g. benzoate and acetate) was observed, while significant accumulation of benzoate was observed when H_2/CO_2 was applied, which confirmed that the syntrophic consortia were necessary in phenol degradation process. In Knoll's later research (Knoll & Winter, 1989), they proposed that the carboxylation of phenol could be the prerequisite for the cleavage of the aromatic ring. Also, according to the thermodynamic calculation carried out by Bakker (1977), who found the free Gibbs energy change is negative (-0.2 kcal/mol) for the hydrogenation process of phenol, while it was positive (20.8 kcal/mol) for the hydration process with the presence of nitrate, which indicated that hydrogenation was the pathway for the cleavage of aromatic ring. Phenol degradation process is further summarized in Figure 2.2 (Fonseca, 2018).

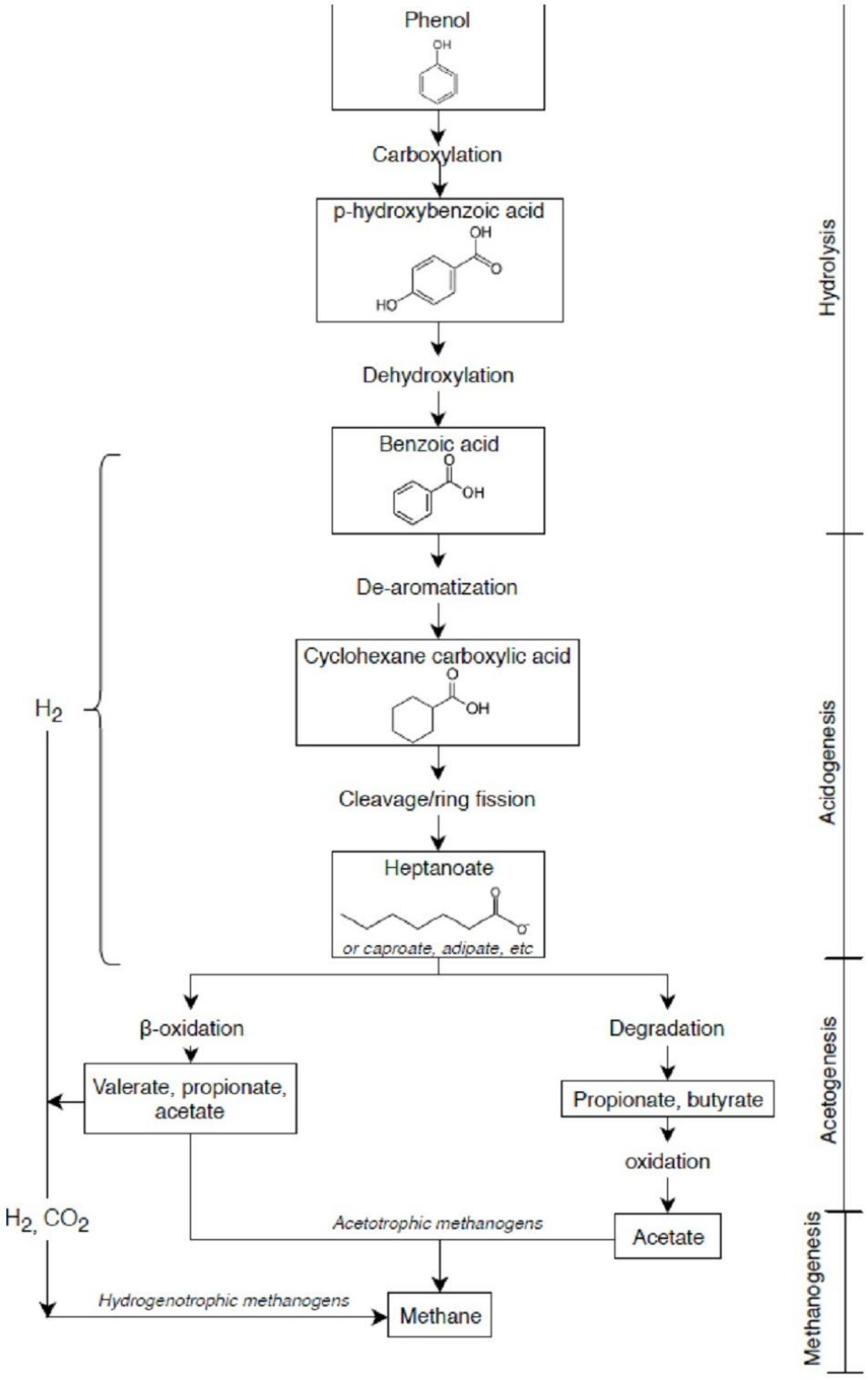

Figure 2.2 Phenol degradation pathway (Young and Rivera,1985; Kobayashi et al.,1989; Fang et al., 1996, 2006)

Depending on the bacteria present (e.g. sulphate reducing bacteria and nitrate reducing bacteria), the degradation pathway might be different. Other possible anaerobic phenol degradation pathways have also been discussed. The pathway of phenol degradation by nitrate-reducing bacteria with hydroxyhydroquinone as intermediate product was proposed by Schink

et al., (2000), see Figure 2.3.

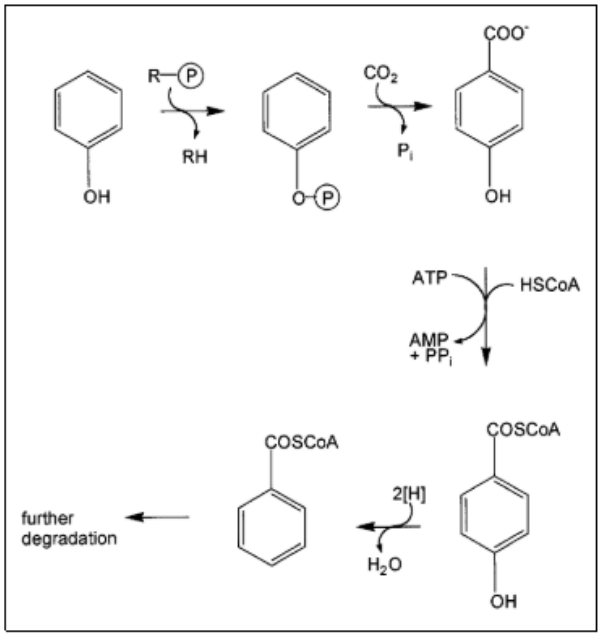

Figure 2.3 Phenol degradation pathway by nitrate-reducing bacteria *Thauera aromatica.* (Schink et al., 2000)

2.3 Anaerobic degradation kinetic

2.3.1 Different equations for inhibition

The basic theory behind biological reactions is the enzyme kinetics reaction, namely the reaction between the substrate and the enzyme to achieve a product.

$$E + S \underset{k_{-1}}{\overset{k_1}{\rightleftharpoons}} S* \xrightarrow{k_2} P + E$$

With Michaelis-Menten kinetic equation, the mechanism could be described by Equation 2.2:

$$r_s = \frac{r_{s,\max} S}{k_S + S} \quad \text{where} \quad k_s = (k_{-1} + k_2)/k_1 \qquad \text{(Equation 2.2)}$$

Based on different mechanisms that interfere substrate interaction with the enzyme and impede the product yield, the inhibition mechanism could be generally divided into: competitive inhibition and non-competitive inhibition. In the first one, the interfering substance take the same enzyme site, while in the second not. Another mechanism is un-competitive inhibition where the inhibitor interacts with the activated complex (intermediate product). The different inhibition mechanisms are summarized in Table 2.2 (Henze et al., 2008).

Table 2.2 Different equations for enzyme inhibition

	Reaction	Equation	Ks	r_{max}
Competitive inhibition	Step A: $E+S \rightleftharpoons S^* \rightarrow P+E$ Step B: $E+I \rightleftharpoons I^*$	$r_s = \frac{r_{s,max} S}{k_S(1+\frac{S_I}{k_I})+S}$	Increase	No effect
Non-competitive inhibition	Step A $E+S \rightleftharpoons S^* \rightarrow P+E$ Step B $E+S \rightleftharpoons S^*+I \rightarrow SI^*$ Step C $E+I \rightleftharpoons I^*+S \rightarrow IS^*$	$r_s = \frac{r_{s,max} S}{(k_S+S)(1+\frac{S_I}{k_I})}$	No effect	Decrease
Un-competitive inhibition	Step A $E+S \rightleftharpoons S^* \rightarrow P+E$ Step B $E+S \rightleftharpoons S^*+I \rightarrow SI^*$	$r_s = \frac{r_{s,max} S}{k_S+S(1+\frac{S_I}{k_I})}$	Decrease	Decrease

k_s represents substrate affinity; k_I represents inhibitor affinity; r_s is specific reaction rate; $r_{s,max}$ is maximum specific reaction rate. Step A, step B and step C are the steps of reactions. In the step A, substrate react with the enzyme, while in the step B and step C, the reactions were interfered by the inhibitor.

Based on Michaelis-Menten kinetic equation, Monod equation was developed. Compared to Michaelis-Menten kinetic equation which is specialized on biochemical reactions for single enzyme and single substrate, Monod equation could better describe the biological treatment processes with various substrates and different microorganisms. The Monod equation is shown in Equation 2.3.

$$\mu_g = \frac{\mu_{max} S}{K_S + S} \quad \text{(Equation 2.3)}$$

where K_s is half saturation coefficient [mgCOD/L], S is concentration of substrate [mgCOD/L], μ_{max} is maximum specific growth rate [1/h], μ_g is specific growth rate [1/h].

Besides substrate-limiting-type model (mainly Monod model), another kind of time-derivative-type model (Gompertz model) is also widely used in the anaerobic fermentative process, especially in hydrogen production process. Although it was shown that Gompertz model could better fit to the experimental data and directly describe the lag phase, Monod model was more popularly used in anaerobic degradation as it could take the anaerobic degradation relevant variables (e.g. substrate concentration) into account and successfully describe the reaction occurring in the biological process (Gadhamshetty et al., 2010; Veluchamy & Kalamdhad, 2017).

However, in the anaerobic modeling practice, Monod equation is sometimes too simplified to determine the biological process with multiple cultures, complex substrates and specific physical factors such as pH and temperature. This might due to the complexity of the anaerobic biological process, for example, when it is inhibited by the substrate or product (Maleki et al., 2018). Underestimating the influence of these factors will lead to an error in the parameter

estimation. At the same time, the biomass concentration change is not considered in the Monod equation which also brings uncertainty to the kinetic parameters' estimation. All these years, many efforts have been done to the modification of Monod equation. For example, Contois's model (Contois, 1959) was developed based on the Monod equation considering the biomass concentration in the biological conversion process.

In addition, other research studies have been carried out on the modification of Monod model based on specific experimental condition, such as inhibition. These models as well as Gomperz models (and its modified format) are summarized as Table 2.3 (Basak et al., 2014; Veluchamy & Kalamdhad, 2017; Wang & Wan, 2009). Recently, some researchers have considered to combine Monod model and Gomperz model to describe the biological process (Siripatana et al., 2016). However, this also means more parameters need to be fitted with limited experimental data and kinetic equations. The freedom of the parameters could easily exceed acceptance and result in an imprecise estimation.

Table 2.3 Models based on Monod equation and Gomperz equation

Models based on Monod equation	Monod model	$\mu=\frac{\mu_{max}S}{K_S+S}$	Monod (1949)
	Haldane's model	$\mu=\frac{\mu_{max}S}{K_S+S+(S^2/K_I)}$	Haldane (1965)
	Yano model	$\mu=\frac{\mu_{max}S}{K_S+S+(S^2/K_I)(1+S/K)}$	Yano et al. (1966)
	Aiba model	$\mu=\frac{\mu_{max}S}{K_S+S}\exp(-S/K_I)$	Aiba et al. (1968)
	Edward's model	$\mu=\mu_{max}S[\exp(\frac{-S}{K_I})-\exp(\frac{-S}{K_S})]$	Edwards (1970)
Models based on Gomperz equation	Gomperz model (for biogas)	$P=P_\infty\exp(-(r_0/\alpha)\exp(-\alpha t))$	Siripatana et al. (2016)
	Zwietering's model (for biogas)	$P=P_\infty\exp(-\exp((R_m\cdot e/P_\infty)(\lambda-t)+1))$	Siripatana et al. (2016)
	Mu's model	$X=\frac{X_0\exp(k_c t)}{1-(X_0/X_{max})(1-\exp(k_c t))}$	Mu et al. (2006)

2.3.2 Phenol and acetate degradation modeling with Haldane kinetic equation

Among the kinetic models used for biological process description, Haldane's model has proven to be the most suitable to describe the inhibition by substrate in the anaerobic degradation. In the research of phenol degradation, the correlation coefficient could reach 0.99 when using Haldane equation for experimental data fitting (Kumar et al., 2005). The reactions and kinetic equation of Haldane equation are shown in Equation 2.4.

Step A $E + S \rightleftharpoons S^* \rightarrow P + E$; Step B $E + S \rightleftharpoons S^* + S \rightleftharpoons S_2^*$

$$\mu_g = \frac{\mu_{max} S}{K_S + S + (S^2 / K_I)} \quad \text{(Equation 2.4)}$$

where K_I is inhibition coefficient of Haldane's growth kinetic [mg COD/L]; Based on the equations, the difference between microbial growth rate with Monod and Haldane equations could be expressed in Figure 2.4.

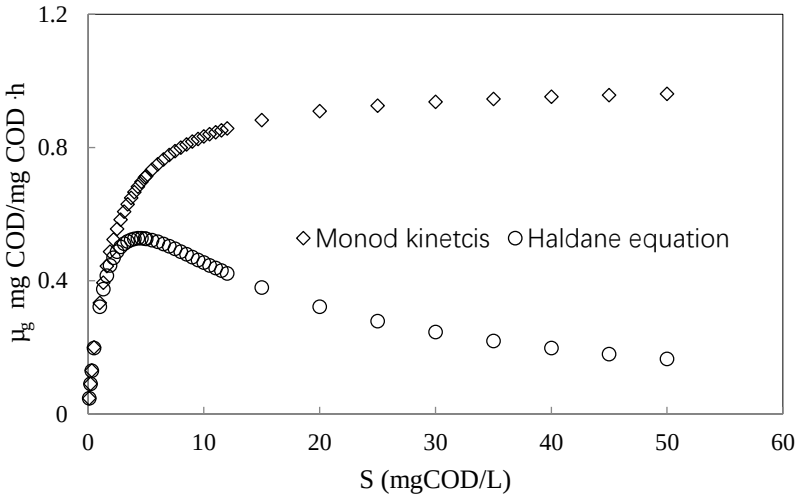

Figure 2.4 Microbial growth rate with Monod and Haldane equations (μ_{max}=1h^{-1}, Ks=2 mg COD/L, K_I =10 mg COD/L)

However, the kinetic parameters (K_s, K_I and μ_{max}) in the Haldane equation and the shape of the degradation curve were affected by many factors. For example, it was reported by Banerjee & Ghoshal (2010) that higher phenol degradation rate could be achieved with higher initial phenol concentration in the case that phenol concentration is lower than 500mg/L. On the other hand, too much phenol could inhibit phenol degradation, for example a 36h lag phase was observed by Arutchelvan et al., (2006) when phenol concentration was higher than 1750 mg/L. This has also been proved by the results of many batch experiments in which different kinetic parameters set were achieved with different initial substrate concentrations (Arutchelvan et al., 2006; Hao, 2002; Vavilin & Lokshina, 1996) while keeping everything else is the same. The Haldane kinetic parameters distribution for phenol degradation in different studies are summarized in Figure 2.5, the references are listed in Appendix 2.1.

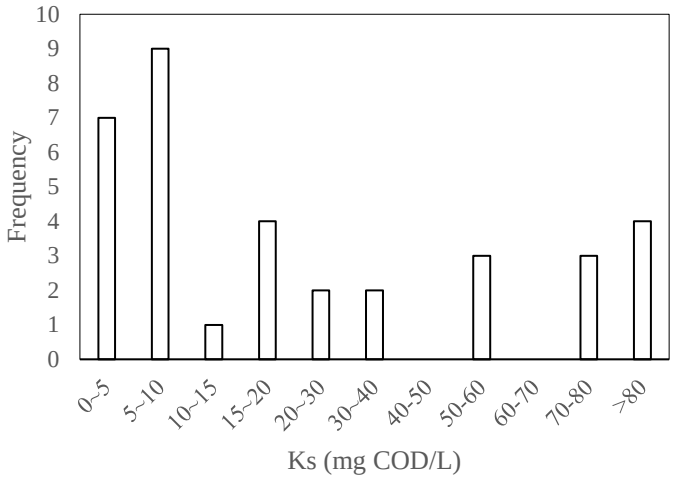

(a)

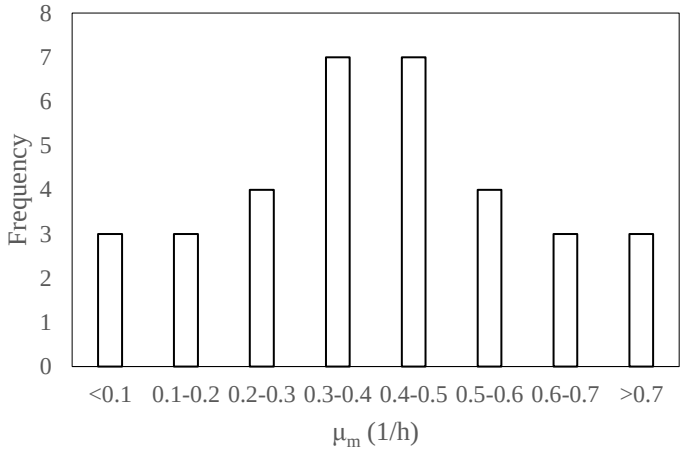

(b)

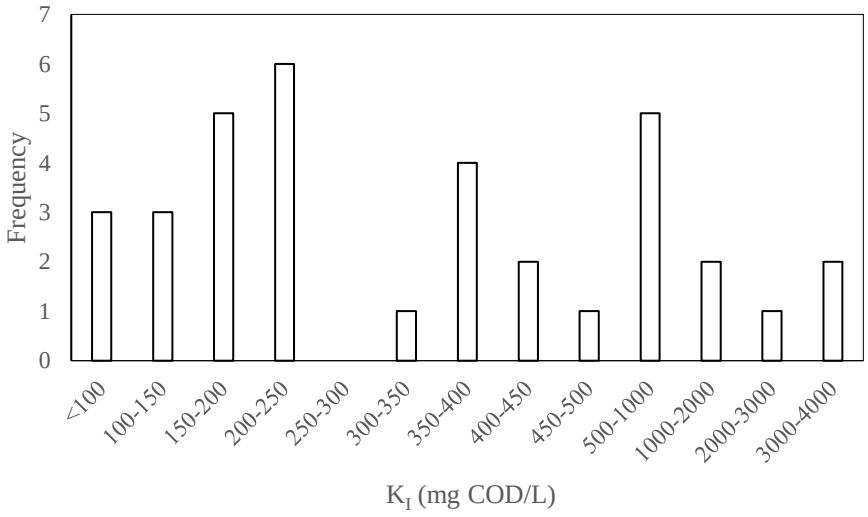

(c)

Figure 2.5 Kinetic parameters distribution from literature. The x axis is the Ks (a), μ_m(b), or K_I (c) value in mg COD/L given by the literature. The y axis is the frequency of these values when reported in the literature. From each figure, it can be seen that the most common used Ks, μ_m and K_I value are 5~10 mg COD/L, 0.3~0.5 h^{-1} and 200~250 mg COD/L, respectively. The range of K_I values varies considerably.

On the other hand, the inhibition caused by acetate is rarely reported compared to the phenol inhibition in the phenolic wastewater treatment. This might be due to that the K_I of acetate degradation at 35ºC is very large so that the inhibition by acetate could be neglected in general (Lokshina et al., 2001; Vavilin & Lokshina, 1996). Without considering the inhibition effect, Henze & Harremoës (1983) proposed a value of Ks= 50 mg COD/L, μ_{max}=0.4 d^{-1}, Y=0.03 mg COD/mgCOD, k_m= μ_{max}/Y=13 mg COD/mgCOD·d for the methanogenesis process. Furthermore, Pavlostathis & Giraldo-Gomez (1991) summarized a concentration range for each kinetic parameter in the acetoclastic methanogenesis process with k_m=2.6~11.6 mg

COD/mgCOD·d, Y=0.01~0.054 mg COD/mg COD, Ks=11~421 mgCOD/L, μ_{max}=0.08~0.7d^{-1}. However, these parameters have not considered the inhibition effect brought by phenol or salinity.

2.3.3 ADM1 model

ADM1 model was developed by the IWA Task Group for Mathematical Modelling of Anaerobic Digestion Processes (Batstone et al., 2002) and is one of the most widely used model to describe the anaerobic process (Maharaj et al., 2019; Peiris et al., 2006; Lohani et al., 2016). In the ADM1 model, the conversion process (hydrolysis, acidogenesis, acetogenesis, and methanogenesis) in the anaerobic degradation are involved, and the gas-liquid mass transfer process was also clearly described. The schematic diagram of ADM1 model implementation in a single tank system is shown in Figure 2.6 (Batstone et al., 2002).

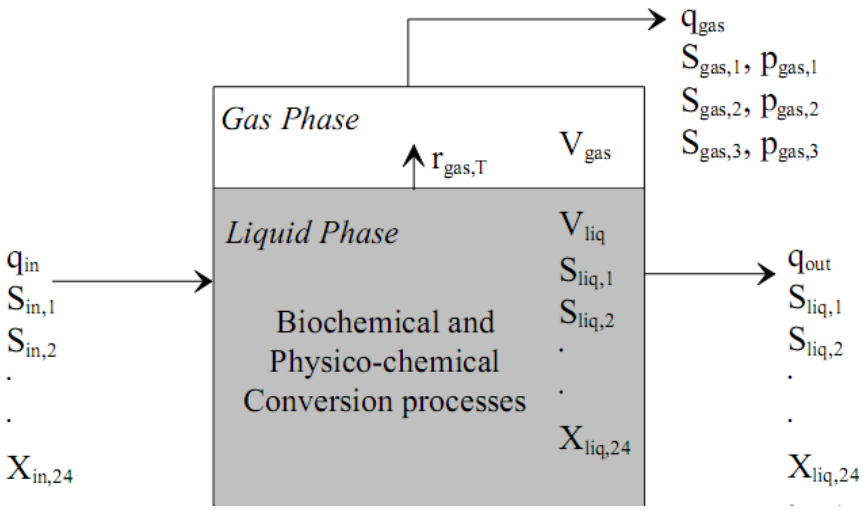

Figure 2.6 Schematic diagram of the ADM1 model implementation in a single tank system. X_i is particle component concentration and S_i is soluble component concentration. r_{gas} represents gas-liquid transfer rate (Batstone et al., 2002).

Many studies have demonstrated that the kinetic parameters given by ADM1 model (or modified/extended ADM1 model) could effectively predict the conversion process from complex organic matter to methane in the anaerobic digestion process (Galí et al. 2009; Derbal et al. 2009; Dereli et al. 2010). The kinetic parameters for acetate degradation given by ADM1 were k_m=8 mgCOD/mgVSS·d, Y=0.05 mgVSS/mgCOD, Ks = 140 mgCOD/L.

Nevertheless, limitations for the application of ADM1, such as less effective description from glucose to VFA production, and uncertainty in parameters estimation were also proposed by Batstone et al. (2006). One of the difficulties in the ADM1 model application is the estimation of initial biomass concentration. Especially in the presence of multiple organisms, their fractions are often difficult to estimate. Nevertheless, the dependence of biological processes on initial biomass concentrations is weak, which allows to predict biological

processes without accurate initial biomass estimation or in the case that initial biomass data are not directly available (Kalyuzhnyi, 1997). On the other hand, the ADM1 model neglects the thermodynamic limitations and the oxidation state difference between substrate and biomass, which makes the assessment on the metabolic process not accurate enough (Kleerebezem & van Loosdrecht, 2006).

Based on specific wastewater characteristics, the extensions of ADM1 were reported by many researchers. For instance, a modified ADM1 model was proved to be an effective tool in the prediction of phenolic wastewater treatment, considering the conversion from phenol to acetate (Chen et al., 2016; Fezzani & Cheikh, 2009). In the latter research, the inhibition of phenol was also considered, using non-competitive inhibition equation, as well as the calibration of the most sensitive parameters using the experimental data.

Since we used synthetic sewage in the lab experiment (no hydrolysis process needs to be considered), and the experiments lasted only for 12 h for dynamic experiment and no more than 5 days for batch experiment, respectively, a simplified ADM1 model was used in our research without considering the growth or decay of the biomass. Only two groups of bacteria were included in our research: phenol degrader and acetate degrader. The parameters for acetate degradation in the ADM1 was used as reference values for sensitivity analysis. The inhibition of phenol was described by the Haldane equation.

2.4 Industrial wastewater treatment by AnMBR

Anaerobic treatment has been widely applied in industrial wastewater treatment since the development of the HRAR (e.g. UASB and EGSB) (Seghezzo, 1998). HRARs could decouple the SRT and HRT by biomass immobilization through granulation, or physical separation of the biomass with the liquid phase by membrane filtration. Compared to other anaerobic reactors such as UASB, AnMBR is particularly suitable for treatment processes that require a complete retention of specific microorganisms. This is useful in the case of microorganisms with low growth rate, or when treating wastewater under adverse conditions, such as saline and toxic (phenolic) wastewater (Vyrides & Stuckey, 2009a; Skouteris et al., 2012). It was proposed by Jeison et al. (2008) that use of microfiltration membrane improves the halotolerant bacteria retention and positively affect its performance in saline water treatment.

At the same time, AnMBR also takes advantage of shorter start-up period because of its longer SRT, and better effluent quality due to the complete solid-liquid separation. However, AnMBRs have drawbacks such as membrane fouling, high operation and capital cost, and low flux (Chernicharo et al., 2015).

AnMBR has two main configurations, vacuum-driven submerged membrane reactor and pressure-driven external cross-flow membrane reactor (Chang, 2014). Among them, the external cross-flow membrane reactor could be more easily hydrodynamically-controlled and

more convenient for membrane replacement, which leads to less membrane fouling and higher flux. However, the cost of energy consumption for recirculation are generally high, which limits its application in full-scale (Lin et al., 2013).

2.4.1 Effect of HRT and SRT on the performance of AnMBR

It is considered that AnMBR operation under long HRT and SRT will be beneficial for methane recovery. It could also contribute to improve the AnMBR treatment performance as well as sludge production reduction (Lin et al., 2013). However, the effect of HRT on AnMBR performance is a little tricky. Besides the direct impact on the loading rate, as explained in Equation 2.5, it is also related to the membrane fouling, microbial activity and physical COD removal. For the fouling control, high flow rate will result in a decrease of cake layer formation and increase the flux. Nevertheless, the cake layers sometimes could act as a protective layer for further clogging of the membrane, so this could pose a negative effect on the membrane fouling. At the same time, the higher cross-flow velocity resulting from the higher flow rate will lead to the increase of cell lysis, and more EPS and SMPs will be released. This will even exacerbate the membrane fouling (Stuckey, 2012). For the microbial activity, on the other hand, high flow velocity could decrease the particle size of the sludge and increase the mass transfer between the substrate and methanogenic biomass. However, the increase of cell lysis will also impede the methanogen's activity. Moreover, high flow rate will hamper the symbiotic association between the hydrogen utilizers and acetogenic bacteria because of violent mixing (Dereli et al., 2012) and destroy the hydrogen transfer association. Furthermore, higher flow rate will lead to a higher hydrolysis rate due to the increase of mixing and shear, which easily results in the accumulation of VFA and pH drop (Stuckey, 2012) and inhibit the activity of methanogens. Although, it was reported by Skouteris et al. (2012) that shorter HRT could improve biomass growth, high flow velocity due to short HRT is generally considered negatively affect the AnMBR biomass activities.

$$vOLR = \frac{C_{in}}{HRT} \qquad \text{(Equation 2.5)}$$

$$sOLR = \frac{C_{in}}{HRT \times X} \qquad \text{(Equation 2.6)}$$

As the cake layer could also act as a barrier to prevent COD flow out with the effluent, thinner cake layer brought by HRT decrease could reduce the COD removal efficiency of the AnMBR. Moreover, shorter HRT also increase the energy requirement for the AnMBR and increase the overall cost.

The implications of SRT on the AnMBR performance are also manifold. On the one hand, it was reported that more biogas could be obtained under longer SRT (Skouteris et al., 2012). This might be due to that longer SRT will contribute to a higher concentration of biomass and help the bacteria better adapt to the extreme conditions, such as toxicity (Dvořák et al., 2016),

which seems to be beneficial for the COD removal. However, longer SRT will also result in higher SMP concentration, leading to a deterioration of effluent quality as well as more serious membrane fouling due to internal pore blocking (Skouteris et al., 2012).

On the other hand, it was also reported by Stuckey (2012) that the growth rate of the bacteria and the active biomass concentration under high SRT could be very low, leading to a poor biodegradability. In industrial practice, the SRT applied for an AnMBR generally fall in the range of 25 days to 335 days.

To conclude, the effect of HRT and SRT on the AnMBR performance can be very complex, depending on the set-up configuration, pump, and the characteristics of the feeding solution (Dereli et al., 2012; Stuckey, 2012; Lin et al., 2013). In general, the COD removal efficiency of an AnMBR could be higher than 90% with vOLR from 2 to 15 g COD/L·d (Lin et al., 2013). However, considering economic factors, it was suggested by Martin et al. (2011) to apply AnMBR only for the industrial wastewater with COD concentrations higher than 4~5 g/L.

2.4.2 AnMBR for saline (and) phenolic wastewater treatment

As mentioned in the last section, AnMBR is preferred for the treatment of wastewater with toxic compounds, in our case, the treatment of saline phenolic wastewater. Many studies have been carried out on the treatment of water with high salinity. The research carried out by Chen et al. (2019) proved that the COD removal efficiency decreased from 96.4% to 77.7% with the stepwise increase of NaCl concentration from 5 to 40 g /L; COD removal was improved to 94.1% during the recovery. Li et al. (2018) conducted a research of saline (35 g Na^+/ L) water treatment with AnMBR and achieved 97.2% COD removal with vOLR of 4 g COD/L· d after 226 days' acclimation. Similar results were reported by Yang (2013) that the COD removal efficiency of AnMBR could be higher than 99% when treating wastewater with NaCl concentration of 32 g/L and sOLR of 0.55 g COD/g VSS·d.

There is very few research regarding to the phenolic wastewater treatment using AnMBR. Ghanbari (2018) studied the performance of AnMBR treating wastewater with phenol concentration from 25 mg/L to 600 mg/L (total COD concentration from 1000 mg/L to 6430 mg/L) using glucose as co-substrate. It was shown that higher COD removal efficiency was achieved with longer HRT and glucose concentration. The highest COD removal efficiency reached 99.85%. Skouteris et al. (2012) reported that the SMA could be improved by granular activated carbon (GAC) dosing and higher methane yield could be achieved.

Although, both high phenol concentration and salinity were proved to be inhibitors to anaerobic degradation (Şeker et al., 1997), there are few studies that take into account the collective effect of them, which might reduce the activity of the biomass more significantly (Muñoz-Sierra et al., 2018). Most of the studies to date were carried out by our group and the BioXtreme project. Muñoz-Sierra et al. (2018), working also with AnMBR, focused on the

effect of sodium concentration on the treatment performance of phenolic wastewater. In his study, phenol conversion rates decreased from 5.1 mg Ph/gVSS·d to 4.7 mg Ph/gVSS·d when the sodium concentration was increased from 16 g Na^+/L to 18 g Na^+/L. In his later research (Muñoz-Sierra et al., 2019) he also pointed out that the specialized microorganisms could be retained in the reactor under a phenol concentration up to 5 g Ph/L in the case of sodium concentration lower than 26 g Na^+/L with the help of the membrane. Similar research but focused on the effect of co-substrate was carried out by Fonseca (Fonseca et al., 2018) who used acetate as co-substrate and achieved PhCR of 115 mg Ph/gVSS·d with 3g Ph/L in the influent, while the PhCR was only 42 mg Ph/gVSS·d using phenol as sole carbon source.

3 Materials and methods

The research had two experimental setups: batch and continuous experiments. Using the batch experiment, a model was built to study the effect of different factors (e.g. phenol and sodium concentration) on acetate degradation. It was assumed that there was no phenol degradation before a complete acetate degradation, so the phenol degradation could be neglected within 3 days' experiment. The acetate degradation kinetics were studied with the adapted biomass from two AnMBRs with different sodium concentrations (AnMBR1: 18.6 g Na^+/L and AnMBR2: 8.0 g Na^+/L). Haldane equation was used to describe the inhibition of acetate and phenol (only for dynamic experiment) in the degradation kinetic (Vavilin & Lokshina, 1996).

In the continuous experiment, the effect of PhLR increase on the phenol removal of AnMBR1 was studied by a short-term dynamic experiment (by decreasing HRT) and a mathematical model. In the model the phenol degradation process was simplified into two stages: from phenol to acetate and from acetate to methane. The kinetic parameters of acetate degradation were the same as those determined in the batch experiment. The maximum PhCR was compared with the results of previous research in the BioXtreme group with lower sodium concentration (Fonseca et al., 2018).

The schedule for the whole experiment is shown in Appendix 3.1. The continuous experiment with the AnMBR operation was divided into an acetate concentration decrease stage, transition stage (maximum PhCR determination), and HRT variation stage (dynamic experiment stage). The biomass was taken out for batch experiments at day 54, and 115 during this period.

3.1Batch experiment

3.1.1 Model establishment and sensitivity analysis

For the batch experiment, a mathematical model was built in Python with the acetate kinetic parameters proposed in literature (Batstone et al., 2002; Vavilin & Lokshina, 1996). Biomass concentration was assumed to be constant so that no decay or biomass growth during this period were considered. The active biomass was assumed to be 50% of the total VSS according to Henze & Harremoës (1983). The yield and fraction of acetate degrader were determined by thermodynamic calculation proposed by Kleerebezem & Van Loosdrecht (2010), which considered a coupled reaction of catabolism and anabolism. In the catabolism reaction, the substrate is consumed to produce energy. In the anabolism reaction, the energy produced as well as the carbon and nitrogen source from the substrates are used for synthesis of biomass. The reaction of each process was determined by stoichiometry calculation. The biomass formula ($C_1H_{1.8}N_{0.2}O_{0.5}$) was taken from Kleerebezem & Van Loosdrecht (2010). As a simplified model, and as we kept the pH constant, the effect of pH variation on degradation

kinetic was neglected in the model.

For determining the dissolved methane in the effluent, the mass transfer coefficient used was the one proposed by Metcalf. et al. (2003). The solubility of the methane was corrected for salinity and temperature as proposed by Weiss (1974). The equations and relative parameters are listed below.

$$\ln \beta = A_1 + A_2(\frac{100}{T}) + A_3 \ln(\frac{T}{100}) + S‰[B_1 + B_2(\frac{T}{100}) + B_3(\frac{T}{100})^2] \qquad \text{(Equation 3.1)}$$

where β is Bunsen solubility coefficient [L CH_4(STP)/L atm]; A and B are constants for Bunsen solubility equation proposed by Yamamoto et al. (1976), see Appendix 3.2; T is temperature [K]; S‰ is salinity expressed in ppt NaCl. For the Na^+ concentration of 8.0 g /L and 18.6 g /L, the S‰ equals to 18.5 ppt and 42 ppt, respectively.

A sensitivity analysis was carried out on Haldane equation instead of ADM1 model for simplification. The most sensitive parameter in the Haldane equation was determined by changing the values of 5% on one of the variables while keeping the other parameters constant. The most sensitive substrate (acetate) concentration range for each parameter was determined by the derivation of the Haldane equation for each of them. The sampling points of the batch experiment were determined according to the sensitivity analysis of the model.

3.1.2 Inoculum

The main composition of the substrate in each batch experiment is shown in Appendix 3.3. Sodium concentration, micro- and macronutrient solutions, and phosphate buffer solutions were maintained the same as in each reactor. Also, due to the limited reactor biomass available, the I/S ratio used for the batch experiment was 1 and each batch experiment condition was carried out in duplicates due to limited biomass available. The bottles used for batch experiment were 500 mL Schott Duran glasses, and the working inoculum + substrate volume was 400 mL. Phenol and acetate concentration measured in the AnMBR biomass mixture was about 0 mg COD/L, so it was assumed that the substrate COD completely came from the acetate or acetate phenol mixture added.

3.1.3 Batch test

At the beginning of the experiment, pH and COD of the solution in each bottle were measured. To ensure anaerobic conditions, each reactor was flushed with nitrogen for one minute. The batch tests were carried out in a temperature controlled shaker (New Brunswick Scientific, Innova 44) at 130 RPM or motors (112 RPM) for getting a complete mixing. Temperature was kept constant at 35°C.

According to the sensitivity analysis, the sampling was done 2-3 times each day for VFAs and phenol measurement. Methane production was measured online by AMPTS system

(Bioprocess Control, Sweden). The final VSS concentration, pH, and COD concentration were also measured at the end of the experiment. The sludge used for the batch tests was recovered prior centrifugation at 5000 g in a Heraeus Labofuge 400 centrifuge (Thermal Scientific, USA) and returned to the reactor.

3.1.4 Kinetic parameters estimation

The actual value of the kinetic parameters (K_s, K_I, μ_{max}) was determined by fitting the model to the experimental data. The effect of the phenol on acetate degradation was determined by comparing the parameters between the group using solely acetate with the group using phenol and acetate. The effect of high sodium concentration was determined by comparing the difference of kinetic parameters achieved by similar groups with a lower Na^+ concentration [8.0 g /L].

3.2 Continuous experiment

3.2.1 Experimental set-up

Two 7L AnMBR reactors, AnMBR1 and AnMBR2, with a working volume of 6 L were continuously operated under different sodium concentration (8.0 g Na^+/L and 18.6 g Na^+/L, respectively) for more than 200 days before the experiment started. Phenol removal efficiency of both reactors were above 99%.

(a)

(b)

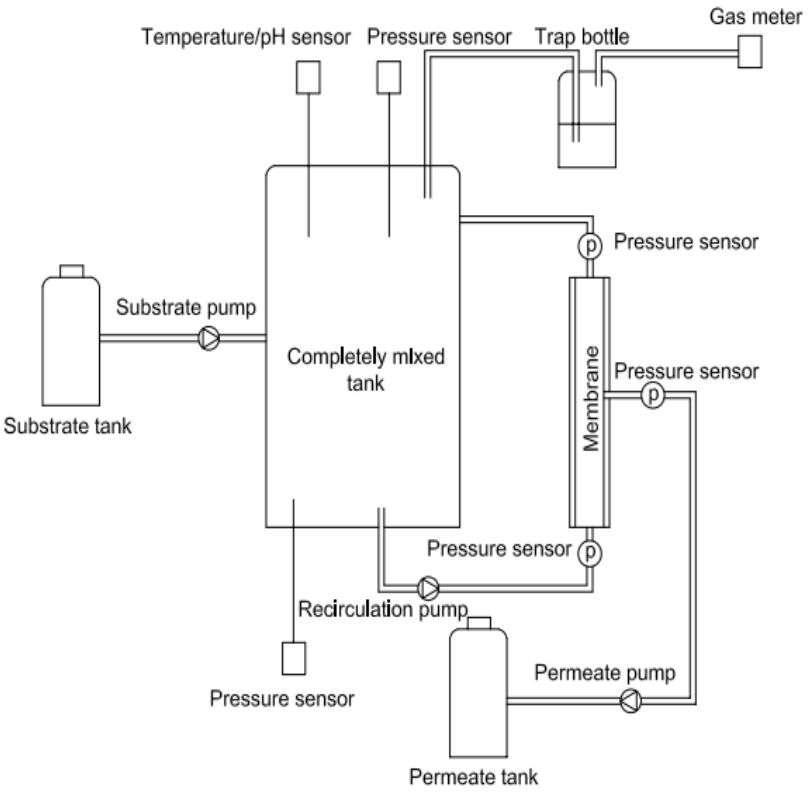

(c)

Figure 3.1 (a) Setup and (c) Scheme of the pilot scale (6 L working volume) AnMBR experimental set-up. Filtration was done by an external ultrafiltration (30 nm nominal pore size) module (b) (Pentair, The Netherlands).

Temperature of both reactors were kept constant at 35 ± 1ºC with a thermostatic water bath (Tamson TC16, Netherlands). The feed water was pumped into the reactor by a peristaltic pump (Watson-Marlow 120U, UK) and fully mixed with the sludge inside. The sludge mixture was ensured by the internal sludge recirculation (Q=1470L/d, $Q_{recriculation}/V_{reactor}$ = 245 1/d). Sludge was pumped into the external membrane module (see Chapter 3.2.3) through a recirculation pump (Watson-Marlow 540Du, UK). Permeate was collected by the permeate pump (Watson-Marlow 120U, UK) and the retentate was recirculated to the reactor. The AnMBRs and their scheme are shown in Figure 3.1.

The initial flow rate of the influent was fixed at 1L/d corresponding to the HRT of 6 d and the PhLR of 49 mg Ph-COD/gVSS-COD·d. The filtration cycle was 500s of pressure driven filtration, followed by a backwash (Q =8L/d) for 15s (Judd, 2010). As the experiment proceeded, the HRT was stepwise changed so that the influent flow was adjusted correspondingly.

The permeate flow rate was controlled by a volume control system of Lab View software (National Instruments, USA) designed by Carya (Carya, NL), and it worked through the measurement of several parameters (e.g. pressure, pH and temperature) by different sensors. So then, the conditions inside the reactor were online-monitored. The pH and temperature were

measured by a pH/temperature sensor (Mettler Toledo M300 for AnMBR 1 and Endress & Hauser for AnMBR 2); The pressures at the membrane module inlet, outlet, and permeate side of the membrane were measured by three pressure sensors (AE Sensors ATM [-800~600 mbar], The Netherlands) and was used to calculate the TMP (carried out by Lab View software automatically). Biogas produced volume was measured by a gas meter (Ritter, MGC-10 PMMA_R). To keep the volume constant in the reactor, the water volume in the reactor was determined by the difference of two pressure sensors, a headspace sensor (AE Sensors ATM [0~20 mbar], The Netherlands) for the gas pressure; and a total pressure (hydrodynamic + gas) sensor (AE Sensors ATM [0~70 mbar], The Netherlands).

3.2.2 Feeding solution of continuous experiment

For a better comparison of the results between the two AnMBR results, the acetate concentration of AnMBR1 was decreased stepwise before the HRT was changed. The final acetate-COD concentration in the AnMBR1 feeding was set at 2 g/L which was the same as in AnMBR2, while the Na^+ concentration in AnMBR1 remained constant at 18.6g Na^+/L. The feeding solution composition of AnMBR1 at different stages are shown in Table 3.1. The volume for micronutrients and macronutrients were 4.5mL/L and 9 mL/L, respectively and the K^+/Na^+ ratio was kept constant at 0.05 (Muñoz-Sierra et al., 2018). At point F, yeast concentration was further decreased to 189 mg/L (0.22g COD/L, 5.4% of the total COD) according to the Hendriks et al. (2018).

Table 3.1 Feeding solution of AnMBR1 at different stages

	Sodium Acetate (g/L)	Phenol (mg/L)	NaCl (g/L)	Yeast (mg/L)	Total COD (g/L)	Total Na^+ (g/L)
Initial-A	41.55	500	29.55	2000	22.83	18.6
A-B	41.55	500	29.55	1200	21.91	18.6
B-C	30.9	500	34	1200	17.08	18.6
C-D	20.6	500	38.4	1200	12.24	18.6
D-E	10.3	500	42.8	1200	7.41	18.6
E-F	4.3	500	45.4	1200	4.57	18.6

3.2.3 Membrane Characteristics

The membranes coupled for both reactors were tubular PVDF ultrafiltration (UF) membranes with a nominal pore size of 30 nm (Pentair, the Netherlands). The characteristics of the membrane are shown in Table 3.2.

Table 3.2. Characteristics of the membrane

	Nominal pore size (nm)	Diameter (mm)	Length (mm)	Surface area (m^2)	Cross-section area (m^2)
Membrane	30	5.2	640	0.0104	2.12E-05

Membrane preparation, permeability and critical flux determination

A new membrane was used at the beginning of the transition stage, so membrane de-coating was done by soaking the membrane with citric acid (5g/L) during one day before the membrane was installed in the module.

Permeability was tested with demi water at room temperature under cross-flow velocity of 1 m/s (Judd, S. 2010). The mass of every 10 minutes' permeate (demi water) was measured after receiving a uniform permeate. The permeability of the membrane was calculated with Equation 3.2.

$$K = \frac{J \times \exp(-0.0239 \times (T-20))}{\Delta P \times A} \quad \text{(Equation 3.2)}$$

where J is permeate flow rate [L/h]; T is temperature [^{o} C]; A is surface area of the membrane, m^2. ΔP is transmembrane pressure[bar]; K is permeability of the membrane, [LMH· bar].

Critical flux

Critical flux was determined by a modification protocol proposed by Le Cleche et al. (2003). The time interval of the measurement was 15 min and the step height of the flux was 4L/(m^2·h). The critical flux was determined by the flux when significant TMP ($\triangle P_0 = TMP_{i,n} - TMP_{f,n-1}$) increase occurred.

Membrane cleaning

Membrane fouling causes negative pressure on the permeate side of the membrane, which results in the AnMBR system shut down (controlled automatically by Lab-view software). Physical cleaning, chemical cleaning, and backwash or membrane relaxation could be applied to relieve this problem. Physical cleaning was accomplished by removing the membrane and injecting demi-water into and out of the membrane module with a syringe. Chemical cleaning was applied when the pressure of membrane on the permeate side decreased to about -200 mbar, or when the pressure at the inlet of the membrane was more than 500 mbar. Chemical cleaning was carried out by soaking the membrane in 300 ppm (active chlorine) NaOCl solution for 2 hours, followed by soaking with a 2 g/L citric acid solution for 2 hours subsequently.

3.2.4 HRT variation

In the dynamic experiment, the effect of PhLR on the PhCR was studied by the increase or decrease of HRT and the maximum PhCR was determined. At the beginning of the dynamic experiment, as the accumulation of phenol was already observed, HRT was stepwise increased by decreasing the influent flow rate from 1 L/d (PhLR = 29.2 mg Ph/gVSS·d) while keeping the substrate composition unchanged. Then, due to the adaptation of the biomass, HRT was decreased from 10 h (PhLR = 17.5 mg Ph/gVSS·d). The corresponding PhLR at different stages are shown in Table 3.3.

Table 3.3 PhLR with HRT variation

Phenol concentration [g/L]	Flow rate [L/d]	Phenol loading rate [mg Ph-COD/gVSS-COD·d]	Phenol loading rate [mg Ph/gVSS·d]	HRT (d)	HRT (h)
0.5	1.0	49	29	6	144
0.5	0.8	39	23	7.5	180
0.5	0.6	29	17	10	240
0.5	1.2	58	35	5	120
0.5	1.5	73	44	4	96
0.5	2.0	98	59	3	72

3.3 Biomass

The biomass inoculum in the reactor came from a UASB reactor of Shell, used for treating petrochemical wastewater. In the batch experiments, the initial VSS concentration of AnMBR1 and AnMBR2 were 2.0 g/L and 2.9 g/L, respectively.

3.4 Chemicals

The specific composition of buffer solution A & B and nutrient solution as specified by Muñoz-Sierra et al., 2018 are shown in Appendix 3.4. The origin and purity of the chemicals used in the experiment are shown in Appendix 3.5.

3.5 Analysis method

3.5.1 Analysis method of sludge

- *Volatile suspended solids*

The VSS concentration in the experiment was measured in triplicates according to standard method (APHA,1999). A 0.7 μm glass-fiber filters (Merck Millipore Ltd.) was ignited at 550 ^{o}C for 2.5 hours in the muffle oven and weighted (Weight 1) after cooling in the desiccator to remove any organic matter. Because of the reduced sludge availability, 2 mL (V) biomass sample were filtered through the prepared filter and heated at 105^{o}C in an oven over night. The weight increase (Weight 2) was the total suspended solid (TSS) of 2 mL biomass sample.

Then, the biomass sample was burned at 550 ^{o}C in a muffle oven for 2.5 hours and weighted after cooling in the desiccator, the weight (Weight 3) decrease was the VSS concentration of the biomass sample.

$$TSS = \frac{W_2 - W_1}{V}$$
$$VSS = \frac{W_2 - W_3}{V} \quad \text{(Equation 3.3)}$$

Note*: For the mathematical model, the concentration of phenol degraders and methanogens was used separately. VSS was used to represent biomass concentration for all other experiments.

3.5.2 Analysis method of biogas composition

10 mL biogas sample was used to determine the biogas composition with gas chromatograph (Agilenttech 7890A), which contains a HP-PLOT Molesieve GC column (Agilent 19095P-MS6) of $60\text{m}\times 0.53mm\times 200\mu m$. A thermal conductivity detector (TCD) was used as front detector with helium as carrier gas (14.8 psi and 23 mL/min flow rate), the operation temperature for injector and detector were both 200 ^{o}C.

3.5.3 Analysis method of permeate

- *Volatile fatty acids composition and concentration*

1.5 mL of permeate were filtered through 0.45 μm membrane filter (Chromafil Xtra PES-45/25, Ireland), and 500 μL of the filtered sample were transferred to a 1.5 mL vial. A dilution ratio of 1:2 with pentanol (320 mg/L) was used in our research. At last, 10 μL of formic acid (98%) were added to the sample for acidification.

The prepared VFA sample was analyzed by a GC (Agilenttech 7890A) with capillary HP-FFAP column size of $25\text{m}\times 0.32mm\times 0.50\mu m$ (Agilent 19091F-112). A flame ionization detector (FID) was used in the chromatograph with helium as the carrier gas (11 psi and 2.45 mL/min flow rate). The operation temperatures for detector and injector were 240°C and 225°C, respectively.

- *Phenol concentration*

The permeate was filtered through a 0.45 μm filter first. Phenol concentration in the permeate was measured with phenol cuvettes (Lange Hach phenol Cuvette Test LCK 346) by a spectrophotometer (Lange Hach DR3900). Concentration was double checked by GC (Agilenttech 7890A) using the same program already described.

- *Chemical oxygen demand*

The chemical oxygen demand (COD) was measured with a COD cuvette (Lange Hach COD Cuvette Test LCK 314 and 514) by spectrophotometer (Lange Hach DR3900) after digested by a thermo-reactor (Merck, Spectroquant TR620). Proper dilution ratios were used in our research to avoid the interference of chloride.

4 Results and discussion

4.1 Effect of acetate decrease on phenol removal of AnMBR

4.1.1 Effect of acetate decreasing on phenol conversion rate

Acetate [Ac^-] as a co-substrate can play an important role in the phenol degradation process (Fonseca, 2018). Hence, the Ac^- concentration in the feeding and thus the Ac^- loading of AnMBR1 and AnMBR2 should be the same to compare the effect of the high sodium concentration on the maximum PhCR. The initial acetate concentration in the AnMBR1 was 19.34 g COD/L corresponding to a biomass specific loading rate of 1.1 [g Ac-COD/gVSS·d], with a yeast concentration of 2 g/L. In the stage A-B, the yeast concentration was decreased to 1.2 g/L. From point B, the Ac^- concentration was decreased through steps of 4.8 g Ac-COD/L. After 69 days, the Ac-COD concentration reached 2 g/L (same with AnMBR2). The variation of PhLR, PhCR, and phenol removal efficiency during this period is shown in Figure 4.1.

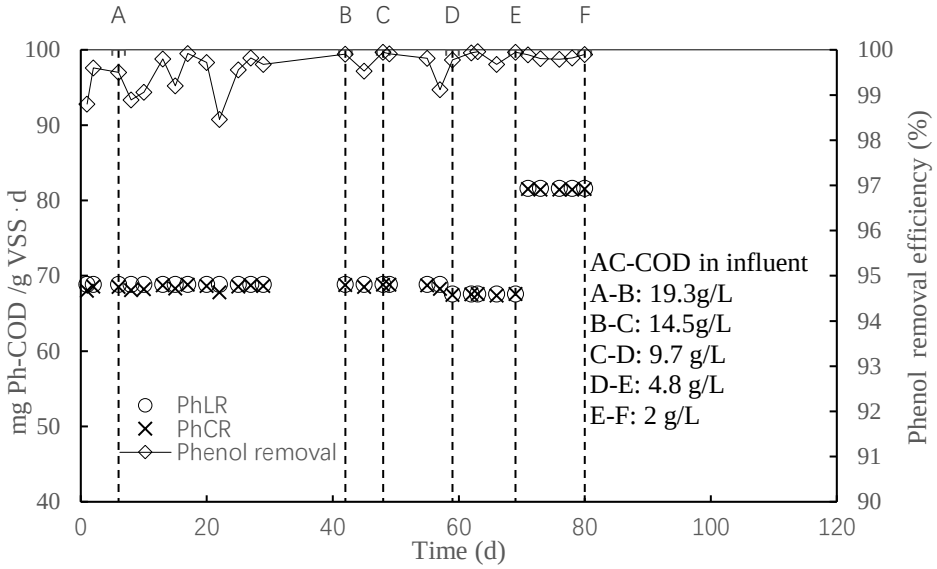

Figure 4.1 PhLR, PhCR and phenol removal efficiency changes of AnMBR1 biomass during the decrease of the acetate loading rate (HRT=6d). Ac- was stepwise decreased, so AnMBR1 [18.6 g Na^+/L] had the same volumetric Ac- loading as AnMBR2 [8.0 g Na^+/L]. At the end of the 5 stages PhCR was the same as the loading, meaning more than 99.5 removal percentage.

During the whole stages of acetate concentration decrease, the PhCR was always equal to the PhLR which indicated the reactor worked properly during this period. Although there were fluctuations in the removal, the efficiency remained above 98% and the phenol concentration in the effluent was below 10 mg/L. Hence, no effect on the PhCR was brought by the decrease of acetate concentration at the used PhLR [about 68~81 mg Ph-COD/gVSS·d].

4.1.2 Effect of acetate decreasing and COD removal efficiency

Unlike PhLR, the decrease of acetate concentration results in the decrease of sOLR as Equation

2.6. Figure 4.2 shows the COD removal efficiency variation with the decrease of sOLR. Besides, the variation in the COD removal remained above 93%. The COD concentration in the effluent was lower than 800 mg/L.

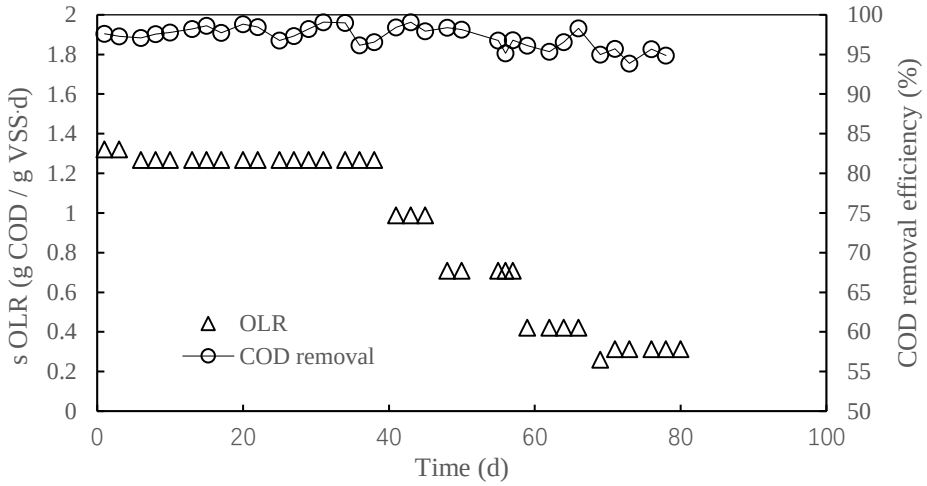

Figure 4.2 COD removal efficiency and sOLR of AnMBR1 biomass with the decrease of acetate loading rate (HRT=6d). sOLR was stepwise decreased from 1.3 to 0.3 g COD/gVSS·d. At the end of the 5 stages, COD was more than 93 removal percentage.

4.1.3 Effect of acetate decrease on biogas production rate

The variation of biogas production with the decrease of acetate loading rate is shown in Figure 4.3.

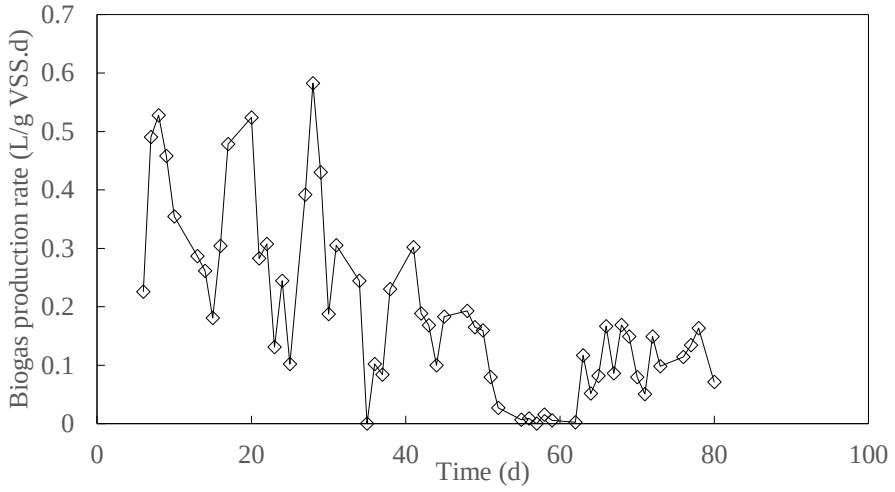

Figure 4.3 Biogas production rate of AnMBR1 biomass with the decrease of acetate loading rate (HRT=6d). Biogas production rate decreased from about 0.5 to 0.1 L/gVSS·d due to the decrease of the acetate concentration.

It can be seen from the figure that the biogas production rate was decreased due to less acetate available for the methanogens. From day 52 to day 62, the biogas production measured was almost zero due to a leakage in the AnMBR's gas tubing system.

4.2 Phenol removal of AnMBR during transition stage

4.2.1 Phenol conversion rate during transition stage

The transition stage is the stage between acetate decrease stage and dynamic experiment stage, where the reactor (or the biomass) was not working properly due to different events. Between day 80 and day 85, the pressure on the permeate side of the membrane was too negative (-250 mbar) even after chemical cleaning. Nevertheless, the PhCR remained similar to the PhLR in this period [45~82 mg Ph-COD/gVSS·d], and phenol removal efficiency was above 90%. A new membrane was set up to cope with the fluxes at day 85. At day 111, the phenol concentration in the influent was raised to 750 mg Ph/L (1785 mg Ph-COD/L) to achieve faster reaching the maximum PhCR through the decrease in the HRT (initial HRT=6d). However, at day 113, a deterioration on the phenol removal efficiency and thus on the PhCR was observed due to the increase of PhLR (phenol concentration increase and biomass taken out for batch experiment). Phenol removal efficiency decreased to 81.81% and the PhCR was lower (in the range of 2%~20%) than the PhLR, with a mean phenol concentration in the permeate of 51.6 mg Ph/L (122.8 mg Ph-COD/L). The maximum PhCR for phenol concentration of 750 mg/L was 134 mg Ph-COD/gVSS·d.

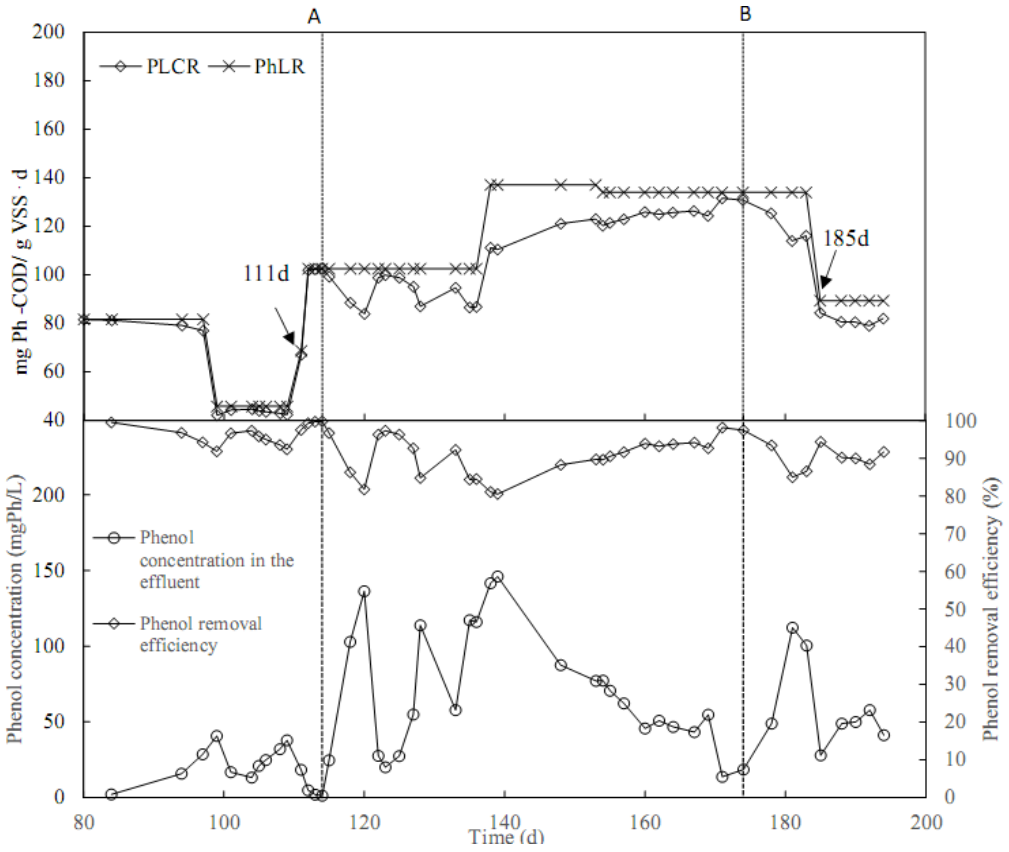

Figure 4.4 Upper: PhLR and PhCR variation of AnMBR1 biomass during the transition stage; Lower: Phenol removal efficiency and phenol concentration in the effluent of AnMBR1. A: Take out sludge for batch experiment; B: AnMBR temperature shock and starvation due to a power outage. At day 111d, phenol concentration was increased to 750 mg Ph/L. At day 185, phenol concentration was decreased to 500 mg

Ph/L.

To avoid further increase in the phenol concentration and an intoxication of the reactor biomass, the phenol concentration in the influent was decreased again to 500 mg Ph/L (1190 mg Ph-COD/L) at day 185. The variation of PhLR, PhCR, and phenol removal efficiency during the transition period is shown in Figure 4.4. Some events which resulted in the deterioration of the reactor performance are also listed in the figure. Based on the phenol concentration in the effluent, which meant that maximum PhCR (about 80 mg Ph-COD/gVSS·d at the end of transition stage) was already surpassed, it was decided to perform a dynamic experiment stage with the change of HRT to confirm the value of the maximum PhCR.

4.2.2 COD removal efficiency during transition stage

The variation of COD removal efficiency is shown in Figure 4.5. The variation of the sOLR was due to the change of phenol concentration in influent as well as the change of biomass concentration in the reactor. COD removal efficiency dropped to 66% during this transition period, indicating that the reactor biomass was not robust enough to deal with the conditions during the negative events such as power outage. The maximum COD concentration in the effluent was 1.5 g/L.

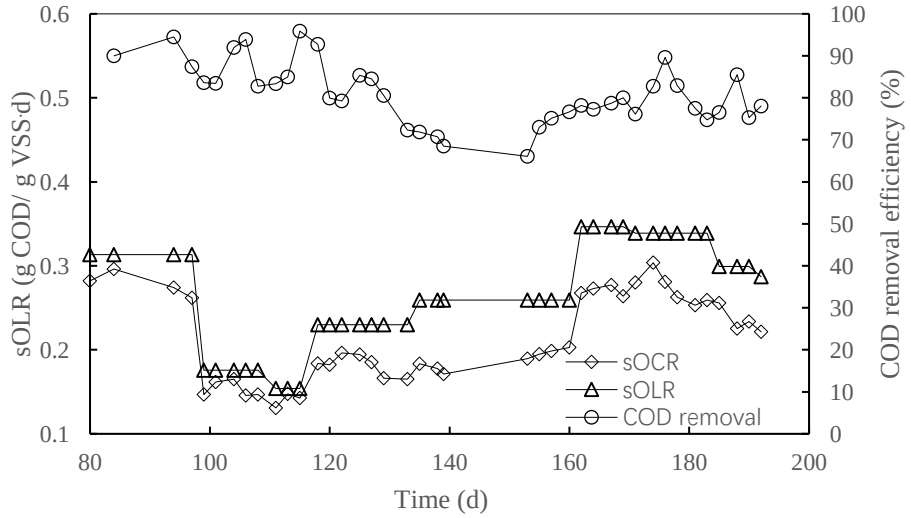

Figure 4.5 COD removal efficiency variation of AnMBR1 during the transition stage. COD removal dropped to 66%, indicating a deterioration during this stage, sOCR was 4%~33% lower than sOLR, with the COD concentration in the effluent of 0.25~1.5g/L.

4.2.3 Benzoate concentration and pH during transition stage

The variation of benzoate concentration and pH in the reactor are shown in Figure 4.6. It can be seen from the figure that pH decreased significantly at day 113 due to the increase of PhLR. This resulted in a shock increase on the PhLR, and lead to the inhibition on the methanogens. The alkalinity was consumed because of lower activity of methanogens than benzoate degraders.

At the same time, as the pH dropped, the activity of benzoate degrader was also reduced, leading to a drastic benzoate accumulation in this transition phase. The concentration of benzoate in the reactor increased from 37 mg/L (73.3 mg COD/L) to 1392 mg/L (2756.2 mg COD/L, 61% of the total COD). After 60 days' recovery, benzoate decreased to 250 mg/L (475 mg COD/L) again. Only a small build-up was observed at day 178 because of the inactivation of benzoate degraders resulted from power malfunction.

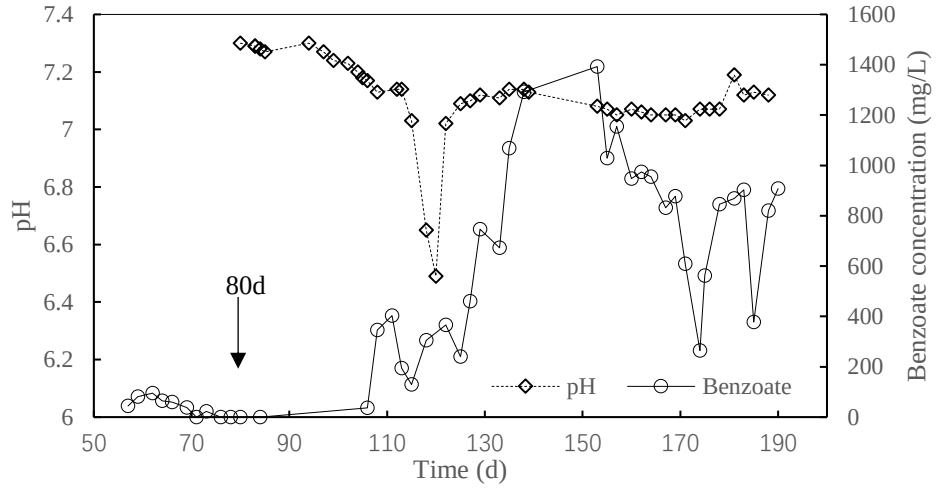

Figure 4.6 Benzoate concentration and pH variation in the AnMBR1 during the transition stage. pH dropped to 6.49 from 7.14 at day 120, followed by the significant increase of benzoate concentration from 37 mg/L to 1392 mg/L. The concentration of benzoate decreased to 250 mg/L after 60 days' recovery.

4.2.4 Biogas production and composition during transition stage

The variation of biogas production and composition at the transition stage is shown in Figure 4.7. Methane accounted for 68% to 83% of the biogas composition in this period. This was higher than the theoretical value (50%) and might due to more carbon dioxide is dissolved than methane. The decrease of methane percentage (e.g. at day 114) might result from the inhibition of methanogens.

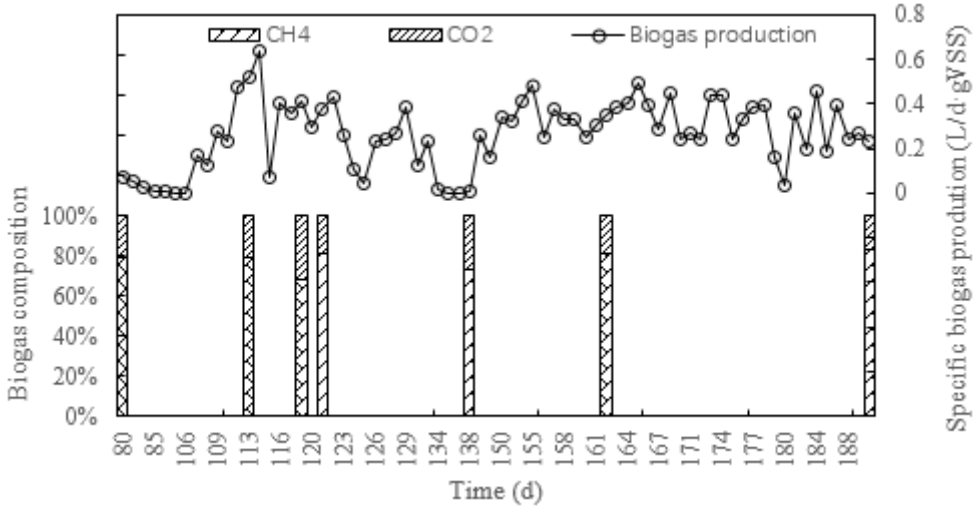

Figure 4.7 Biogas production and composition of AnMBR1 during the transition stage. Methane accounts for 68% to 83% of the biogas during the whole transition stage. The specific methane production was about 0.158 g CH_4-COD/gVSS·d.

There was no biogas production at the beginning which was due to the system leakage. It could be observed that when benzoate concentrations reached a peak in the reactor (e.g. at day 133 and day 178), there was almost no biogas observed, comparing with the figure 4.6 and 4.7. Except that the specific biogas production was relatively steady at about 0.3-0.6 L/d·gVSS. This value was higher than that reported of AnMBR2 by previous study of Bioxtreme group (lower than 0.2 L/d·gVSS) with the same phenol and acetate composition (Fonseca, 2018), indicating the higher activity of the biomass in AnMBR1.

4.3 Membrane properties

4.3.1 Permeability of the membrane

The results of permeability in the first, second, and third 10 minutes are shown in Figure 4.8.

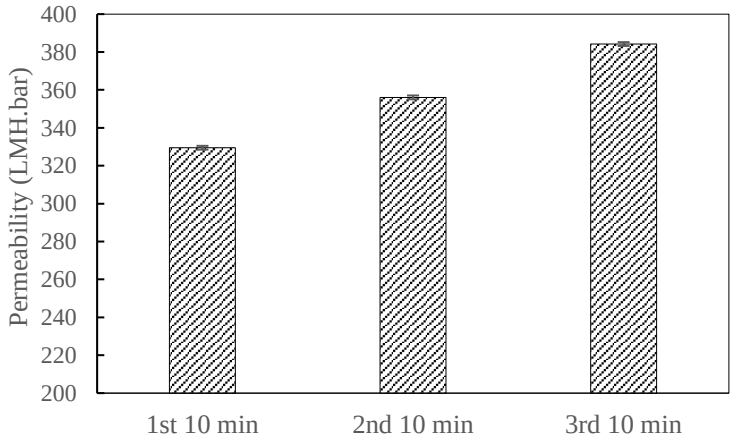

Figure 4.8 Permeability determination. The test was carried out three times subsequently in 30 minutes. The average value of 357 LMH • bar was used for the permeability of the membrane and the error bar stands for the standard deviation for each test.

The average value of 357 LMH • bar was used for the permeability of the membrane in our case. The difference of permeability between periods might be due to the reactor pipelines were not completely clean before the beginning of test, which resulted in the contamination of the membrane with small particles once the experiment was started. As the experiment proceeded, some of the particles could have been removed by the demi water, leading to the increase of permeability in the latter two groups.

4.3.2 Critical flux determination

The 10 min' average TMP value against flux is presented in Figure 4.9. The TMP increase became significant with a flux higher than 56 LMH with the VSS concentration of 4.3 g/L. In our continuous experiment, the maximum flow rate was 2 L/d corresponding to a flux which

was substantially smaller than the critical flux (about 14L/d).

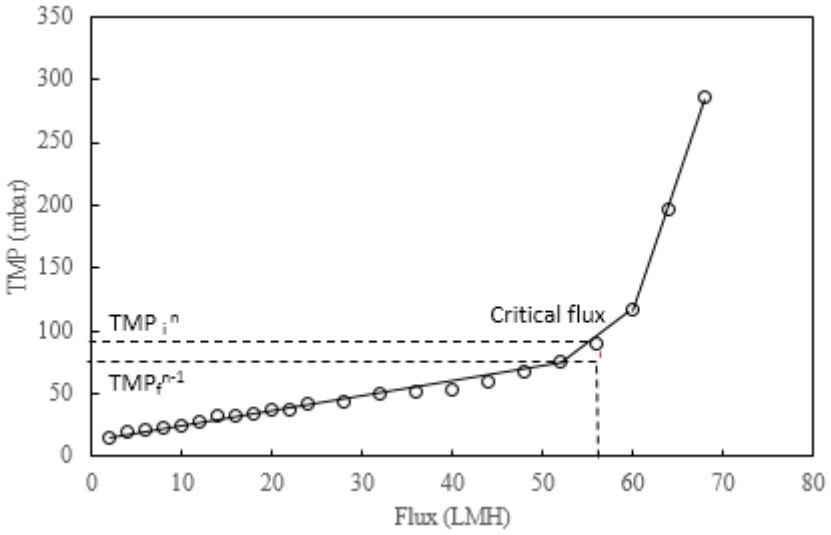

Figure 4.9 Critical flux determination. TMP_f^{n-1}=74.8 mbar, TMP_i^{n}=89.3mbar, $\triangle P_0$ = 14.5 mbar at flux 56 LMH. The flow rate corresponding to the critical flux was about 14L/d.

4.4 Mathematical modeling for phenol degradation

4.4.1 Mathematical model of the batch experiment

A model for Equation 4.1~4.3 was built with Python 3.0 to describe the conversion from acetate to methane in the batch experiment. The codes are shown in the Appendix 4.1.

$$r_{Ac} = -k_{m,Ac} \frac{S_{Ac}}{K_{s,Ac} + S_{Ac} + \frac{S_{Ac}^{2}}{K_{I,Ac}}} \cdot X_{Ac} \cdot I \qquad \text{(Equation 4.1)}$$

$$r_{CH_4} = (1 - Y_{Ac}) \cdot (-r_{Ac}) - r_{gas} \qquad \text{(Equation 4.2)}$$

$$r_{gas} = k_l a \cdot (S_{CH_4} - C_s) \qquad \text{(Equation 4.3)}$$

In Equation 4.1, r_{Ac} is the reaction rate of acetate degradation [mg Ac-COD/L·h]. S_{Ac} is the acetate concentration [mg Ac-COD/L]. $\mu_{m,Ac}$ ($k_{m,Ac} \times Y_{Ac}$), $K_{s,Ac}$ and $K_{I,Ac}$ were the Haldane kinetic parameters for acetate degradation. Among them, $k_{m,Ac}$ is the acetate uptake rate [mg Ac-COD/mgX_{Ac}-COD·h] and Y_{Ac} is the biomass yield of the methanogens [mg X_{Ac}-COD/mg Ac-COD·h]; $K_{s,Ac}$ is the half saturation coefficient [mg Ac-COD/L], $K_{I,Ac}$ is the inhibition coefficient [mg Ac-COD/L]. X_{Ac} is the biomass concentration of methanogens [mg X_{Ac}-COD/L]; Assuming that the acetate degradation could be inhibited by both salinity and phenol we proposed the total inhibition factor $I = I_{Na^+} \times I_{phenol}$, where I_{Na^+} and I_{phenol} are the inhibition factors of sodium and phenol, respectively.

In Equation 4.2, r_{CH4} is the dissolution rate of methane in the liquid phase [mg Ac-COD/L·h]. r_{gas} is the methane production rate in the gas phase [mg Ac-COD/L·h].

In Equation 4.3, Cs is the saturation concentration for methane in the liquid [mg CH_4-COD/L]; k_{la} is the gas-liquid transfer coefficient [1/h]; S_{CH4} is the methane concentration dissolved [mg CH_4-COD/L].

It was assumed that there was no phenol degradation before the complete acetate consumption, so the acetate produced by the phenol degradation was neglected in the batch experiment, while sodium concentration remained constant so the inhibition factor I was constant too. The kinetic parameters of $k_{m,Ac}$, $K_{s,Ac}$, $K_{I,Ac}$, and the inhibition factor I were the ones needed to be calibrated with the batch experimental data. However, as the I and $k_{m,Ac}$ were difficult to calibrate separately, they are reported as a product.

4.4.2 Mathematical modeling for the AnMBR dynamic experiment

The mathematical models for the dynamic experiment are shown in Equation 4.4~4.7. The scripts to implement the mathematical model in Python are shown in Appendix 4.2.

$$r_{Ph} = -k_{m,Ph} \cdot \frac{S_{Ph}}{S_{Ph} + K_{S,Ph} + \frac{S_{Ph}^{\ 2}}{K_{I,\mathrm{Ph}}}} \cdot X_{Ph} \qquad \text{(Equation 4.4)}$$

$$\frac{dS_{Ph}}{dt} = r_{Ph} + \frac{Q}{V} \cdot (S_{\mathrm{Ph},in} - S_{\mathrm{Ph}}) \qquad \text{(Equation 4.5)}$$

$$\frac{dS_{Ac}}{dt} = (1 - Y_{Ph}) \cdot (-r_{Ph}) + r_{Ac} + \frac{Q}{V} \cdot (S_{Ac,in} - S_{Ac}) \qquad \text{(Equation 4.6)}$$

$$\frac{dS_{CH_4}}{dt} = r_{CH_4} - \frac{Q}{V} \cdot S_{CH_4} \qquad \text{(Equation 4.7)}$$

In Equation 4.4, r_{Ph} is the reaction rate of phenol degradation [mg Ph-COD/L·h]. S_{Ph} is the phenol concentration in the reactor [mg Ph-COD/L]. $\mu_{m,\,Ph}$ ($k_{m,Ph} \times Y_{Ph}$), $K_{s,\,Ph}$ and $K_{I,\,Ph}$ are the Haldane kinetic parameters for phenol degradation. Among them, $k_{m,\,Ph}$ is the phenol uptake rate [mg Ph-COD/mgX_{Ph}-COD·h]; $K_{s,\,Ph}$ is the half saturation coefficient [mg Ph-COD/L], $K_{I,Ph}$ is the inhibition coefficient [mg Ph-COD/L]. X_{Ph} is the biomass concentration of phenol degrader [mg X_{Ph}-COD].

In Equation 4.5, Q is the flow rate [L/d]; V is the volume of the reactor [L]. Y_{Ph} is the biomass yield of the phenol degrader [mg X_{Ph}-COD/mg Ph-COD·h]; $S_{Ph,in}$ is the phenol concentration in the influent [mg Ph-COD/L]; In Equation 4.6, $S_{Ac,in}$ is the acetate concentration in the influent [mg Ac-COD/L].

Compared with the batch model, the variation in the acetate and phenol concentration

in the reactor due to the influent and effluent flows is included in this mathematical model; also, the degradation of phenol is considered.

To have a prediction of how the curve (e.g. S_{ph} vs time) should look like, the analysis of these equations was carried out. It is derived from the model that dS_{ph}/dt, that corresponds to the slope, is the highest when S_{Ph} equals to zero ($r_{Ph}=0$), and the concentration of phenol starts to increase. When r_{Ph} equals to $\frac{Q}{V}\cdot(S_{ph,in}-S_{ph})$, dS_{Ph}/dt equals to zero, indicating a constant phenol concentration in the reactor. On the other hand, as the concentration of phenol in the reactor infinitely goes to $S_{ph,in}$ with different HRTs, the effect of changing HRT on dS_{Ph}/dt becomes not significant any more. When S_{Ph} in the reactor equals to $\sqrt{K_{s,Ph}\times K_{I,Ph}}$, the degradation rate of the phenol reaches the maximum ($r_{Ph,max}$). This analysis also applies to acetate degradation.

Furthermore, for acetate, the Monod equation was used in the ADM1 model, while the Haldane equation was used in our case instead of describing the inhibition by acetate and phenol (Vavilin, V. A., & Lokshina, L. Y. 1996). It can be seen from the Haldane equation that, S^2/K_I was close to zero when K_I tends to infinite. That means in the case of large values of K_I, Haldane equation tends to approach the Monod equation.

In comparison to ADM1, in our case dX/dt was neglected. This was due to the fact that the measurement of the active biomass concentration was difficult in practice, especially for dynamic experiments, where two groups of microbials need to be considered. The biomass fraction could be variable due to different yields for phenol degraders and methanogens, and dX_{AC}/dt and dX_{Ph}/dt should be considered separately if the biomass concentration change was included in the model. However, the measurements of concentration change of phenol degraders and methanogens were very difficult.

4.4.3 Methane solubility in the permeate

According to the Equation 3.1, the corresponding β values calculated for AnMBR1 [18.6 g Na^+/L] and AnMBR2 [8.0 g Na^+/L] were 0.0207 LCH_4/(L·atm) and 0.0242 LCH_4/(L·atm), namely 8.20×10^{-4} mol CH_4/ (L·atm) and 9.58 $\times10^{-4}$ mol CH_4/(L·atm), respectively. For dynamic experiment, the pressure in the reactor was the atmospheric pressure plus 5 mbar according to the instruction of Ritter. The batch experiments were performed at atmospheric pressure plus 6 cm of water pressure. Hence, a value of 5 mbar (500 Pa) was used to calculate the average pressure in the reactors. The biogas composition was assumed to be constant and the same as that in the reactor for simplification, where methane accounts for 78% (see Figure 4.7).

$$P_{CH_4}=101325+500\times78\%=101715Pa$$

For the substrate of 8.0 g Na^+/L, the saturation methane COD concentration dissolved in the effluent is:

$$S_{CH_4} = P_{CH_4} \times \beta = 101715 \times 0.000958 = 0.000974 \text{ mol } CH_4/L = 62.34 \text{ mg } CH_4\text{-COD/L}$$

For the substrate of 18.6 g Na^+/L, the saturation methane COD concentration dissolved in the effluent is

$$S_{CH_4} = P_{CH_4} \times \beta = 101715 \times 0.000820 = 0.000834 \text{ mol } CH_4/L = 53.41 \text{ mg } CH_4 - COD/L$$

4.4.4 Determination of biomass yield and fraction based on thermodynamic calculations

The metabolic reactions considered in the mathematical model (phenol to acetate and acetate to methane) were derived by stoichiometry and thermodynamic calculations. The catabolic and anabolic reactions for each conversion process are shown in Table 4.1. The biomass yield was determined by the Gibbs energy dissipation method (Heijnen & Kleerebezem, 2010). The standard Gibbs energy and enthalpy of formation from different compounds are shown in the Appendix 4.3. From these, the standard Gibbs energy and enthalpy of each reaction could be derived.

Table 4.1 Metabolic reactions by stoichiometry calculation

Phenol conversion to acetate		
Catabolism	Oxidation reaction	$C_6H_6O + 5H_2O \rightarrow 3C_2H_3O_2^- + 7H^+ + 4e^-$
	Reduction reaction	$2H^+ + 2e^- \rightarrow H_2$
	Catabolic reaction	$5H_2O + C_6H_6O \rightarrow 3H^+ + 2H_2 + 3C_2H_3O_2^-$
Anabolism	Oxidation reaction	$0.17C_6H_6O + 0.33H_2O + 0.2NH_4^+ \rightarrow CH_{1.8}O_{0.5}N_{0.2} + 0.66H^+ + 0.46e^-$
	Reduction reaction	$2H^+ + 2e^- \rightarrow H_2$
	Anabolic reaction	$0.33H_2O + 0.17C_6H_6O + 0.2NH_4^+ \rightarrow CH_{1.8}O_{0.5}N_{0.2} + 0.2H^+ + 0.23H_2$
Acetate conversion to methane		
Catabolism	Oxidation reaction	$C_2H_3O_2^- + 2H_2O \rightarrow 2CO_2 + 7H^+ + 8e^-$
	Reduction reaction	$C_2H_3O_2^- + 9H^+ + 8e^- \rightarrow 2H_2O + 2CH_4$
	Catabolic reaction	$C_2H_3O_2^- + H^+ \rightarrow CO_2 + CH_4$
Anabolism	Oxidation reaction	$C_2H_3O_2^- + 2H_2O \rightarrow 2CO_2 + 7H^+ + 8e^-$
	Reduction reaction	$0.5C_2H_3O_2^- + 0.2NH_4^+ + 0.5H^+ + 0.2e^- \rightarrow 0.5H_2O + CH_{1.8}O_{0.5}N_{0.2}$
	Anabolic reaction	$0.53C_2H_3O_2^- + 0.2NH_4^+ + 0.33H^+ \rightarrow 0.45H_2O + 0.05CO_2 + CH_{1.8}O_{0.5}N_{0.2}$

The calculations of standard Gibbs energy and enthalpy of catabolic reaction from phenol to acetate, Equations 4.8 and 4.9 are shown as examples.

$$\Delta G_{cat}{}^{0} = 3\times(-369.4)-(-29.7)-5\times(-237.2) = 107.5 kJ/mol \quad \text{(Equation 4.8)}$$

$$\Delta H_{cat}{}^{0} = 3\times(-485.5)-(-93.3)-5\times(-285.8) = 65.8 kJ/mol \quad \text{(Equation 4.9)}$$

The change of Gibbs energy was first corrected by ion activity according to Equation 4.10 and 4.11 (Kleerebezem & Van Loosdrecht, 2010).

$$\Delta G_{cat}{}^{1}(Ts) = \Delta G_{cat}{}^{0}(Ts) + RT\sum_{i=1}^{n} Y_i \times \ln(C_i) \quad \text{(Equation 4.10)}$$

$$\Delta H_{cat}{}^{1}(Ts) = \Delta H_{cat}{}^{0}(Ts) + RT\sum_{i=1}^{n} Y_i \times \ln(C_i) \quad \text{(Equation 4.11)}$$

where *Ci* is the ion concentration in mole, and *Yi* is the stoichiometry coefficient of each ion. Then, the catabolic energy change ($Y_G{}^{cat}$) was corrected to the working temperature (35°C) with Equation 4.12.

$$Y_G{}^{cat} = \Delta G_{cat}{}^{1}(Ts)\times\frac{T}{Ts} + \Delta H_{cat}{}^{1}(Ts)\times\frac{Ts-T}{Ts} \quad \text{(Equation 4.12)}$$

where $\Delta G_{cat}{}^{1}$ and $\Delta H_{cat}{}^{1}$ are the changes of Gibbs energy and enthalpy respectively at 298.15K. T is the working temperature (308.15K); Ts is standard temperature, 298.15 K. Similarly, the change of Gibbs energy in the anabolic reaction *($Y_G{}^{an}$)* was corrected for the temperature and ion activity.

The minimum Gibbs energy requirement for 1C-mol biomass (*$Y_G{}^{max}$)* could be calculated as in Equation 4.13 (Heijnen & Kleerebezem, 2009).

$$-Y_G{}^{max} = 200+18\times(6-NoCs)^{1.8}+\exp(((3.8-\gamma_{cs})^{2})^{0.16}\times(3.6+0.4NoCs)) \quad \text{(Equation 4.13)}$$

where NoC_S is the carbon chain length, and γ_{cs} is the degree of reduction of the carbon source. For phenol and acetate, γ_{cs} equals to 4.67 and 4.00, respectively; The calculation results for $Y_G{}^{an}$, $Y_G{}^{cat}$ and $Y_G{}^{max}$ are shown in Table 4.2.

Table 4.2 Gibbs energy change in the metabolic process

	$Y_G{}^{an}$ *(kJ/mol)*	$Y_G{}^{cat}$ *(kJ/mol)*	$Y_G{}^{max}$ *(kJ/Cmol)*
Phenol conversion to acetate	88.26	-229.03	-429.7
Acetate conversion to methane	45.51	-26.25	-426.3

λ_{cat} is the multiplication factor of the catabolic reaction. In the Gibbs energy dissipation method, it is assumed that all the energy harvest from the catabolic reaction could be used for the biomass synthesis. With Equation 4.14, λ_{cat} could be calculated for each conversion process, which were 2.3 and 18.0 for the conversion from phenol to acetate and from acetate to methane,

respectively. Hence, the metabolic equation for the microorganisms involved in each process could be derived.

$$\lambda_{cat} = \frac{Y_G^{max} - Y_G^{an}}{Y_G^{cat}} \quad \text{(Equation 4.14)}$$

Metabolic equation for phenol degraders:

$$11.64H_2O + 2.43C_6H_6O + 0.2NH_4^+ \rightarrow CH_{1.8}O_{0.5}N_{0.2} + 6.98H^+ + 4.75H_2 + 6.78C_2H_3O_2^- \quad \text{(Equation 4.15)}$$

Metabolic equation for acetate degraders

$$36.47C_2H_3O_2^- + 0.2NH_4^+ + 36.27H^+ \rightarrow 0.45H_2O + 36CO_2 + CH_{1.8}O_{0.5}N_{0.2} + 35.95CH_4 \quad \text{(Equation 4.16)}$$

From Equations 4.15 and 4.16, the theoretical biomass yield for phenol and acetate were:

$Y_{\frac{X}{Ph}}$ = 1/2.43 =0.412 mol X_{Ph}/mol Ph = 0.064 g X_{Ph}-COD/g Ph-COD

$Y_{\frac{X}{AC}}$ = 1/36.47=0.027 mol X_{Ac} /mol Ac = 0.015 g X_{Ac}-COD/g Ac-COD

The biomass yield of methanogens fell in the range [0.01~0.054mgCOD/mgCOD] proposed by Pavlostathis & Giraldo-Gomez (1991). The biomass yield of phenol degraders also fell in the range proposed by the literatures which varied from 0.01~0.44 mgCOD/mgCOD (Hao et al., 2002; Fezzani & Cheikh, 2009). In addition, a rough determination of the methanogenic microorganisms fraction in the AnMBR1 sludge was carried out by fluorescence microscopy to confirm the calculation result (see Appendix 4.4).

The acetate and phenol concentration in the feeding substrate were 2000 mg COD/L and 1190 mg COD/L. The theoretical fraction of phenol degrader and acetate degrader could be calculated as 72% and 28%. However, the active biomass fraction heavily relies on the SRT of the system. The SRT of the biomass was calculated according to Equation 4.17.

$$SRT = \frac{VX}{(Q - Q_W)X_e + Q_W X_R} \quad \text{(Equation 4.17)}$$

where X_e is the biomass concentration in the effluent [mg/L]. Q_W is the flowrate of excess sludge removal [L/d]. X_R is the biomass concentration of the sludge recycled. V is the reactor working volume [L]; X is the biomass concentration in the reactor [mg/L]. In our case, X_e equaled 0 mg/L because the biomass was fully retained by the UF membrane. The biomass concentration in the reactor and sample were the same. The total operation period was about 163 days, while 97.2 mL biomass was taken out for sampling. Hence, the SRT in our experiment was about 10062 days, which was much longer than the industrial practice (Stuckey, 2012) and could lead to the over-estimation on the active biomass concentration with the theoretical yield.

The theoretical increase in the methanogen concentration with 2000 mg Ac-COD/L was 30 mg X_{Ac}-COD/L with the yield calculated (neglecting decay). As a I/S ratio of 1 was used in the batch experiment, the biomass concentration was 2000 mg X_{Ac}-COD /L, among which, the concentration of methanogens in the batch experiment was $2000 \times 0.28 = 560$ mg VSS-COD/L. Assuming the acetate could be degraded in 48h (linear degradation rate and excluding lag phase), and the sampling was carried out every 6 hours. For each sampling point, the estimated error of dS/dt due to neglecting biomass concentration increase was about 0.67%~5.3% (dS/dt =0 at the last point). Actually, as the theoretical calculation overestimated the yield of the biomass, the error resulted from neglecting biomass concentration increase could be even smaller.

As the main goal of the batch experiment was to provide kinetic parameters for acetate degradation, little effect would be observed by neglecting biomass concentration change as long as the same microbial activity ($k_m X_{AC}$) was used in the batch and dynamic experiment. Hence, it was reasonable to neglect the variation of biomass concentration as a simplified model.

4.4.5 Sensitivity analysis of the kinetic parameters for acetate degradation

In general, the parameters to be calibrated in the ADM1 model are not unique, however the experimental data that could be applied to the calibration are indeed limited. Priority should be given to the parameters that are most sensitive to the final results, in our case, acetate degradation rate. A sensitivity analysis of the parameters should be applied to determine which parameters need to be calibrated. As X_{Ac}, $Y_{Ac,}$ and I are constant in Equation 4.1, the sensitivity analysis of the kinetic parameters in Haldane equation was carried out for simplification in the software Maple 2018. The results are shown in Figure 4.10.

From the analysis, it is concluded that μ_m is the most sensitive parameter in the Haldane equation, while 5% variation of Ks and K_I has little effect on the microbial growth rate. This suggested the importance of accurately estimating biomass activity ($k_m X_{AC}$). Regarding to the most sensitive concentration range, it could be concluded that, μ_m was more sensitive in the concentration range higher than 500 mg Ac-COD/L, whereas Ks was more sensitive in the lower concentration range [about 150 mg Ac-COD/L]. The sensitivity of K_I increased in the concentration range of 0~2000 mg Ac-COD/L, which might make it difficult to estimate in our case.

The initial acetate concentration in the batch experiment was 2000 mg Ac-COD/L, which was the same as that in the AnMBR1 reactor. Hence, the acetate concentration was within the sensitive concentration range of Ks and $\mu_{m.}$ Although the estimation of K_I was difficult because of the selected concentration range, the results of the modeling were still considered to be

acceptable. This is because K_I has less effect on biomass growth compared to the other parameters according to Figure 4.10 (a).

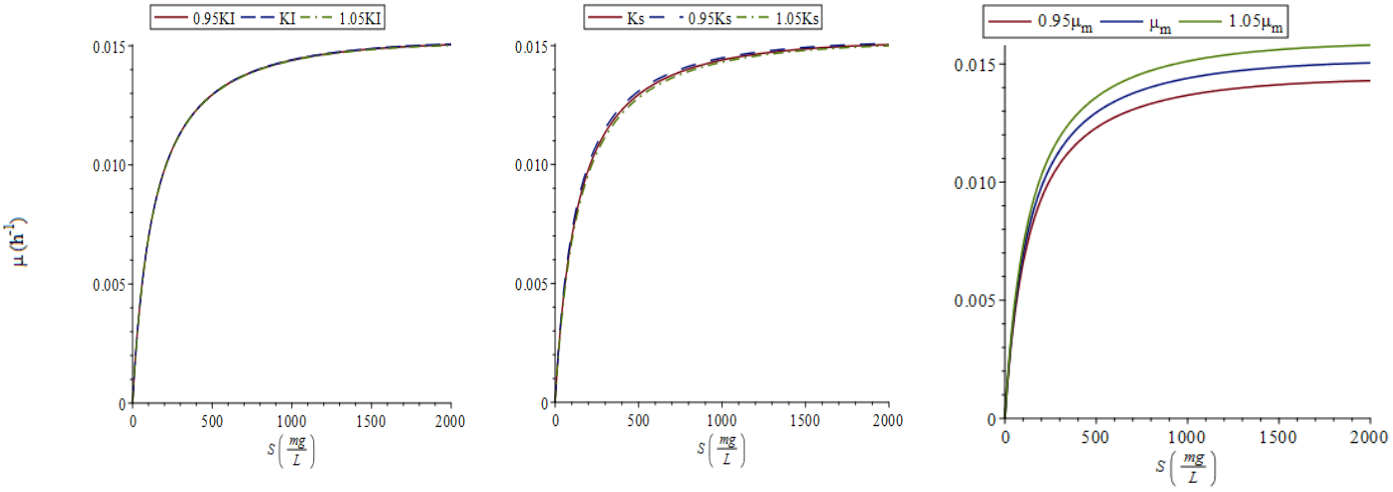

(a)

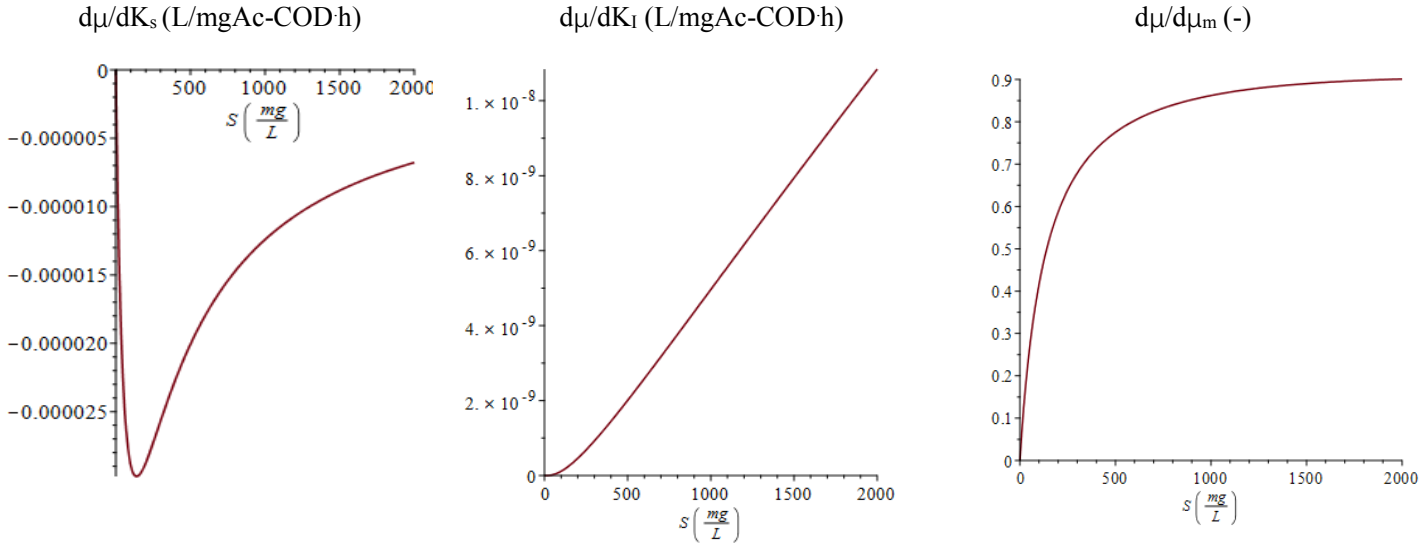

(b)

Figure 4.10 (a) Sensitivity analysis of the kinetic parameters in the Haldane equation (b) Sensitive analysis of the concentration range for each parameter: growth rate for the biomass $\mu = \frac{\mu_{max} S}{K_S + S + (S^2 / K_I)}$; k_m = 0.33 mg Ac-COD /mgX_{Ac}-COD·h, Y=0.05 mg X_{Ac}-COD/mg Ac-COD, Ks=140 mg COD/L, K_I=50000 mg COD/L. $\mu_m = k_m \times Y = 8/24 \times 0.05 = 0.0167 h^{-1}$.

Based on the sensitivity analysis results (Figure 4.11), a complete degradation of acetate was expected within 24 hours. As the acetate degradation rate was almost linear according to the model, the sampling points for the batch experiment were determined to be 2~3 times a day.

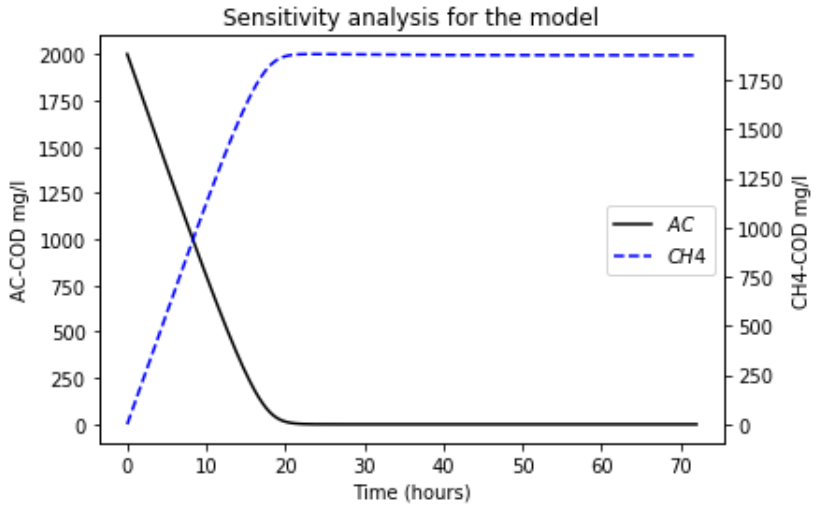

Figure 4.11 Sensitivity analysis of the batch model. A complete acetate degradation was expected within 24 hours with initial acetate concentration of 2000 mg Ac-COD/L, and the sampling points were determined to be 2~3 times a day.k_m = 0.33 mg Ac-COD /mgX_{Ac}-COD·h, Y=0.05 mg X_{Ac}-COD/mg Ac-COD, Ks=140 mg COD/L, K_I=50000 mg COD/L. $\mu_m = k_m \times Y = 8/24 \times 0.05 = 0.0167 h^{-1}$.

4.5 Batch experiment

The objective of the batch experiment was to determine the kinetic parameters for acetate degradation and discuss the factors that could affect them. In the batch experiment, the effect of phenol inhibition and sodium concentration on the acetate degradation as well as on the methane production were studied. At last, the kinetic parameters were given for different sodium concentrations [8.0 g Na^+/L and 18.6 g Na^+/L] and different phenol concentrations [0 mg/L and 300 mg/L] by model fitting. Results for different initial acetate concentration and AnMBR specific biomass loading rate are shown in Appendix 4.5 and 4.6.

4.5.1 Effect of phenol on acetate degradation and methane production

To determine if there was an effect by the addition of phenol on the acetate conversion, the acetate degradation with and without phenol addition was studied. One group was fed with Ac^- at a concentration of 2000 mg COD/L and phenol concentration of 714 mg COD/L (300 mg/L), while the other group was fed only with acetate at a concentration of 2000 mg COD/L. It was assumed that there was no phenol degradation before all the acetate was consumed. The variation of the phenol concentration as function of time is shown in Figure 4.12. It can be seen from the figure that the phenol concentration was almost constant throughout the batch experiment, which supported our previous assumption.

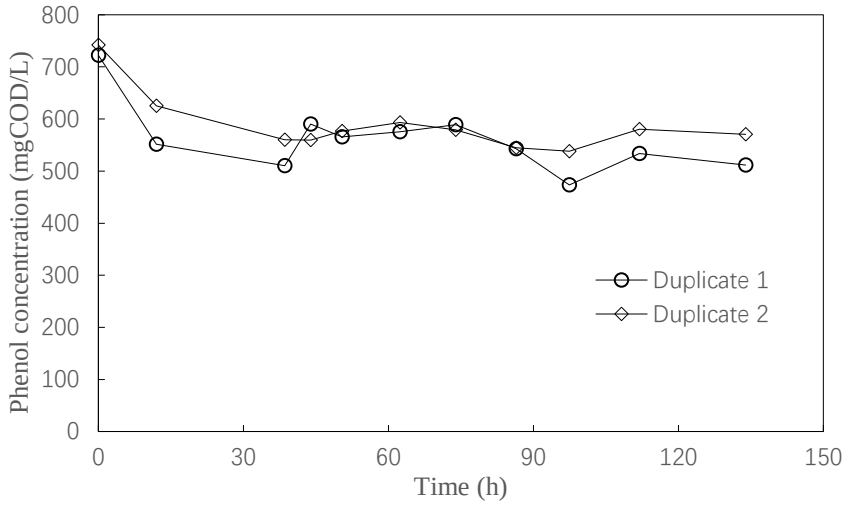

Figure 4.12 Phenol concentration variation with time in the batch experiment. The experiments were carried out duplicated with the biomass of AnMBR1, the specific methane production rate of the biomass in the reactor was 0.158 g CH_4-COD/gVSS·d (assuming the methane accounts for 78% of the biogas). In the batch experiment, the phenol concentration in both groups were almost constant throughout the batch experiment.

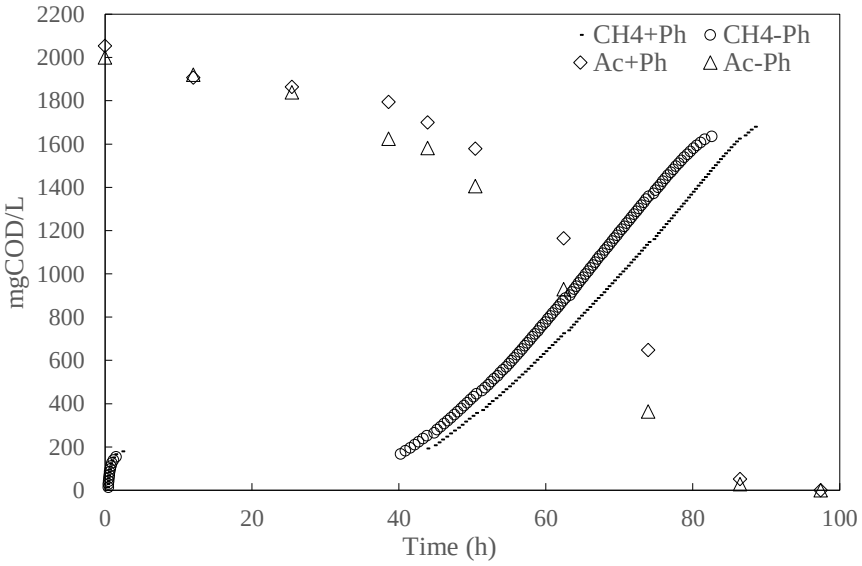

Figure 4.13 Acetate degradation and methane production with and without phenol inhibition. The SMA for the group with and without phenol inhibition were 0.152±0.016 g CH_4-COD/gVSS·d and 0.18 g CH_4-COD/gVSS·d (only one group of result available), respectively, phenol concentration remained close to 300 mg/L during the whole experiment.

The effect of phenol on the acetate degradation and methane production is shown in Figure 4.13. The lag phase of methane production for both groups were about 40h, that might be due to the time needed for the biomass to get active after inoculation. However, as the Haldane equation can only be used to predict the inhibition on the microbial growth rate, this lag phase can not be modeled with the Haldane equation. On the other hand, as there was no lag phase observed in the dynamic experiment because of the low acetate concentration in the reactor

and continuously running, the lag phase was removed from the curve when the model was calibrated in the batch experiment. After the lag phase, complete acetate degradation was observed within two days. The acetate degradation rate and methane production rate for the group without phenol were faster (18.4%) than that with phenol addition. The difference on the COD balance might be due to the energy consumed for cell maintenance. The small build-up of the gas production at the beginning of the curve was due to the expansion of nitrogen when it was heated up to 35ºC.

4.5.2 Effect of different sodium concentration on acetate degradation and methane production

To determine if there was an effect by the sodium concentration on the acetate conversion, we studied the acetate degradation of high sodium concentration [18.6 g Na^+/L] and lower sodium concentration [8.0 g Na^+/L]. The biomass applied to this batch experiment had been acclimated to each sodium concentration in two continuously running AnMBR reactors (AnMBR1 and AnMBR2). The effect of different sodium concentrations on the acetate degradation and methane production are shown in Figure 4.14.

The acetate degradation and methane production of the biomass from AnMBR1 was 168.6% faster than that of AnMBR2 biomass. This result was consistent with what was observed during the operation of reactor (see Chapter 4.2.4) and might be due to the biomass was well acclimated in both groups for a long time, but the biomass of AnMBR1 was working under a higher specific acetate loading rate [1.1 g Ac-COD/gVSS·d] before the acetate concentration decrease in comparison with the AnMBR 2 biomass [0.067 g Ac-COD/gVSS·d]. This might result in a higher biomass fraction of methanogens in AnMBR1. The SMA observed in the batch experiment for the biomass from AnMBR1 was similar to that in the continuous experiment, indicating no acetate inhibition on the biomass activity. However, according to the result of Appendix 4.5, there might be inhibition of acetate on methane production in the batch experiment for the biomass from AnMBR2.

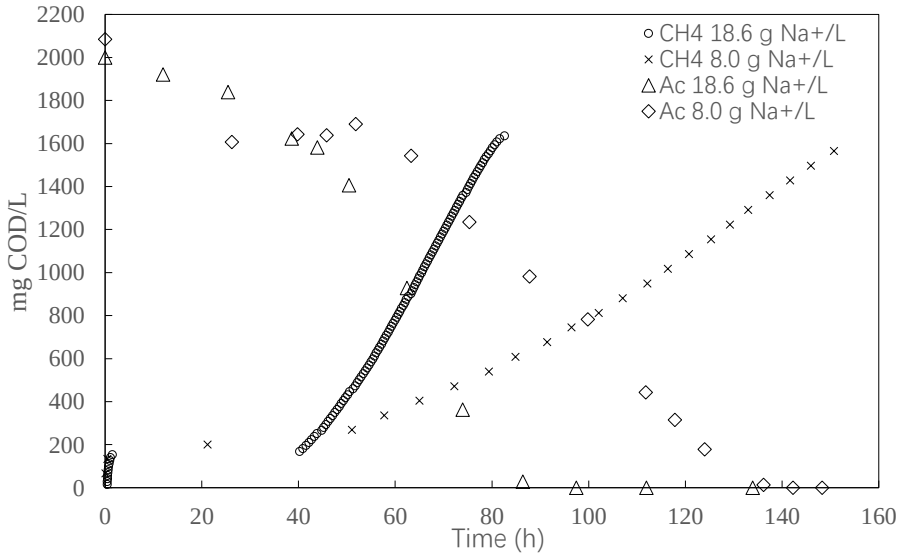

Figure 4.14 Acetate degradation and methane production for the AnMBR biomasses at a concentrations of 8.0 g Na^+/L and 18.6 g Na^+/L. The SMA for the group of 8.0 g Na^+/L and 18.6 g Na^+/L were 0.067±0.003 CH_4-COD/gVSS·d and 0.18 g CH_4-COD/gVSS·d, respectively. About 43 hours (except lag phase) was needed for completely acetate degradation with sodium concentration of 18.6 g Na^+/L while 100 hours was needed with sodium concentration of 8.0 g Na^+/L.

4.5.3 Model fitting to the batch experimental data

It can be seen from Figure 4.13 and Figure 4.14 that the number and time of sampling points were not the same for the methane production and the acetate degradation, which might lead to the difference on parameters estimation. However, as methane production was continuously measured than VFA (acetate degradation) and the experimental data of methane production were measured automatically by AMPTS, it was considered that the kinetic parameters derived were more accurate. Hence, the experimental data of methane production were used for model fitting.

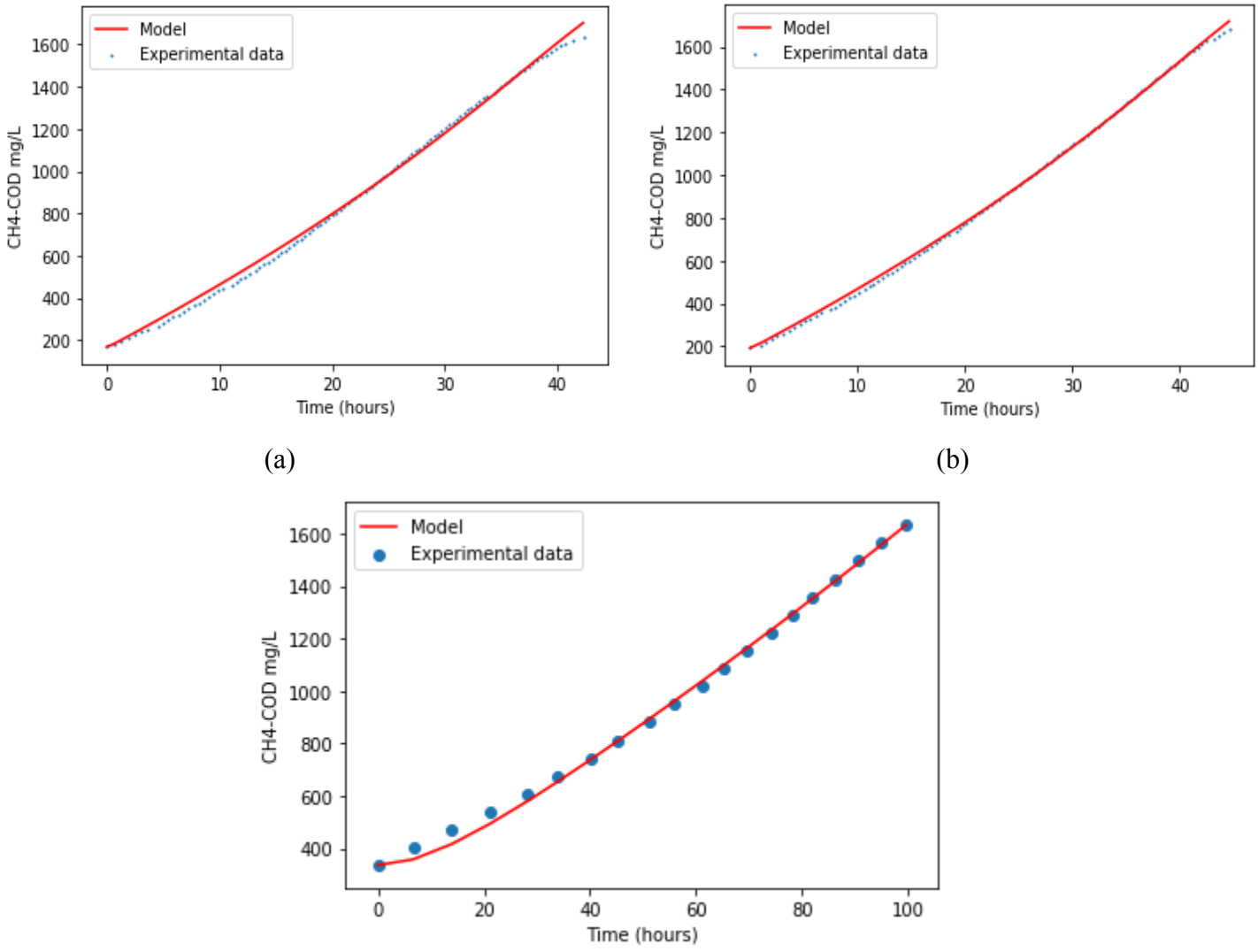

Figure 4.15 Model fitting to the experimental data of methane production (a) with solely acetate, 18.6 g

Na^+/L (b) Acetate and phenol, 18.6 g Na^+/L (c) solely acetate, 8.0 g Na^+/L. The lag phase was removed in each figure and the initial concentration was corrected after the removal. Euler's method was used to solve the differential equations, and the fitting was carried out by curve-fit command in Python with least square method.

The model fittings to the experimental data of the batch experiments in the chapter 4.5.1 and 4.5.2 for methane production are shown in Figure 4.15. The kinetic parameters derived are reported in Table 4.3.

Table 4.3 Kinetic parameters estimated by model fitting and root mean square error (RMSE) in batch tests

	K_s	K_I	$k_m \times I$	RMSE
	mg COD/L	mg COD/L	mg COD/ (mg COD·h)	
Solely acetate 18.6 g Na^+/L	300	821	0.246	21.85
Acetate and phenol 18.6 g Na^+/L	300	806	0.236	11.97
Solely acetate 8.0 g Na^+/L	6.7×10^{-9}	5670	0.043	22.15

Regarding the kinetic parameters estimated with or without phenol addition, there were slight differences on $K_{I,Ac}$ (806 and 821 mg COD/L) and $k_{m,Ac} \times I$ (0.236 and 0.246 mg COD/mgCOD·h). This indicates that the Haldane kinetic parameters for acetate degradation of phenol-acclimated biomass could be even less modified by phenol concentrations lower than 300 mg/L (714 mg COD /L).

Comparing the $k_{m,Ac} \times I$ with the experimental data of methane (with and without phenol addition), it can be seen that the inhibition factor brought by phenol addition was about 0.96 in the batch experiment (neglecting the difference of K_I). However, as the phenol concentration (maximum 48 mg Ph-COD/L) in the reactor for the dynamic experiment was lower than that in the batch experiment, the inhibition factor of phenol on acetate degradation was neglected. Hence, the kinetic parameters $K_{s,Ac}$ = 300 mg COD/L, $K_{I,Ac}$ = 806 mg COD/L, $k_{m,Ac} \times I$ = 0.246 mg COD/mg COD· h (considering the inhibition by salinity) were used for acetate degradation in the mathematical model for dynamic experiment. Also, the $k_{m,AC} \times I$ estimated in our case was 25.4% smaller than that reported in the ADM1 model (Batstone et al., 2002), which might due to the overestimation of biomass concentration or the inhibition of sodium, while the difference of $K_{S,Ac}$ was relatively larger (114.3%). However, the result might be still acceptable according to the sensitivity analysis.

Compared with the kinetic parameters estimated at higher sodium concentration [18.6 g Na^+/L], the set of parameters for the biomass at 8.0 g Na^+/L are different. For example, with lower Ks value for the biomass of 8.0 g Na^+/L, the inhibition on the acetate degradation at lower acetate concentration might be lower, however the maximum biomass activity was also lower. On the other hand, the biomass acetate loading rate in the reactor may also have had an effect on this modification (see Appendix 4.6).

4.5.4 Robustness of the model

To test if the model is robust to small fluctuation of the experimental data, the robustness of the model was analyzed in this section. With the kinetic parameters estimated from the batch experiment (with both phenol and acetate addition) for the biomass of AnMBR1, the robustness of the model was analyzed by adding random noise ($m = 0.02 \times yT_0 \times n$), where yT_0 is the calculated methane production rate with estimated parameters and n is the random value following normal distribution with an average value of 1. The codes for robustness analysis implemented in Python are shown in the Appendix 4.7.

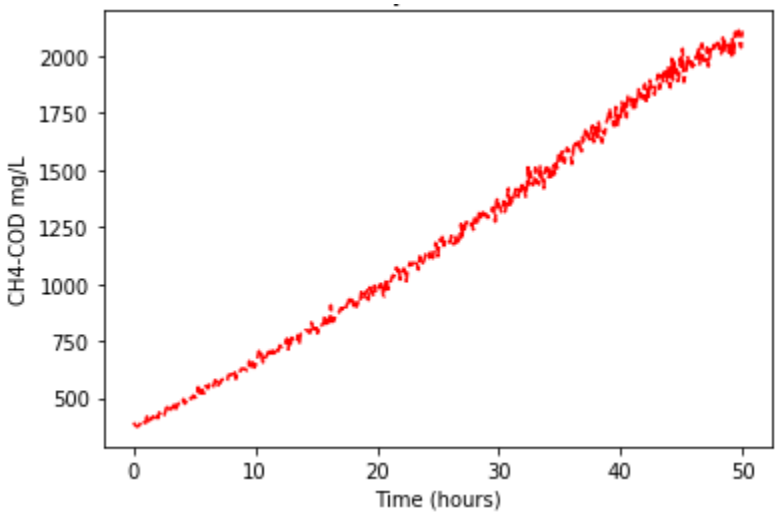

Figure 4.16 Noise analysis for methane production of AnMBR1 biomass with phenol addition. The parameters achieved in the batch experiment were applied by adding random noise ($m = 0.02 \times yT0 \times n$), where y is the calculated methane production rate with estimated parameters and n is the random values followed normal distribution with an average value of 1.

The results of robustness analysis were shown in Table 4.4. It can be seen from the table that the solution of the model could converge to a certain region with the time step of 0.01. The difference between the input parameters and the parameters achieved after adding noise was about 3% for K_I and $k_m \times I$, indicating the robustness of the model was acceptable. Although smaller time step could be used to get a more accurate value on the cost of calculation time.

Table 4.4 Results of the robustness analysis

	K_s mg COD/L	K_I mg COD/L	$k_m \times I$ mg COD/(mgCOD·h)
Input parameter of methane	300	806	0.236
Parameters with noise (methane)	297	791	0.239

4.6 Dynamic experiment in the AnMBR

The objective of the dynamic experiment in the AnMBR was to validate the kinetic parameters

of acetate degradation estimated in the batch experiment and determine the maximum PhCR in the reactor. The dynamic experiment was carried out as the following steps: 1, adjusting the influent and effluent flow according to a fixed HRT (see Table 3.3); 2, continuously feeding of the AnMBR with the influent containing phenol [1190 Ph-COD mg/L] and acetate [2000 mg Ac-COD/L] for about 12h (8 sampling points); and 3, continuously feeding of the AnMBR with influent containing only acetate [2000 mg Ac-COD/L] for approx. 24 h until the concentration of phenol in the reactor was below 20 mg Ph-COD/L, then the reactor was ready to start a new experiment with another HRT.

The first experiment (HRT increase group) started with an HRT = 6 d (influent flow rate of 1 L/d). Then the HRT was stepwise increased (flow rate decreased) from 6 d (1 L/d) to 7.5 d (0.8 L/d), and 10 d (0.6 L/d). For the last part of the experiment (HRT decrease group), the HRT was stepwise decreased (flow rate increased) from 10 d (0.6 L/d), to 5 d (1.2 L/d), 4 d (1.5 L/d), and 3 d (2 L/d).

4.6.1 Phenol concentration in the AnMBR during different PhLRs

The phenol concentrations in the reactor with the different HRTs are shown in Figure 4.17 (a) (HRT increase) and Figure 4.18 (HRT decrease), respectively. Compared with the groups of different HRTs, and so different PhLRs, it could be observed that faster phenol accumulation occurred with shorter HRTs (higher PhLR) in general. However, compared with the results of HRT= 6 d (PhLR of 49.0 mg Ph-COD/gVSS-COD·d) (Figure 4.17) and HRT= 5 d (PhLR of 58.8 mg Ph-COD/gVSS-COD·d) in Figure 4.18, it can be seen that, the phenol concentration increase in the reactor was lower with higher PhLR, indicating an adaptation of biomass in this period.

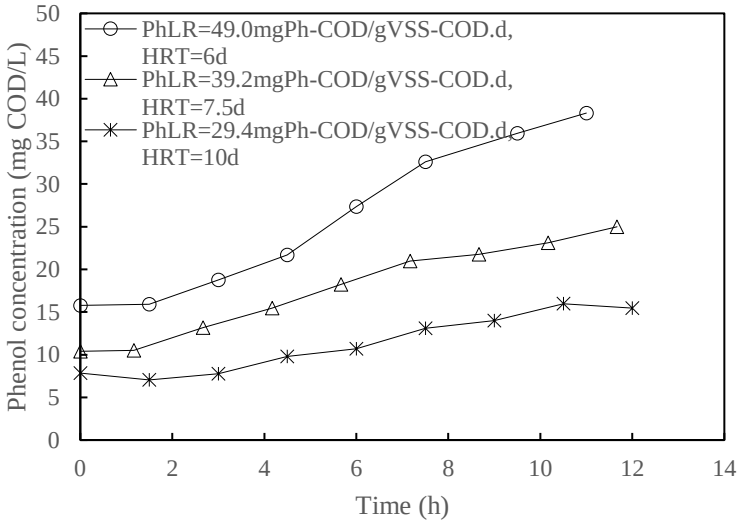

(a)

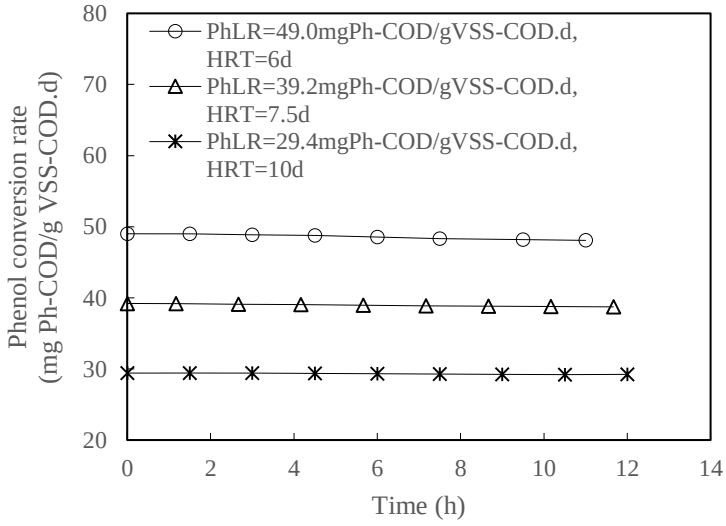

(b)

Figure 4.17 (a) Phenol concentration (b) PhCR with the increase of HRT. The PhCR increased with PhLR indicating the maximum PhCR had not yet reached. This was consistent with the result of 4.2.1, where the maximum PhCR was about 56 mg Ph-COD/gVSS-COD·d (80 mg Ph-COD/gVSS·d) at the end of transition stage. Faster phenol accumulation was observed with higher PhLR.

When the PhLR was increased to 98 mg Ph-COD /gVSS-COD·d at HRT of 3d, the PhCR was similar to that achieved at HRT of 4d (Figure 4.19). This suggested the maximum PhCR was reached at the HRT of 4d. The maximum PhCR at 18.6 g Na^+/L was ≈73 mg Ph-COD/gVSS-COD·d, (43.55 mg Ph/gVSS·d) while it was 193 mg Ph-COD/g VSS-COD·d (115 mg Ph/gVSS·d) at 8.0 g Na^+/L according to the observation of Fonseca (2018). This might indicate that at higher Na^+ concentration the PhCR is lower than at lower Na^+ concentration. However, as the experiments for the maximum PhCR determination at different sodium concentrations were not carried out at the same time, the difference on biomass condition might also contribute to the difference on the maximum PhCR achieved.

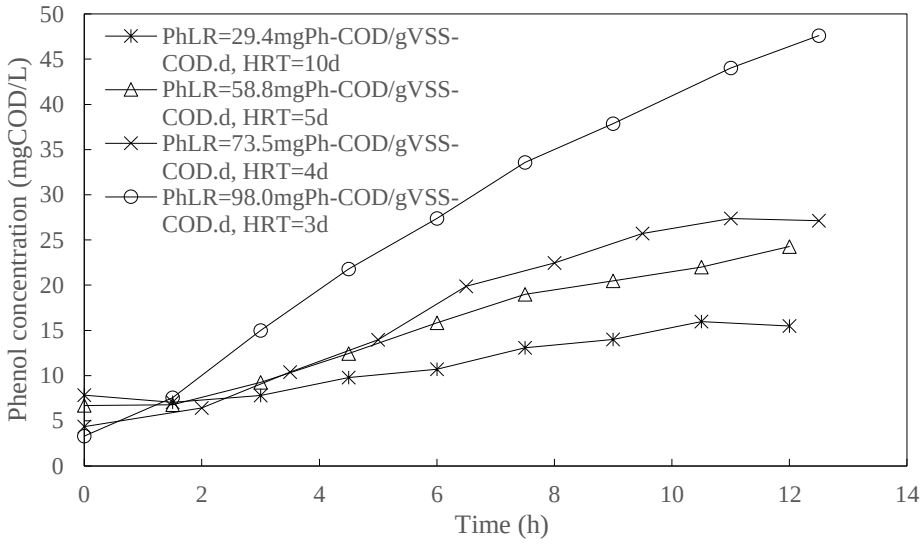

Figure 4.18 Phenol concentration increase in the AnMBR with the decrease of HRT. Faster phenol accumulation occurred with shorter HRTs (higher PhLR). The phenol concentration at HRT of 3d reached 47.6 mg COD/L after 12 hours.

On the other hand, compared to the maximum PhCR achieved at the end of transition stage (56 mg Ph-COD/gVSS-COD·d), the higher maximum PhCR achieved in this dynamic experiment also demonstrated the biomass adaptation in this period. At the same time, it could be observed from the figure that the PhCR slightly decreased with time for each group, which was consistent with the observed increase in the phenol effluent concentration. The PhCR decreased much faster at HRT of 3d than other HRT conditions due to the faster accumulation of phenol in the reactor.

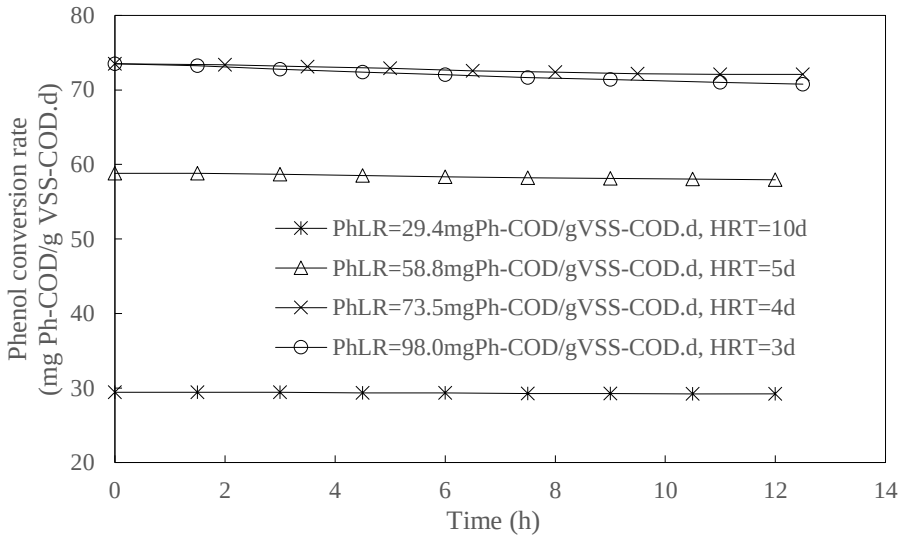

Figure 4.19 PhCR with the decrease of HRT. The maximum PhCR at 18.6 g Na^+/L was about 73 mg Ph-COD/gVSS-COD·d, which was achieved at HRT of 4d. Higher PhCR was achieved at higher PhLR before the maximum PhCR was reached.

4.6.2 Acetate and benzoate accumulation in the reactor at HRT of 3d

To study which degradation process was more inhibited by the increased PhLR, the measurement of acetate and benzoate concentration in the reactor was carried out. There was no significant acetate and benzoate accumulation in the AnMBR with HRTs higher than 3d. However, accumulation became noticeable at HRT of 3d. The variation of acetate and benzoate concentration with time is shown in Figure 4.20.

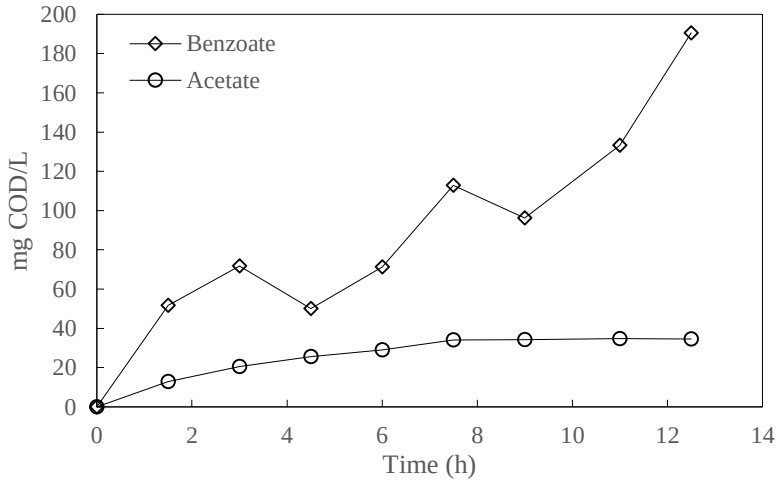

Figure 4.20 Acetate and benzoate concentration accumulation at HRT=3d. After 7.5 hours, acetate concentration in the reactor reached its maximum concentration while benzoate kept increasing, indicating the inhibition of increased PhLR on benzoate degraders.

The concentration of benzoate kept increasing within 12 hours while the acetate concentration stayed constant after 7.5h. This indicated that, the inhibition of benzoate degrader was more serious than that of methanogens with higher PhLR. However, in our case, the

conversion process from phenol to acetate was simplified without considering benzoate as intermediate product in the mathematical model for dynamic experiment. This was due to the concentration of benzoate was lower (190 mg COD/L) compared to the concentration of acetate (2000 mg COD/L) and phenol (1190 mg COD/L) in the influent and the benzoate accumulation was not obvious except the condition of HRT = 3 d.

4.6.3 Biogas production under different PhLRs

As the biogas volume could only be recorded every 19.4 mL by the biogas meter. Accumulated methane production was shown in Figure 4.21 instead of methane production every time interval.

Accumulated methane production was increased with the decrease of HRT as the COD loading also increased. Compared with the other HRT conditions, methane production rate at HRT of 3 d was faster and it became constant after 7.5 hours. This resulted from the acetate concentration reached the maximum value after 7.5 hours ($dS_{Ac}/dt = 0$), which was consistent with the observations in Figure 4.20.

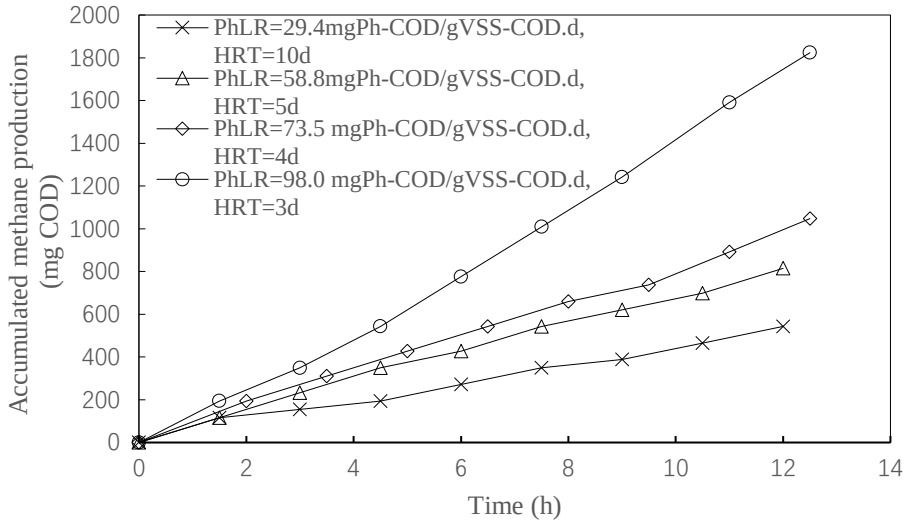

Figure 4.21 Accumulated methane production of different HRTs. Higher methane production was achieved with higher PhLR. Methane production rate became constant after 10 hours in general.

4.6.4 Biogas composition at different PhLRs

The biogas composition at different HRTs and their variation with time are shown in Figure 4.22 and 4.23, respectively.

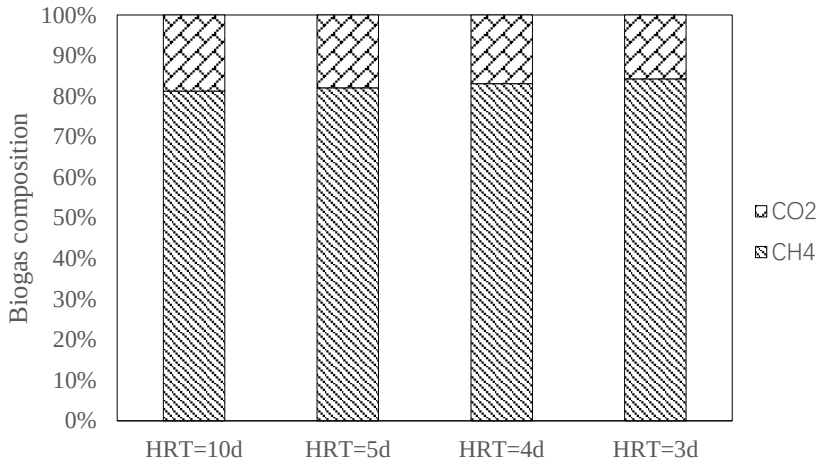

Figure 4.22 Biogas composition under different HRTs. Methane accounted for 81% to 84% with an average value of 82.6% in the biogas composition during dynamic experiment and increased with the decrease of HRT.

An average value of 78 % (the same as that in the batch experiment) in the biogas composition was applied for methane prediction in the model for dynamic experiment. Although, it can be seen from Figure 4.22, that the methane percentage varied between 81% and 84% and increased with the decrease of the HRT. The difference by underestimating methane production was about 84 mg COD (1.12 mg COD/L· h) at most (at HRT of 3d) which was negligible. On the other hand, the percentage of methane in the biogas increased slightly (about 1.3%) with time due to the increase of methane production.

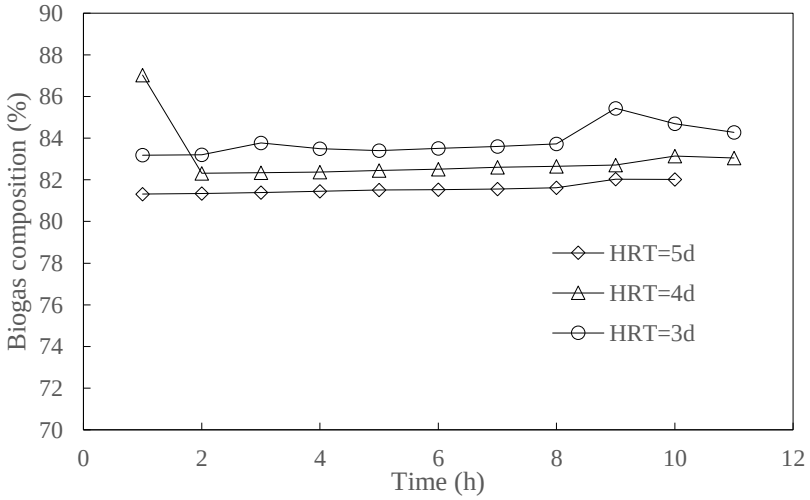

Figure 4.23 Methane concentration variation with time. The percentage of methane in the biogas increased slightly (about 1.3%) with time due to the increase of methane production.

4.6.7 Dynamic experiment model fitting

As the reactor was continuously running before the start of dynamic experiment, the initial value for the methane concentration dissolved was assumed to be its saturation concentration. The results for the model fitting of dynamic experiment are shown in Figure 4.24. In the model,

$k_{m,ph}$ already considers the inhibition of salinity. The kinetic parameters estimated for phenol degradation by model fitting were $K_{s,Ph}$ = 20 mgCOD/L, $K_{I,Ph}$ = 300 mgCOD/L, and $k_{m,Ph}$ = 0.008 mgCOD/mgCOD· h with the experimental data of HRT increase group, these values fell in the range proposed by the literatures (Figure 2.5). Then the validity of the parameters was tested with the experimental data of HRT decrease group.

The phenol concentration in the reactor with the highest phenol degradation rate was $\sqrt{K_{s,ph} \times K_{I,ph}}$ = 0.4 mg COD/L; This indicated that the maximum PhCR was achieved immediately at the beginning of the experiment once the phenol concentration started to accumulate and was consistent with the result of Figure 4.19 where the decrease of PhCR with time was observed throughout the experiment.

It can be seen from Figure 4.24 (a) that, the kinetic parameters estimated from the model fitting could well describe the phenol degradation of groups with HRT higher than 6 d. However, the difference between the experimental data and model prediction was relatively larger (4% of the total Ph-COD in the influent) for the other HRT groups with the same kinetic parameter set. This might be due to the variation of kinetic parameters between different PhLRs (see Table 3.3) or the variation of biomass concentration.

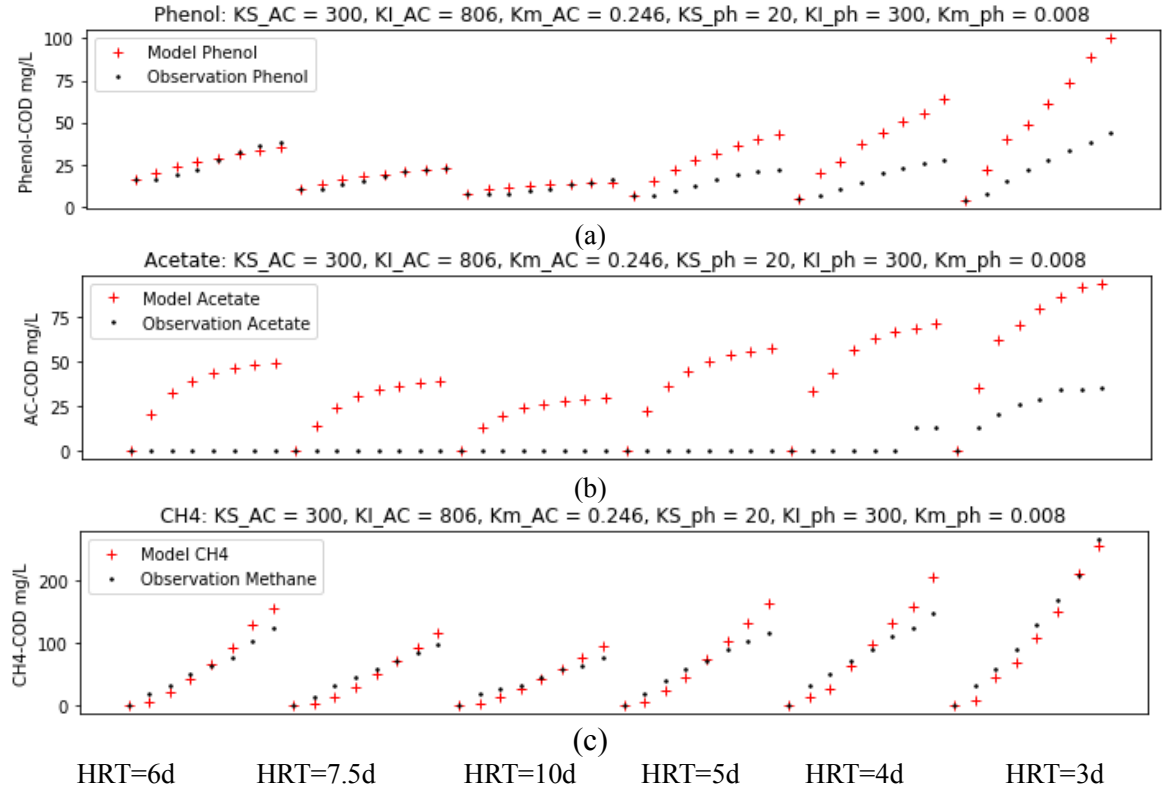

Figure 4.24 Results of the model fitting for (a) Phenol concentration in the reactor (b) acetate concentration in the reactor (c) methane production per liquid volume in the dynamic experiment. The horizontal axis represents time (in hour) and varies from 0 to 12 for each HRT condition. The kinetic parameters for acetate degradation were proposed from batch experiments. The estimated error accounts for 2.5%~4% of the total COD for each group, indicating an acceptable predicting result with this simplified ADM1 model.

On the other hand, it can be seen from Figure 4.24 (b) that the kinetic parameters estimated in the batch experiment cannot fit the experimental data of the continuous experiment, that is why the acetate concentration error between the model and measurement was about 50 mg Ac-COD/L. However, the prediction could be considered acceptable as it only accounted for 2.5% of the AC-COD in the influent. Furthermore, as dS_{Ac}/dt was not zero at the beginning of the experiment when $S_{AC}=0$, it was not possible for the acetate concentration in the reactor to be 0 mg/L according to the model. As 3 times dilution was used for the acetate (VFA) measurements, the acetate concentration value was under the GC detection limit which could have led to this error.

It also can be seen from Figure 4.24 (c) that the kinetic parameters of acetate degradation estimated from the batch experiment could predict the methane production at different HRTs compared to the parameters of phenol degradation which were modified by different HRTs when a constant biomass concentration was assumed. The modification of the kinetic parameters by different specific loadings in the AnMBR could be seen as an adaptation of biomass to the phenol in the medium (Arutchelvan et al., 2006; Hao, 2002). However, as the biomass yield of phenol degrader is 4.3 times larger than acetate degrader, this difference might also be due to the more obvious biomass concentration change of phenol degrader in the reactor.

To be concluded, as the estimated error only accounts for 2.5%~4% of the total COD, the prediction of the phenol concentration, acetate concentration, and methane production with this simplified ADM1 model is considered to be acceptable. Nevertheless, further experiments on the modeling of biomass concentration change and identification of the kinetic parameters still need to be carried out.

4.7 Summary of the results

This research determined the effect of increasing PhLR on PhCR by decreasing the HRT, of a mesophilic (35 °C) AnMBR (AnMBR1) at high sodium concentration [18.6 g Na^+/L].

The reactor was operated for 196 days before the HRT decrease. In the first 80 days, acetate loading of the AnMBR1 was step-wise decreased to the same loading as the one for AnMBR2 which was at lower sodium concentration [8.0 g Na^+/L]. In this process, the phenol removal efficiency remained above 98% with the phenol concentration in the effluent lower than 10 mg/L. The COD removal efficiency was above 93% and the PhCR [68~81 mg Ph-COD/gVSS·d] remained the same with PhLR indicating that all the phenol was converted by the biomass.

After 113 days, the phenol removal efficiency dropped to 81.81% due to the phenol concentration increase and sludge taken out for batch experiment which in turn increased the PhLR, the average phenol concentration in the effluent increased to 51.6 mg/L. The PhCR was 2 to 20% lower than PhLR indicating the maximum PhCR had been surpassed in this stage. The maximum PhCR during this stage were about 94 and 56 mg Ph-COD/gVSS-COD·d for

phenol concentration of 750 mg/L and 500 mg/L, respectively. On the other hand, the COD removal efficiency dropped to 66% in this stage and a significant benzoate accumulation (1392 mg /L) was observed in the effluent.

In addition, a simplified ADM1 model was used to model the conversion from acetate to methane in the batch experiment, where the degradation of phenol was neglected. The inhibition of acetate and phenol (only for dynamic experiment) on microbial growth rate was described by Haldane equation and the biomass yield and fraction were achieved by thermodynamic calculation. The calculated biomass yields for acetate and phenol were 0.015 gX_{Ac}-COD/gAC-COD, and 0.064 gX_{Ph}-COD/gPh-COD, the fraction of these microbial population in the VSS were estimated as 14% and 36% (considering the active component), respectively.

At the same time, the effect of phenol and sodium concentration on acetate degradation was studied by a series of batch experiments. The SMAs were 0.152 ± 0.016 and 0.18 CH_4-COD/gVSS·d for the groups with 300 mg/L phenol and without phenol addition at high sodium concentration [18.6 g Na^+/L], while it was 0.067 ± 0.003 CH_4-COD/g VSS·d at lower sodium concentration [8.0 g Na^+/L] without phenol addition.

Regarding to the effect of phenol addition and sodium concentration on the kinetic parameters, the effect of phenol addition was negligible ($K_{s,AC}$=300 mg COD/L, $K_{I,AC}$=806 mg COD/L, $k_{m,AC} \times I$=0.236 mg COD/mgCOD·h with phenol addition and $K_{s,AC}$=300 mg COD/L, $K_{I,AC}$=821 mg COD/L, $k_{m,AC} \times I$=0.246 mg COD/mgCOD·h without phenol addition), while the parameters were significantly modified by lower sodium concentration ($K_{s,AC}=6.7 \times 10^{-9}$ mg COD/L; $K_{I,AC}$=5670 mg COD/L; $k_{m,AC} \times I$=0.043 mg COD/mgCOD·h). Considering that the phenol concentration is lower than 48 mg Ph-COD/L in the reactor, $K_{s,AC}$=300 mg COD/L, $K_{I,AC}$=806 mg COD/L, $k_{m,AC} \times I$ =0.246 mg COD/mgCOD·h were used in the mathematical model for dynamic experiment.

In the dynamic experiment carried out in the AnMBR1, the maximum PhCR achieved at high sodium concentration [18.6 g Na^+/L] by HRT decrease was about 73 mg Ph-COD/gVSS-COD·d, with acetate as co-substrate [2 g AC-COD/L]. This result was lower than that reported by previous study of Bioxtreme (193 mg Ph-COD/gVSS-COD·d) at lower sodium concentration [8.0 g Na^+/L]. At the same time, the larger maximum PhCR in the dynamic experiment than that at the end of the transition stage indicated the adaptation of the biomass.

The kinetic parameters for phenol degradation derived by model fitting were $K_{s,Ph}$= 20 mg COD/L; $K_{I,Ph}$=300 mg COD/L; $k_{m,Ph}$=0.008 mg COD/mgCOD·h. The kinetic parameters for acetate degradation were validated at different HRTs. It was demonstrated that the simplified ADM1 model could well describe the phenol degradation process and predict methane production at different HRTs.

4.8 Limitations and recommendations for the model

For the modeling part some flaws both in the model, as well as in the parameter determination were found which affected the results that were obtained. For example, in the batch experiment, because of the duration of the test, the biomass concentration (VSS) was assumed to be constant, and the biomass fraction and yield for methanogens were derived from thermodynamic calculation. This might be not according to the reality, due to the biomass fractions change in the reactor (e.g. biomass concentration change resulting from acetate concentration variation or power outage), which bring uncertainty to the estimation of k_m. In addition, as cited in the literature (Henze & Harremoës, 1983), the active biomass concentration was assumed to be 50% of the VSS in the model, while this value could be lower than 10% due to high SRT according to Kleerebezem & van Loosdrecht (2006).

Furthermore, regarding to the gas-liquid transfer process, as it was difficult to determine the kla value in the anaerobic batch experiment, the kla value of the model was taken from literature. However, as the kla value varies between different experiment, this could also result in an increase on the uncertainty of the kinetic parameters estimated. At the same time, the gas liquid transfer process was simplified in the model. The variation of methane partial pressure due to the production of biogas was not considered, and the pressure change in the headspace due to sampling was not considered, either.

Some kinetic parameters such as K_I were not sensitive to the experimental data, which brought more uncertainty to the model. There were no confidence intervals of the kinetic parameter values given by the model, and the correlation coefficient between each two kinetic parameters were not further studied in our research. Some identification analysis (e.g. Bayesian method and Monte Carlo method) of the kinetic parameters could be carried out in the further research.

Because of the uncertainty in the estimation of the kinetic parameters, we believe that a more strict analysis for the parameters estimation should be done. The results in the model fitting for the dynamic experiment showed that the parameters estimated in the batch experiment could not be used for the continuous operation, for example ks value might be lower than the value that we determined; however, ks in the batch experiments was difficult to measure because of the reported ranges that were under the limit of detection of our research equipment.

In the model, we used explicit Euler's method (conditional convergent at small time step) to solve the differential equations. Considering the cost of computing time, the model only converged to a certain region instead of a certain value. Furthermore, the boundaries of the kinetic parameters in the model were taken from the literatures, however the literatures for acetate degradation with Haldane equation were very few, so the information provided might be not accurate enough.

To summarized, as the first experience in mathematical modeling, the model was an effective tool for better understanding the acetate and phenol degradation process. However, there is still a lot of work need to be done for the uncertainty of the kinetic parameter estimation, as well as in the improvement of the model structure.

5 Conclusion and recommendation

5.1 Conclusions

- Considering a Haldane kinetic, what are the values of the kinetic parameters that could predict the acetate degradation by the AnMBR biomass at a high Na^+ concentration (18.6 g Na^+/L)?

The kinetic parameters for acetate degradation were $K_{s,Ac}$=300 mg COD/L, $K_{I,Ac}$=821 mg COD/L, $k_{m,Ac} \times I$=0.246 mg COD/mgCOD·h at 18.6 g Na^+/L.

- Is there any inhibition effect on acetate degradation caused by phenol addition?

Negligible effect was caused by phenol (300 mg/L) on the Haldane kinetic parameters for acetate degradation. The kinetic parameters for acetate degradation in the presence of phenol were $K_{s,Ac}$=300 mg COD/L, $K_{I,Ac}$=806 mg COD/L, $k_{m,Ac} \times I$=0.236 mg COD/mgCOD·h at 18.6 g Na^+/L.

- How are those kinetic parameters compared to that of an AnMBR biomass under a lower Na^+ concentration (8.0 g Na^+/L)?

High sodium concentration could modify the kinetic parameters of acetate degradation. However, the specific biomass loading of AnMBR1 was higher than that of AnMBR2 (at acetate decrease stage) which might also have an effect on this modification. The kinetic parameters for acetate degradation were $K_{s,Ac}=6.7 \times 10^{-9}$ mg COD/L; $K_{I,Ac}$= 5670 mgCOD/L; $k_{m,Ac} \times I$=0.043 mg COD/mgCOD·h at lower sodium concentration.

- What is the maximum PhCR of a mesophilic AnMBR at high Na^+ concentration (18.6 g Na^+/L) condition?

The maximum PhCR at high sodium concentration was 73 mg Ph-COD/gVSS-COD·d, while higher maximum PhCR (193 mg Ph-COD/gVSS-COD·d) was obtained at lower sodium concentration (8.0 g Na^+/L) according to the previous study in the Bioxtreme group.

5.2 Recommendations

- The biomass fraction was determined by thermodynamic calculation. However, this theoretical value might be not accurate enough, and brought uncertainty to the parameter's estimation, especially k_m. Modern advanced technology (e.g. flow cytometry) could be applied to for more precise estimation of biomass fraction.
- In our experiment, the change of the biomass concentration was not considered due to a short experiment period. However, this should be included for a long-term prediction if the model was applied to industrial practice. The yield and decay value of the biomass could be achieved by the experimental data of long-term operation.

- The mechanism of the lag phase was not further studied in the experiment. Different models such as Gompertz model could be used to model this lag phase.
- The effect of sodium concentration on the kinetic model was not clearly studied in the batch experiment, due to the fact that the specific biomass loading of AnMBR1 used to be higher than that of AnMBR2. The biomass should always stay in the same condition.
- The batch experiment was carried out only in duplicates due to limited AnMBR sludge. This resulted in the experiment results less reliable (e.g. SMA of AnMBR1 biomass with phenol addition in Chapter 4.5.1). More parallel experiments are needed if possible.
- The role of acetate as co-substrate was not further investigated in this thesis; although, the effect and mechanisms of acetate as a co-substrate on phenol degradation was out of the scope of this thesis. Nevertheless, the effect is being analyzed in other experiment of our research group.
- For the dynamic experiment, the kinetic parameters of acetate degradation were estimated from the batch experiments. Comparison could be carried out with the kinetic parameters estimated directly from the experimental data of dynamic experiment.

Reference

Aiba S, Shoda M, Nagatani M (1968) Kinetics of product inhibition in alcohol fermentation. Biotechnol Bioeng 10(6):845–864.

Alhraishawi, A. A., & Alani, W. K. (2018). The co-fermentation of organic substrates: A review performance of biogas production under different salt content. In *Journal of Physics: Conference Series* (Vol. 1032, No. 1, p. 012041). IOP Publishing.

Allen, K.D. and White, R.H. (2018) Identification of the Radical SAM Enzymes Involved in the Biosynthesis of Methanopterin and Coenzyme F420 in Methanogens. *Methods Enzymol,* 606, 461-483.

APHA (1999). Standard Methods for the Examination of Water and Wastewater, 20th ed. American Public Health Association/American Water Works Association/ Water Environment Federation, Washington, DC.

Arutchelvan, V., Kanakasabai, V., Elangovan, R., Nagarajan, S., & Muralikrishnan, V. (2006). Kinetics of high strength phenol degradation using Bacillus brevis. *Journal of Hazardous Materials*, *129*(1-3), 216-222.

Bakker, G. (1977). Anaerobic degradation of aromatic compounds in the presence of nitrate. *FEMS Microbiology Letters*, *1*(2), 103-107.

Banerjee, A., & Ghoshal, A. K. (2010). Phenol degradation by Bacillus cereus: pathway and kinetic modeling. *Bioresource Technology*, *101*(14), 5501-5507.

Basak, B., Bhunia, B., Dutta, S., Chakraborty, S., & Dey, A. (2014). Kinetics of phenol biodegradation at high concentration by a metabolically versatile isolated yeast Candida tropicalis PHB5. *Environmental Science and Pollution Research*, *21*(2), 1444-1454.

Batstone, D. J., Keller, J., Angelidaki, I., Kalyuzhnyi, S. V., Pavlostathis, S. G., Rozzi, A., Sanders, W.T.M., Siegrist, H. & Vavilin, V. A. (2002). The IWA anaerobic digestion model no 1 (ADM1). *Water Science and Technology*, *45*(10), 65-73.

Batstone, D. J., Keller, J., & Steyer, J. P. (2006). A review of ADM1 extensions, applications, and analysis: 2002–2005. *Water science and technology*, *54*(4), 1-10.

Blagodatskaya, E. and Kuzyakov, Y. (2013). Active microorganisms in soil: Critical review of estimation criteria and approaches. *Soil Biology & Biochemistry*, 67, 192-211.

Busca, G., Berardinelli, S., Resini, C., & Arrighi, L. (2008). Technologies for the removal of phenol from fluid streams: a short review of recent developments. *Journal of Hazardous Materials*, *160*(2-3), 265-288.

Castillo-Carvajal, L. C., Sanz-Martín, J. L., & Barragán-Huerta, B. E. (2014). Biodegradation of organic pollutants in saline wastewater by halophilic microorganisms: a review. *Environmental Science and Pollution Research*, *21*(16), 9578-9588.

Chang, S. (2014). Anaerobic membrane bioreactors (AnMBR) for wastewater treatment. *Advances in Chemical Engineering and Science*, *4*(1), 56-61.

Chen, L., Hu, Q., Zhang, X., Chen, Z., Wang, Y., & Liu, S. (2019). Effects of salinity on the biological

performance of anaerobic membrane bioreactor. *Journal of environmental management*, *238*, 263-273.

Chen, Y., He, J., Wang, Y. Q., Kotsopoulos, T. A., Kaparaju, P., & Zeng, R. J. (2016). Development of an anaerobic co-metabolic model for degradation of phenol, m-cresol and easily degradable substrate. *Biochemical engineering journal*, *106*, 19-25.

Chernicharo, C. A. L., Van Lier, J. B., Noyola, A., & Ribeiro, T. B. (2015). Anaerobic sewage treatment: state of the art, constraints and challenges. *Reviews in Environmental Science and Bio/Technology*, *14*(4), 649-679.

Contois, D. (1959). Kinetics of bacterial growth: Relationship between population density and specific growth rate of continuous cultures, J. Gen. Microbiol., 21(1), 40–50.

Dahiya, S., Sarkar, O., Swamy, Y. V., & Mohan, S. V. (2015). Acidogenic fermentation of food waste for volatile fatty acid production with co-generation of biohydrogen. *Bioresource technology*, *182*, 103-113.

Dereli, R. K., Ersahin, M. E., Ozgun, H., Ozturk, I., Jeison, D., van der Zee, F., & van Lier, J. B. (2012). Potentials of anaerobic membrane bioreactors to overcome treatment limitations induced by industrial wastewaters. *Bioresource Technology*, *122*, 160-170.

Derbal, K., Bencheikh-Lehocine, M., Cecchi, F., Meniai, A. H., & Pavan, P. (2009). Application of the IWA ADM1 model to simulate anaerobic co-digestion of organic waste with waste activated sludge in mesophilic condition. *Bioresource Technology*, *100*(4), 1539-1543.

Dereli, R. K., Ersahin, M. E., Ozgun, H., Ozturk, I., & Aydin, A. F. (2010). Applicability of Anaerobic Digestion Model No. 1 (ADM1) for a specific industrial wastewater: Opium alkaloid effluents. *Chemical Engineering Journal*, *165*(1), 89-94.

De Vrieze, J., Coma, M., Debeuckelaere, M., Van der Meeren, P., & Rabaey, K. (2016). High salinity in molasses wastewaters shifts anaerobic digestion to carboxylate production. *Water research*, *98*, 293-301.

Dinçer, A. R., & Kargi, F. (2001). Salt inhibition kinetics in nitrification of synthetic saline wastewater. *Enzyme and microbial technology*, *28*(7-8), 661-665.

Dvořák, L., Gómez, M., Dolina, J., & Černín, A. (2016). Anaerobic membrane bioreactors—a mini review with emphasis on industrial wastewater treatment: applications, limitations and perspectives. *Desalination and Water Treatment*, *57*(41), 19062-19076.

Edwards, V.H. (1970). The influence of high substrate concentrations on microbial kinetics. Biotechnol. Bioeng. 12, 679–712.

Fang, H.H.P., Chen, T., Li, Y.-Y., Chui, H.-K. (1996). Degradation of phenol in wastewater in an upflow anaerobic sludge blanket reactor. *Water Res.* 30, 1353–1360.

Fang, H. H. P., Liu, Y., Ke, S. Z., & Zhang, T. (2004). Anaerobic degradation of phenol in wastewater at ambient temperature. *Water Science and Technology*, 49(1), 95-102.

Fang, H.H.P., Liang, D.W., Zhang, T., Liu, Y. (2006). Anaerobic treatment of phenol in wastewater under thermophilic condition. *Water Res*. 40, 427–434.

Fedorak, P. M., & Hrudey, S. E. (1984). The effects of phenol and some alkyl phenolics on batch anaerobic

methanogenesis. *Water Research*, *18*(3), 361-367.

Feng, X. M., Karlsson, A., Svensson, B. H., & Bertilsson, S. (2010). Impact of trace element addition on biogas production from food industrial waste–linking process to microbial communities. *FEMS microbiology ecology*, *74*(1), 226-240.

Ferry, J.G. (2010). The chemical biology of methanogenesis. *Planetary and Space Science,* 58(14–15), 1775-1783.

Fezzani, B., & Cheikh, R. B. (2009). Extension of the anaerobic digestion model No. 1 (ADM1) to include phenol compounds biodegradation processes for simulating the anaerobic co-digestion of olive mill wastes at mesophilic temperature. *Journal of hazardous materials*, *172*(2-3), 1430-1438.

Fezzani, B., & Cheikh, R. B. (2009). Extension of the anaerobic digestion model No. 1 (ADM1) to include phenolic compounds biodegradation processes for the simulation of anaerobic co-digestion of olive mill wastes at thermophilic temperature. *Journal of hazardous Materials*, *162*(2-3), 1563-1570.

Fonseca Aponte, L. M. (2018). Influence of the addition of acetate as an external carbon and energy source in phenol conversion rate in an AnMBR under salinity and mesophilic conditions.

Gadhamshetty, V., Arudchelvam, Y., Nirmalakhandan, N., & Johnson, D. C. (2010). Modeling dark fermentation for biohydrogen production: ADM1-based model vs. Gompertz model. *international journal of hydrogen energy*, *35*(2), 479-490.

Gagliano, M. C., Ismail, S. B., Stams, A. J. M., Plugge, C. M., Temmink, H., & Van Lier, J. B. (2017). Biofilm formation and granule properties in anaerobic digestion at high salinity. *Water research*, *121*, 61-71.

Galí, A., Benabdallah, T., Astals, S., & Mata-Alvarez, J. (2009). Modified version of ADM1 model for agro-waste application. *Bioresource Technology*, *100*(11), 2783-2790.

Ghanbari, R. (2018). *Study of Anaerobic Membrane Bioreactor (AnMBR) Efficiency in treatment of synthetic wastewater containing phenol* (Doctoral dissertation, Qazvin university of Medical Sciences).

Gujer, W., & Zehnder, A. J. (1983). Conversion processes in anaerobic digestion. *Water science and technology*, *15*(8-9), 127-167.

Haldane, J.B.S., 1965. Enzyme. MIT Press, Cambridge, MA.

Hanselmann, K. W. (1991). Microbial energetics applied to waste repositories. Experientia, 47(7), 645-687.

Hao, O. J., Kim, M. H., Seagren, E. A., & Kim, H. (2002). Kinetics of phenol and chlorophenol utilization by Acinetobacter species. *Chemosphere*, *46*(6), 797-807.

Heijnen, J. J., & Kleerebezem, R. (2009). Bioenergetics of microbial growth. *Encyclopedia of Industrial Biotechnology: Bioprocess, Bioseparation, and Cell Technology*, 1-66.

Heijnen, J.J., Kleerebezem, R., 2010. Bioenergetics of Microbial Growth, in: Encyclopedia of Industrial Biotechnology. John Wiley & Sons, Inc., Hoboken, NJ, USA.

Hendriks, A. T. W. M., Van Lier, J. B., & De Kreuk, M. K. (2018). Growth media in anaerobic fermentative processes: the underestimated potential of thermophilic fermentation and anaerobic digestion. *Biotechnology advances*, *36*(1), 1-13.

Henze, M., & Harremoës, P. (1983). Anaerobic treatment of wastewater in fixed film reactors–a literature review. *Water science and technology*, *15*(8-9), 1-101.

Henze, M., van Loosdrecht, M. C., Ekama, G. A., & Brdjanovic, D. (Eds.). (2008). *Biological wastewater treatment*. IWA publishing.

Ismail, S. (2013). *Anaerobic wastewater treatment of high salinity wastewaters: impact on bioactivity and biomass retention*. PhD thesis, Wageningen UR.

Ismail, S. B., Gonzalez, P., Jeison, D., & Van Lier, J. B. (2008). Effects of high salinity wastewater on methanogenic sludge bed systems. *Water Science and Technology*, *58*(10), 1963-1970.

Jeison, D., Kremer, B., & van Lier, J. B. (2008). Application of membrane enhanced biomass retention to the anaerobic treatment of acidified wastewaters under extreme saline conditions. *Separation and Purification Technology*, *64*(2), 198-205.

Ji, Q., Tabassum, S., Hena, S., Silva, C. G., Yu, G., & Zhang, Z. (2016). A review on the coal gasification wastewater treatment technologies: past, present and future outlook. *Journal of cleaner production*, *126*, 38-55.

Judd, S. (2010). *The MBR book: principles and applications of membrane bioreactors for water and wastewater treatment*. Elsevier.

Kalyuzhnyi, S. V. (1997). Batch anaerobic digestion of glucose and its mathematical modeling. II. Description, verification and application of model. *Bioresource technology*, *59*(2-3), 249-258.

Kargi, F. (2002). Enhanced biological treatment of saline wastewater by using halophilic bacteria. *Biotechnology letters*, *24*(19), 1569-1572.

Kargi, F., & Dincer, A. R. (1997). Biological treatment of saline wastewater by fed‐batch operation. *Journal of Chemical Technology & Biotechnology: International Research in Process, Environmental AND Clean Technology*, *69*(2), 167-172.

Kargi, F., & Dinçer, A. R. (1998). Saline wastewater treatment by halophile-supplemented activated sludge culture in an aerated rotating biodisc contactor. *Enzyme and Microbial Technology*, *22*(6), 427-433.

Karlsson, A., Ejlertsson, J., Nezirevic, D., & Svensson, B. H. (1999). Degradation of phenol under meso- and thermophilic, anaerobic conditions. *Anaerobe*, *5*(1), 25-35.

Kleerebezem, R. (1999). *Anaerobic treatment of Phthalates: microbiological and technological aspects*.

Kleerebezem, R. and van Loosdrecht, M.C.M. (2006). Critical analysis of some concepts proposed in ADM1. Water Science and Technology, 54(4), 51–57.

Kleerebezem, R., & Van Loosdrecht, M. C. (2010). A generalized method for thermodynamic state analysis of environmental systems. *Critical Reviews in Environmental Science and Technology*, *40*(1), 1-54.

Knoll, G., & Winter, J. (1987). Anaerobic degradation of phenol in sewage sludge. *Applied microbiology and biotechnology*, *25*(4), 384-391.

Knoll, G., & Winter, J. (1989). Degradation of phenol via carboxylation to benzoate by a defined, obligate syntrophic consortium of anaerobic bacteria. *Applied Microbiology and Biotechnology*, *30*(3), 318-324.

Kobayashi, T., Hashinaga, T., Mikami, E., Suzuki, T. (1989). Methanogenic Degradation of Phenol and

Benzoate in Acclimated Sludges. Water Sci. Technol. 21, 55–65.

Kotturi, G., Robinson, C. W., & Inniss, W. E. (1991). Phenol degradation by a psychrotrophic strain of Pseudomonas putida. *Applied Microbiology and Biotechnology*, *34*(4), 539-543.

Kumar, A., Kumar, S., & Kumar, S. (2005). Biodegradation kinetics of phenol and catechol using Pseudomonas putida MTCC 1194. *Biochemical Engineering Journal*, *22*(2), 151-159.

Lambrecht, J., Cichocki, N., Hübschmann, T., Koch, C., Harms, H. and Müller, S. (2017) Flow cytometric quantification, sorting and sequencing of methanogenic archaea based on F(420) autofluorescence. *Microb Cell Fact,* 16(1), 180.

Lay, J. J., & Cheng, S. S. (1998). Influence of hydraulic loading rate on UASB reactor treating phenolic wastewater. *Journal of Environmental Engineering*, *124*(9), 829-837.

Le Clech, P., Jefferson, B., Chang, I. S., & Judd, S. J. (2003). Critical flux determination by the flux-step method in a submerged membrane bioreactor. *Journal of membrane science*, *227*(1-2), 81-93.

Lefebvre, O., & Moletta, R. (2006). Treatment of organic pollution in industrial saline wastewater: a literature review. *Water research*, *40*(20), 3671-3682.

Lin, H., Peng, W., Zhang, M., Chen, J., Hong, H., & Zhang, Y. (2013). A review on anaerobic membrane bioreactors: applications, membrane fouling and future perspectives. *Desalination*, *314*, 169-188.

Li, J., Jiang, C., Shi, W., Song, F., He, D., Miao, H., Wang, T., Deng, J.X., & Ruan, W. (2018). Polytetrafluoroethylene (PTFE) hollow fiber AnMBR performance in the treatment of organic wastewater with varying salinity and membrane cleaning behavior. *Bioresource technology*, *267*, 363-370.

Lohani, S., Wang, S., Lackner, S., Horn, H., Khanal, S., & Bakke, R. (2016). ADM1 modeling of UASB treating domestic wastewater in Nepal. *Renewable Energy*, 95, 263-268. doi:10.1016/j.renene.2016.04.014.

Lokshina, L. Y., Vavilin, V. A., Kettunen, R. H., Rintala, J. A., Holliger, C., & Nozhevnikova, A. N. (2001). Evaluation of kinetic coefficients using integrated Monod and Haldane models for low-temperature acetoclastic methanogenesis. *Water Research*, *35*(12), 2913-2922.

Maharaj, B. C., Mattei, M. R., Frunzo, L., van Hullebusch, E. D., & Esposito, G. (2019). ADM1 based mathematical model of trace element complexation in anaerobic digestion processes. *Bioresource technology*, *276*, 253-259.

Maleki, E., Bokhary, A., & Liao, B. (2018). A review of anaerobic digestion bio-kinetics. *Reviews in Environmental Science and Biotechnology*, 17(4), 691-705. doi:10.1007/s11157-018-9484-z

Martin, I., Pidou, M., Soares, S., Judd, S., Jefferson, B. (2011). Modelling the energy demands of aerobic and anaerobic membrane bioreactors for wastewater treatment. *Environ. Technol.* 32 (9), 921–932.

Metcalf & Eddy, Burton, F. L., Stensel, H. D., & Tchobanoglous, G. (2003). *Wastewater engineering: treatment and reuse*. McGraw Hill.

Monod, J. (1949). The growth of bacterial cultures, Annu. Rev. Microbiol., 3(1), 371–394.

Mu Y, Wang G., Yu H.Q. (2006). Kinetic modeling of batch hydrogen production process by mixed anaerobic cultures. *Bioresour Technol*, 97 (11), 1302–7.

Neff, J. M. (2002). *Bioaccumulation in marine organisms: effect of contaminants from oil well produced water*. Elsevier.

Pavlostathis, S. G., & Giraldo-Gomez, E. (1991). Kinetics of anaerobic treatment. *Water science and technology*, *24*(8), 35-59.

Peiris, B., Rathnasiri, P., Johansen, J., Kuhn, A., & Bakke, R. (2006). ADM1 simulations of hydrogen production. Water Science and Technology: A Journal of the International Association on Water Pollution Research,53(8), 129-37.

Quartaroli, L., Silva, L. C. F., Silva, C. M., Lima, H. S., de Paula, S. O., de Oliveira, V. M., ... & Souza, R. S. (2017). Ammonium removal from high-salinity oilfield-produced water: assessing the microbial community dynamics at increasing salt concentrations. *Applied microbiology and biotechnology*, *101*(2), 859-870.

Riffat, R., & Krongthamchat, K. (2006). Specific methanogenic activity of halophilic and mixed cultures in saline wastewater. *International Journal of Environmental Science & Technology*, *2*(4), 291-299.

Riffat, R., & Krongthamchat, K. (2007). Anaerobic treatment of high‐saline wastewater using halophilic methanogens in laboratory‐scale anaerobic filters. *Water environment research*, *79*(2), 191-198.

Rath, K. M., Maheshwari, A., Bengtson, P., & Rousk, J. (2016). Comparative toxicities of salts on microbial processes in soil. *Appl. Environ. Microbiol.*, *82*(7), 2012-2020.

Schink, B., Philipp, B., & Müller, J. (2000). Anaerobic degradation of phenolic compounds. *Naturwissenschaften*, *87*(1), 12-23.

Seghezzo, L., Zeeman, G., van Lier, J. B., Hamelers, H. V. M., & Lettinga, G. (1998). A review: the anaerobic treatment of sewage in UASB and EGSB reactors. *Bioresource technology*, *65*(3), 175-190.

Şeker, Ş., Beyenal, H., Salih, B., & Tanyolac, A. (1997). Multi-substrate growth kinetics of Pseudomonas putida for phenol removal. *Applied Microbiology and Biotechnology*, *47*(5), 610-614.

Shi, K., Zhou, W., Zhao, H., & Zhang, Y. (2012). Performance of halophilic marine bacteria inocula on nutrient removal from hypersaline wastewater in an intermittently aerated biological filter. *Bioresource technology*, *113*, 280-287.

Sierra, J. D. M., Lafita, C., Gabaldón, C., Spanjers, H., & van Lier, J. B. (2017). Trace metals supplementation in anaerobic membrane bioreactors treating highly saline phenolic wastewater. *Bioresource technology*, *234*, 106-114.

Sierra, J. D. M., Oosterkamp, M. J., Wang, W., Spanjers, H., & van Lier, J. B. (2018). Impact of long-term salinity exposure in anaerobic membrane bioreactors treating phenolic wastewater: Performance robustness and endured microbial community. *Water research*, *141*, 172-184.

Sierra, J. D. M., Oosterkamp, M. J., Wang, W., Spanjers, H., & van Lier, J. B. (2019). Comparative performance of upflow anaerobic sludge blanket reactor and anaerobic membrane bioreactor treating phenolic wastewater: Overcoming high salinity. *Chemical Engineering Journal*, *366*, 480-490.

Siripatana, C., Jijai, S., & Kongjan, P. (2016, October). Analysis and extension of Gompertz-type and Monod-type equations for estimation of design parameters from batch anaerobic digestion experiments. In *AIP Conference Proceedings* (Vol. 1775, No. 1, p. 030079). AIP Publishing.

Skouteris, G., Hermosilla, D., López, P., Negro, C., & Blanco, Á. (2012). Anaerobic membrane bioreactors for wastewater treatment: a review. *Chemical Engineering Journal*, *198*, 138-148.

Speece, R. E. (1983). Anaerobic biotechnology for industrial wastewater treatment. *Environmental science & technology*, *17*(9), 416A-427A.

Stuckey, D. C. (2012). Recent developments in anaerobic membrane reactors. *Bioresource technology*, *122*, 137-148.

Suidan, M. T., Najm, I. N., Pfeffer, J. T., & Wang, Y. T. (1988). Anaerobic biodegradation of phenols inhibition kinetics and system stability. *Journal of environmental engineering*, *114*(6), 1359-1376.

Sudmalis, D., Gagliano, M. C., Pei, R., Grolle, K., Plugge, C. M., Rijnaarts, H. H. M., Zeeman, G. & Temmink, H. (2018). Fast anaerobic sludge granulation at elevated salinity. *Water research*, *128*, 293-303.

Tay, J. H., He, Y. X., & Yan, Y. G. (2001). Improved anaerobic degradation of phenol with supplemental glucose. *Journal of environmental engineering*, *127*(1), 38-45.

Van Lier, J. B., Tilche, A., Ahring, B. K., Macarie, H., Moletta, R., Dohanyos, M., Hulshoff Pol, L. W., Lens, P. & Verstraete, W. (2001). New perspectives in anaerobic digestion. *Water Science and Technology*, *43*(1), 1-18.

Van Lier, J.B., Mahmoud, N. and Zeeman, G. (2002) Biological Wastewater Treatment: Principles, Modelling and Design.

Vavilin, V. A., & Lokshina, L. Y. (1996). Modeling of volatile fatty acids degradation kinetics and evaluation of microorganism activity. *Bioresource Technology*, *57*(1), 69-80.

Veeresh, G. S., Kumar, P., & Mehrotra, I. (2005). Treatment of phenol and cresols in upflow anaerobic sludge blanket (UASB) process: a review. *Water research*, *39*(1), 154-170.

Veluchamy, C., & Kalamdhad, A. S. (2017). Biochemical methane potential test for pulp and paper mill sludge with different food/microorganisms ratios and its kinetics. *International Biodeterioration & Biodegradation*, *117*, 197-204.

Vyrides, I., Stuckey, D.C., 2009a. Saline sewage treatment using a submerged anaerobic membrane reactor (SAMBR): effects of activated carbon addition and biogas-sparging time. Wat. Res. 43 (4), 933–942.

Wang, J., & Wan, W. (2009). Kinetic models for fermentative hydrogen production: a review. *International Journal of Hydrogen Energy*, *34*(8), 3313-3323.

Weiss, R. (1974). Carbon dioxide in water and seawater: the solubility of a non-ideal gas. *Marine chemistry*, *2*(3), 203-215.

Yamamoto, S., Alcauskas, J. B., & Crozier, T. E. (1976). Solubility of methane in distilled water and seawater. *Journal of Chemical and Engineering Data*, *21*(1), 78-80.

Yang, J. (2013). Prospects for flux enhancement in anaerobic membrane bioreactors treating saline wastewater.

Yang, J., Spanjers, H., Jeison, D., & Van Lier, J. B. (2013). Impact of Na^+ on biological wastewater treatment and the potential of anaerobic membrane bioreactors: A review. Critical Reviews in Environmental Science and Technology,43(24), 2722-2746.

Yano, T., Nakahara, T., Kamiyama, S., Yamada, K., 1966. Kinetic studies on microbial activities in concentrated solutions. I. Effect of excess sugars on oxygen uptake rate of a cell-free respiratory system. Agric. Biol. Chem. 30, 42–48.

Young, L. Y., & Rivera, M. D. (1985). Methanogenic degradation of four phenolic compounds. *Water Research*, *19*(10), 1325-1332.

Zhao, Q., & Liu, Y. (2016). State of the art of biological processes for coal gasification wastewater treatment. *Biotechnology advances*, *34*(5), 1064-1072.

Zhao, J., Liu, Y., Wang, D., Chen, F., Li, X., Zeng, G., & Yang, Q. (2017). Potential impact of salinity on methane production from food waste anaerobic digestion. *Waste Management*, *67*, 308-314.

Appendix 2.1 Literature review of the kinetic parameters in Haldane kinetic equation for phenol degradation

	K_S (mg COD/L)	K_I (mg COD/L)	u_m (h^{-1})	S (mg/L)	Bacteria (mixed culture or not) Other conditions	Source
1	25.4	173	0.26	0-900	Y	Arutchelvan et al., 2006
2	5.86	934.5	0.223	0-1000	Y	
3	0.015	470	0.534	0-700	N	
4	2.39	106	0.567	0-500	N	
5	1.66	380	0.464	0-900	N	
6	5.94	227	0.369	0-700	N	
7	2.9	370	0.418	0-500	N	
8	36.2	145	0.542	60-500	N	
9	71.4	241	0.618	85-890	N	
10	53.9	516	0.456	300-710	N	
11	18	430	0.051	50	N	
12	2.2-29.3	868-2434.7	0.026-0.078	750-1750	N	
13	1.06	903	0.388	0-200	N	Kumar et al., 2005
14	5.27	377	0.119	0-200	N	
15	8.2	170	0.325	0-170	N	
16	53.9	516	0.459	300-710	N	
17	71.4	241	0.618	85-590	N	
18	36.33	129.79	0.305	-	N	
19	59.15	2.411?	27.85	-	N	Banerjee et al., 2010
20	9.706	3873	1.635	-	N	
21	10500	50000	0.09	31000	Thermophilic temperature	Fezzani et al., 2009
22	5.27	377	0.119	<200	Psychrotrophic	Kotturi et al., 1991
23	0.16-5.2	7.5-19.4	0.44-1.61	-	N	
24	15.81	169	0.3407	-	N	Basak et al., 2014
25	2.22	245.37	0.15	1600	N	
26	129.4	637.8	0.4396	<2000	N	

27	5.16	1033.7	0.29	1000	N	
28	6.19	54.1	0.436	100	N	
29	77.7	319.4	0.094	745	N	
30	11.7	207.9	0.48	2000	N	
31	130.4	200	0.312	1800	N	
32	1167	58.5	0.28	1000	N	
33	160	3760	0.66	2400	N	
34	6.7	234	0.54	2600	N	
35	15.81	169	0.3407	2400	N	
36	30500	50000	0.625	24000	N	Fezzani et al., 2009

Appendix 3.1 Time series of the experiment

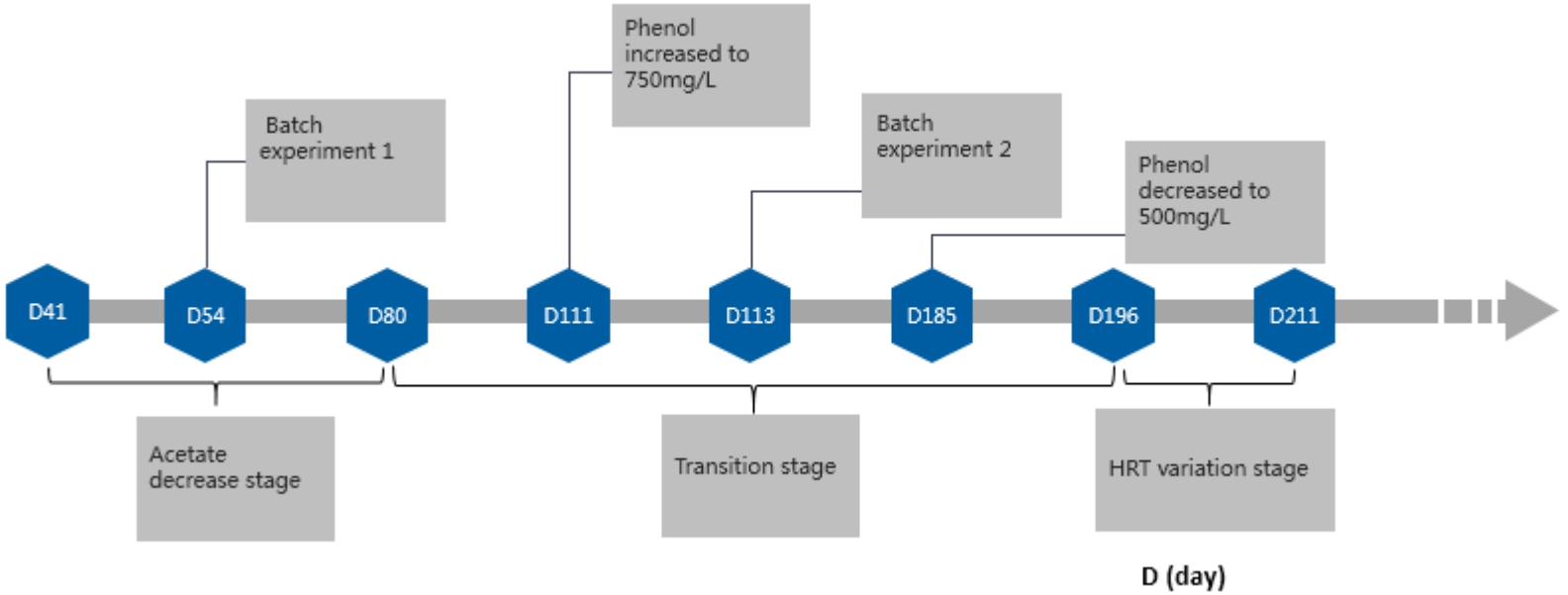

Batch experiment 1: 8.0 g Na^+/L with solely acetate
Batch experiment 2: 18.6 g Na^+/L with phenol and acetate
18.6 g Na^+/L with solely acetate

Appendix 3.2 Constant for Bunsen solubility coefficient calculation

A1	-67.1962	B1	-0.072909
A2	99.1624	B2	0.041674
A3	27.9015	B3	-0.006460

Appendix 3.3 Composition of the substrate in the batch experiment

	Na^+ concentration (g/L)	Acetate concentration (g/L)	AC-COD concentration (g/L)	Phenol concentration (mg/L)	Phenol-COD concentration (mg/L)
AnMBR1 (acetate)	18.6	4.2	2	0	0
AnMBR1 (acetate and phenol)	18.6	4.2	2	300	714
AnMBR2 (acetate)	8	4.2	2	0	0
AnMBR2 (acetate and phenol)	8	4.2	2	300	714

Appendix 3.4 Composition of buffer solution and nutrient solution

Solution	Composition and concentration
Buffer Solution A	0.2M $K_2HPO_4.3H_2O$
Buffer Solution B	0.2M $NaH_2PO_4.2H_2O$
Micronutrients	$FeCl_3 \cdot 6H_2O$ 2g/L; $CoCl_2 \cdot 6H_2O$ 2g/L; $MnCl_2 \cdot 4H_2O$ 500 mg/L; $CuCl_2 \cdot 2H_2O$ 30 mg/L; $ZnCl_2$ 50 mg/L; H_3BO_3 50 mg/L; $(NH4)_6Mo_7O_2 \cdot 4H_2O$ 90 mg/L; Na_2SeO 100 mg/L; $NiCl_2 \cdot 6H_2O$ 50 mg/L; EDTA 1 g/L, $Na_2WO_4 \cdot 2H_2O$ 80 mg/L.
Macronutrients	NH_4Cl 170g/L; $CaCl_2.2H_2O$ 8g/L; $MgSO_4.7H_2O$ 9g/L;

Appendix 3.5 Chemical origin and purity

Chemical	Origin	Purity	Chemical	Origin	Purity
Phenol	Merck	>99%	$CH_3COONa{\cdot}3H_2O$	Merck	Analysis grade
NaCl	VWR	Technical degree	Yeast	Sigma Aldrich	Technical degree
$K_2HPO_4.3H_2O$	Sigma Aldrich	⩾98%	$NaH_2PO_4.2H_2O$	Carl Roth	⩾99%
$FeCl_3{\cdot}6H_2O$	Merck	⩾99%	$CoCl_2{\cdot}6H_2O$	Merck	Analysis grade
$MnCl_2{\cdot}4H_2O$	VWR	99,6%	$CuCl_2{\cdot}2H_2O$	VWR	Analysis grade
$ZnCl_2$	VWR	⩾98%	H_3BO_3	Merck	Analysis grade
$(NH4)_6Mo_7O_2{\cdot}4H_2O$	Merck	⩾99%	Na_2SeO	VWR	Analysis grade
$Na_2WO_4{\cdot}2H_2O$	Sigma Aldrich	⩾99%	EDTA	Carl Roth	⩾99% USP
$NiCl_2{\cdot}6H_2O$	Riedel-deHaen	⩾97%	NH_4Cl	Merck	Analysis grade
$CaCl_2.2H_2O$	Merck	⩾99%	$MgSO_4.7H_2O$	Sigma Aldrich	⩾99%
Citric acid	VWR	100%	Sulfuric acid	Sigma Aldrich	95%-97%
Pentanol	Sigma Aldrich	>99%	Formic acid	Sigma Aldrich	>99%

Appendix 4.1 Codes for mathematical model of batch experiment

```
import numpy as np
import matplotlib.pyplot as plt
%matplotlib inline

R3_AC = np.loadtxt('R3_SMA_AC.txt')
R3_Ph = np.loadtxt('R3_SMA_ph.txt')

kla = 178/24  # 1 / h
R = 8.314  # Pa * m3 / K / mol
T = 273 + 35 # K
V_liq = 0.4 # Effective volume of the bottke L
X = 2000 * 0.5 * 1.42 # Biomass concentration mg XAc-COD / L
f_AC = 0.28 # Biomass fraction of acetate
Y_AC = 0.015 # Biomass yield of methanogens mg XAc-COD / mg AC-COD / h
Time = 300 # h
N = 30001  # Time step
C = 53.41 #  Saturation concentration of methane mg CH4-COD / L
```

```
# Unit conversion

V_AC = 2.07 / (10 ** 6)        # Vial volume of the AMPTS without phenol, m3
V_Ph = 2.04 / (10 ** 6)        # Vial volume of the AMPTS with phenol, m3

P_AC = R3_AC[:,2] * 10 ** 3    # Pressure without phenol, Pa
P_Ph = R3_Ph[:,2] * 10 ** 3    # Pressure with phenol, Pa
x1 = R3_AC[:,0]                # Time of click without phenol, h
x2 = R3_Ph[:,0]                # Time of click with phenol, h
T_AC = R3_AC[:,1] + 273        # Temperature with phenol,K
T_Ph = R3_Ph[:,1] + 273        # Temperature without phenol,K

n_AC = P_AC * V_AC / R / T_AC  # molAc
S_AC = n_AC * 64 / V_liq * 1000# mg Ac-COD/L
n_Ph = P_Ph * V_Ph / R / T_Ph  # molPh
S_Ph = n_Ph * 64 / V_liq * 1000 #mg Ph-COD/L
```

```
# State variables
y_AC = np.zeros(118)
y_Ph = np.zeros(123)
C_AC = np.zeros(118)
C_Ph = np.zeros(123)
V_AC = np.zeros(118)
V_Ph = np.zeros(123)

for i in range(len(y_AC)):

    #Initialization
    if i ==0:
        y_AC[i] = V_AC[0]
        C_AC[i] = S_AC[0]
    else:
        # model
        y_AC[i] = y_AC[i-1] + V_AC[i]
        C_AC[i] = C_AC[i-1] + S_AC[i]

for i in range(len(y_Ph)):
    if i ==0:
        y_Ph[i] = V_Ph[0]
        C_Ph[i] = S_Ph[0]
        V_Ph[i] = V_Ph[0]
    else:
        y_Ph[i] = y_Ph[i-1] + V_Ph[i]
        C_Ph[i] = C_Ph[i-1] + S_Ph[i]
```

```
Time_2 = 300
N_2 = 30001
t_2 = np.linspace(0,Time_2,N_2)

Air_2 = np.zeros(N_2)
S_AC_2 = np.zeros(N_2)
S_CH4_2 = np.zeros(N_2)

def Model_2(a,KS_AC_2,KI_AC_2,km_AC_2,I2):

    # initialization
    for i in range (N_2):
            if i == 0:
                Air_2[i] = S_CH4_0
                S_AC_2[i] = S_AC_0
                S_CH4_2[i]= C
            else:
                # Model
                C_AC = (km_AC_2 * S_AC_2[i-1] * X * f_AC) / (KS_AC_2 + S_AC_2[i-1] + S_AC_2[i-1] ** 2 / KI_AC_2)
                S_AC_2[i] = S_AC_2[i-1] - Time_2 / (N_2-1) * C_AC * I2
                S_CH4_2[i] = S_CH4_2[i-1] + Time_2 / (N_2-1) * ((1 - Y_AC) * C_AC * I2 - kla * (S_CH4_2[i-1] - C))
                Air_2[i] = Air_2[i-1] + (kla * (S_CH4_2[i-1] - C))* Time_2 / (N_2-1)

            aaa = np.abs(t_2[i] - a)
            if aaa < 10 ** -5:
                return(Air_2[i])
```

```
# Remove lag phase
y_data4 = C_Ph[13::]
B = np.ones(len(y_data4)) * 43.84
x_data4 = R3_Ph[13::,0]- B
S_AC_0 = 2052-y_data4[0]
S_CH4_0 = y_data4[0]

m2 = len(x_data4)
v2 = np.zeros(m2)

# Fitting the model to the experiemntal data
def fitcurve4(x_data4,KS_AC_2,KI_AC_2,km_AC_2,I2):
    for i in range (m2):
        v2[i] = Model_2(x_data4[i],KS_AC_2,KI_AC_2,km_AC_2,I2)
    return v2

from scipy.optimize import curve_fit
popt4,pcov4 = curve_fit(fitcurve4,x_data4,y_data4,p0=(0,2000,0.1,0.5),bounds=([0,300,0,0],[300,50000,1,1]),method='trf')
y_model4 = fitcurve4(x_data4,popt4[0],popt4[1],popt4[2],popt4[3])

print('Optimal parameters:',popt4)
plt.plot(x_data4,y_model4,color = 'r',label = 'Model')
plt.scatter(x_data4,y_data4,label = 'Experimental data',s = 1)
plt.xlabel('Time (hours)')
plt.ylabel('CH4-COD mg/L')
plt.title('Modeling of methane with acetate and phenol')
plt.legend()
```

Appendix 4.2 Codes for mathematical model of dynamic experiment

```
# Phenol data mg COD/L
R3_Ph = np.loadtxt('ph_data.txt')
S_AC_1 = 0
S_phenol_1 = 6.63 * 2.38
S_AC_2 = 0 * 1.08
S_phenol_2 = 4.37 * 2.38
S_AC_3 = 0
S_phenol_3 = 3.29 * 2.38
S_AC_4 = 0 * 1.08
S_phenol_4 = 2.81 * 2.38
S_AC_5 = 0 * 1.08
S_phenol_5 = 1.83 * 2.38
S_AC_6 = 0 * 1.08
S_phenol_6 = 1.39 * 2.38

x1 = R3_Ph[:,0]
y1 = R3_Ph[:,1] * 2.38            # Q = 1 L/d
x2 = R3_Ph[:,2]
y2 = R3_Ph[:,3] * 2.38            # Q = 0.8 L/d
x3 = R3_Ph[:,4]
y3 = R3_Ph[:,5] * 2.38            # Q = 0.6 L/d
x4 = R3_Ph[:,6]
y4 = R3_Ph[:,7] * 2.38            # Q = 1.2 L/d
x5 = R3_Ph[:,8]
y5 = R3_Ph[:,9] * 2.38            # Q = 1.5 L/d
x6 = R3_Ph[:,10]
y6 = R3_Ph[:,11] * 2.38            # Q = 2 L/d
```

```
# Methane data  mg COD/L
R3_CH4 = np.loadtxt('CH4_data1.txt')   # mg COD

y_1 = R3_CH4[:,0]/6          # Q = 1 L/d
y_2 = R3_CH4[:,1]/6          # Q = 0.8 L/d
y_3 = R3_CH4[:,2]/6          # Q = 0.6 L/d
y_4 = R3_CH4[:,3]/6          # Q = 1.2 L/d
y_5 = R3_CH4[:,4]/6          # Q = 1.5 L/d
y_6 = R3_CH4[:,5]/6          # Q = 2 L/d

# Acetate data mg COD/L
R3_AC = np.loadtxt('AC_data.txt')

y_AC_1 = R3_AC[:,0]          # Q = 1 L/d
y_AC_2 = R3_AC[:,1]          # Q = 0.8 L/d
y_AC_3 = R3_AC[:,2]          # Q = 0.6 L/d
y_AC_4 = R3_AC[:,3]          # Q = 1.2 L/d
y_AC_5 = R3_AC[:,4]          # Q = 1.5 L/d
y_AC_6 = R3_AC[:,5]          # Q = 2 L/d
```

```
def Continuous_Experiment_Model(Q_i, S_AC_0, S_phenol_0, KS_AC, KI_AC, km_AC, KS_ph, KI_ph, km_ph):

    # Gobal Settings
    f_AC = 0.28  # biomass fraction of acetate
    f_ph = 0.72  # biomass fraction of phenol
    kla = 178/24  # 1/ h
    X = 2850 * 0.5 * 1.42# mgCOD/L
    Y_ph = 0.064   # mgX-COD/ mgPh-COD
    Y_AC = 0.015   ## mgX-COD/ mgAC-COD
    Time = 12 #hour
    N = 5000  # time step
    C = 53.41 # mgCH4-COD/L/h
    V_liq = 6 # L

    time = np.linspace(0,Time,N)

    time_index = pd.date_range(start = '00:00:00', end = '{}:00:00'.format(Time), periods = N)
    C_PH_i = 500 * 2.38 #mg Ph-COD/L
    C_AC_i = 2000 # mg AC-COD/L

    # State Variables
    R_AC =  np.zeros(N)
    R_phenol =  np.zeros(N)

    S_AC =  np.zeros(N)
    S_phenol =  np.zeros(N)
    S_CH4 =  np.zeros(N)
    S_CH4_air = np.zeros(N)
```

```
    # initialization
    for i in range(N):
        if i == 0:
            R_AC[i] = 0
            R_phenol[i] = 0
            S_AC[i] = S_AC_0
            S_CH4[i]= C
            S_CH4_air[i] = 0
            S_phenol[i] = S_phenol_0

        else:
            # Model
            delta_t = time[i] - time[i-1] # Delta time

            R_AC[i] = (km_AC * S_AC[i-1] * X * f_AC) / (KS_AC + S_AC[i-1] + (S_AC[i-1] ** 2 / KI_AC))
            R_phenol[i] = (km_ph * S_phenol[i-1] * X * f_ph) /(KS_ph + S_phenol[i-1] + (S_phenol[i-1]** 2 / KI_ph))

            # Concentrations
            S_phenol[i] = S_phenol[i-1] + delta_t * (Q_i / V_liq * (C_PH_i - S_phenol[i-1]) - R_phenol[i-1])
            S_AC[i] = S_AC[i-1] + delta_t * (Q_i / V_liq * (C_AC_i - S_AC[i-1]) + (1 - Y_ph) * R_phenol[i-1] - R_AC[i-1])
            S_CH4[i] = S_CH4[i-1] + delta_t * ((1 - Y_AC) * R_AC[i-1] - kla * (S_CH4[i-1] - C) - Q_i * S_CH4[i-1] / V_liq)
            S_CH4_air[i] = S_CH4_air[i-1] + delta_t * kla * (S_CH4[i-1] - C)

    data_model = pd.DataFrame(data = np.vstack([S_phenol, S_AC, S_CH4, S_CH4_air, R_AC, R_phenol]).T,
                              index = time_index, columns = ['S_phenol', 'S_AC', 'S_CH4', 'S_CH4_air', 'R_AC', 'R_phenol'])
    return data_model

def reindex_and_interpolate(df, new_index):
    return df.reindex(df.index | new_index).interpolate(method='index', limit_direction='both').loc[new_index]
```

```
# Sample model layout
# Set global parameters:

KS_AC_i = 300 # mg AC-COD/L
KI_AC_i = 806 # mg AC-COD/L
Km_AC_i = 0.246# mg AC-COD/(mgX-COD.h)

KS_ph_i = 20   # mg Ph-COD/L
KI_ph_i = 300  # mg Ph-COD/L
Km_ph_i = 0.008# mg Ph-COD/(mgX-COD.h)

data_model_1 = Continuous_Experiment_Model(Q_i = 1/24., S_AC_0 = S_AC_1, S_phenol_0 = S_phenol_1,
                                           KS_AC = KS_AC_i, KI_AC = KI_AC_i, km_AC = Km_AC_i,
                                           KS_ph = KS_ph_i, KI_ph = KI_ph_i, km_ph = Km_ph_i)

data_model_2 = Continuous_Experiment_Model(Q_i = 0.8/24., S_AC_0 = S_AC_2, S_phenol_0 = S_phenol_2,
                                           KS_AC = KS_AC_i, KI_AC = KI_AC_i, km_AC = Km_AC_i,
                                           KS_ph = KS_ph_i, KI_ph = KI_ph_i, km_ph = Km_ph_i)

data_model_3 = Continuous_Experiment_Model(Q_i = 0.6/24., S_AC_0 = S_AC_3, S_phenol_0 = S_phenol_3,
                                           KS_AC = KS_AC_i, KI_AC = KI_AC_i, km_AC = Km_AC_i,
                                           KS_ph = KS_ph_i, KI_ph = KI_ph_i, km_ph = Km_ph_i)

data_model_4 = Continuous_Experiment_Model(Q_i = 1.2/24., S_AC_0 = S_AC_4, S_phenol_0 = S_phenol_4,
                                           KS_AC = KS_AC_i, KI_AC = KI_AC_i, km_AC = Km_AC_i,
                                           KS_ph = KS_ph_i, KI_ph = KI_ph_i, km_ph = Km_ph_i)

data_model_5 = Continuous_Experiment_Model(Q_i = 1.5/24., S_AC_0 = S_AC_5, S_phenol_0 = S_phenol_5,
                                           KS_AC = KS_AC_i, KI_AC = KI_AC_i, km_AC = Km_AC_i,
                                           KS_ph = KS_ph_i, KI_ph = KI_ph_i, km_ph = Km_ph_i)
```

```
data_model_6 = Continuous_Experiment_Model(Q_i = 2/24., S_AC_0 = S_AC_6, S_phenol_0 = S_phenol_6,
                                           KS_AC = KS_AC_i, KI_AC = KI_AC_i, km_AC = Km_AC_i,
                                           KS_ph = KS_ph_i, KI_ph = KI_ph_i, km_ph = Km_ph_i)


data_model_1_reindexed = reindex_and_interpolate(data_model_1,
                                                 [pd.to_datetime('00:00:00') + pd.Timedelta('{}S'.format(int(x*60*60))) for x in x1])
data_model_2_reindexed = reindex_and_interpolate(data_model_2,
                                                 [pd.to_datetime('00:00:00') + pd.Timedelta('{}S'.format(int(x*60*60))) for x in x2])
data_model_3_reindexed = reindex_and_interpolate(data_model_3,
                                                 [pd.to_datetime('00:00:00') + pd.Timedelta('{}S'.format(int(x*60*60))) for x in x3])
data_model_4_reindexed = reindex_and_interpolate(data_model_4,
                                                 [pd.to_datetime('00:00:00') + pd.Timedelta('{}S'.format(int(x*60*60))) for x in x4])
data_model_5_reindexed = reindex_and_interpolate(data_model_5,
                                                 [pd.to_datetime('00:00:00') + pd.Timedelta('{}S'.format(int(x*60*60))) for x in x5])
data_model_6_reindexed = reindex_and_interpolate(data_model_6,
                                                 [pd.to_datetime('00:00:00') + pd.Timedelta('{}S'.format(int(x*60*60))) for x in x6])
```

```
# compose model layout

Model_Layout_ph = np.array([data_model_1_reindexed['S_phenol'].values,
                            data_model_2_reindexed['S_phenol'].values,
                            data_model_3_reindexed['S_phenol'].values,
                            data_model_4_reindexed['S_phenol'].values,
                            data_model_5_reindexed['S_phenol'].values,
                            data_model_6_reindexed['S_phenol'].values]).flatten()

Model_Layout_ac = np.array([data_model_1_reindexed['S_AC'].values,
                            data_model_2_reindexed['S_AC'].values,
                            data_model_3_reindexed['S_AC'].values,
                            data_model_4_reindexed['S_AC'].values,
                            data_model_5_reindexed['S_AC'].values,
                            data_model_6_reindexed['S_AC'].values]).flatten()
```

```
Model_Layout_CH4 = np.array([data_model_1_reindexed['S_CH4'].values,
                             data_model_2_reindexed['S_CH4'].values,
                             data_model_3_reindexed['S_CH4'].values,
                             data_model_4_reindexed['S_CH4'].values,
                             data_model_5_reindexed['S_CH4'].values,
                             data_model_6_reindexed['S_CH4'].values]).flatten()

Model_Layout_CH4_air = np.array([data_model_1_reindexed['S_CH4_air'].values,
                             data_model_2_reindexed['S_CH4_air'].values,
                             data_model_3_reindexed['S_CH4_air'].values,
                             data_model_4_reindexed['S_CH4_air'].values,
                             data_model_5_reindexed['S_CH4_air'].values,
                             data_model_6_reindexed['S_CH4_air'].values]).flatten()

# Generate Observation layout
Observation_Layout_ph = np.array([y1, y2, y3, y4, y5, y6]).flatten()
Observation_Layout_CH4_air = np.array([y_1, y_2, y_3, y_4, y_5, y_6]).flatten()
Observation_Layout_AC = np.array([y_AC_1, y_AC_2, y_AC_3, y_AC_4, y_AC_5, y_AC_6]).flatten()
```

```
fig = plt.figure(figsize = (10,8))

ax = fig.add_subplot(411)
plt.plot(Model_Layout_ph, 'r+', label = 'Model Phenol')
plt.plot(Observation_Layout_ph, 'k.', ms = 3, label = 'Observation Phenol')

plt.ylabel('Phenol-COD mg/L')
plt.title('Phenol: KS_AC = {}, KI_AC = {}, Km_AC = {}, KS_ph = {}, KI_ph = {}, Km_ph = {}'.format(KS_AC_i, KI_AC_i, Km_AC_i,
                                                                                                  KS_ph_i, KI_ph_i, Km_ph_i))
plt.legend()
plt.xticks([])

ax = fig.add_subplot(412)
plt.plot(Model_Layout_ac, 'r+', label = 'Model Acetate')
plt.plot(Observation_Layout_AC, 'k.', ms = 3, label = 'Observation Acetate')

plt.ylabel('AC-COD mg/L')
plt.title('Acetate: KS_AC = {}, KI_AC = {}, Km_AC = {}, KS_ph = {}, KI_ph = {}, Km_ph = {}'.format(KS_AC_i, KI_AC_i, Km_AC_i,
                                                                                                   KS_ph_i, KI_ph_i, Km_ph_i))
plt.legend()
plt.xticks([])
```

```
ax = fig.add_subplot(413)
plt.plot(Model_Layout_CH4_air, 'r+', label = 'Model CH4')
plt.plot(Observation_Layout_CH4_air, 'k.', ms = 3, label = 'Observation Methane')

plt.ylabel('CH4-COD mg/L')
plt.title('CH4: KS_AC = {}, KI_AC = {}, Km_AC = {}, KS_ph = {}, KI_ph = {}, Km_ph = {}'.format(KS_AC_i, KI_AC_i, Km_AC_i,
                                                                                               KS_ph_i, KI_ph_i, Km_ph_i))
plt.legend()
plt.xticks([])


plt.tight_layout()
plt.savefig('Fit_Observationlayout_ParamLiteratureOptChao.png')
```

Appendix 4.3 Standard Gibbs energy and enthalpy of different chemicals

Composition	$\triangle G_f^{01}$ (kJ/mol)	$\triangle H_f^{01}$ (kJ/mol)
Phenol (C_6H_6O)	-29.7	-93.3
Acetate ($C_2H_3O_2^-$)	-369.4	-485.8
$CH_{1.8}O_{0.5}N_{0.2}$	-67.0	-91.0
H_2O	-237.2	-285.8
CO_2	-394.4	-393.5
CH_4	-50.7	-74.8
NH_4^+	-79.4	-133.3
H^+	0	0
e^-	0	0

(Heijnen, J.J., Kleerebezem, R., 2010; Hanselmann, K. W., 1991)

Appendix 4.4 Rough determination of methanogenic microorganisms fraction by fluorescence microscopy

Introduction

For modeling of the kinetics of the anaerobic digestion (AD) process, the fractions of active microorganisms are needed. In Equation A 4.4.1, this fraction is required to determine the substrate uptake, so do for a case in which biomass growth is considered (Eq. A 4.4.2). However, the determination of both the fraction and especially the active part of microorganisms in that fraction has been a constant challenge.

$$\frac{dS_{Ac}}{dt} = \frac{\mu_g X_{Ac}}{Y_{Ac}} \quad \text{where} \quad X_{Ac} = X \cdot f_{Ac} \qquad \text{Equation A 4.4.1}$$

$$\frac{dX_{Ac}}{dt} = Y_{Ac} \cdot \mu_g \cdot X_{Ac} - k_{d,Ac} \cdot X_{Ac} \qquad \text{Equation A 4.4.2}$$

Some methods have been proposed for the determination of the active fraction of microorganisms (Blagodatskaya& Kuzyakov 2013). These include plate count and microbial cultures, microorganism staining coupled to microscopy, molecular biology techniques, etc. In this regard, proteins, cofactors, or other molecules that are specific for a certain population are from special interest as the marking, labeling, or detection techniques could be focused on these molecules. This is the case of the protein F_{420}, which has been proposed as a marker to determine the methanogenic microorganisms.

The protein or coenzyme F_{420} is a dezaflavin hydride carrier which is used in two reduction steps during the hydrogenotrophic methanogenesis (Allen & White 2018; Ferry 2010), it supplies hydrogen as reducing equivalents, and it gets oxidized during this process (Lambrecht et al., 2017). This protein has autofluorescence properties when excited at a maximum of 420 nm in its oxidized form. The study of this protein either by flow cytometry or fluorescence microscopy, has been proposed and documented as a way to determine the methanogenic microbial population (Lambrecht et al., 2017).

In this experiment, we aimed to have a rough estimation of the methanogenic microorganisms present in the anaerobic membrane bioreactor (AnMBR) sludge at 18.6 g Na^+/L by fluorescence microscopy targeting the autofluorescence of protein F_{420}. Although the results were not used in the model, the images supported our idea that methanogens would not represent more than 40% of the biomass we proposed in the model.

Materials and methods

For the determination of the F_{420}-positive methanogenic microorganisms, we measured the autofluorescence of the protein by fluorescence microscopy. Approximately, 5 mL of the mixed liquor suspended solids (MLSS) were taken out of the AnMBR1. 20 µL were put in a crystal microscope slide and then visualized in an Olympus total internal reflection (TIRF)

microscope (Olympus, Japan). F_{420} autofluorescence was determined by excitation with a 424 – 444 nm filter and 477 – 500 nm detection filter. Images were processed using the program ImageJ (NIH, Md, USA).

Results

The micrographs obtained by the fluorescent microscope are shown in figure Appendix 4.4.1. In the figures, it is possible to observe both the micrographs in the visible spectrum and the ones excited at 424-444 nm. The figures show the presence of microorganisms with different morphologies such as rods, long rods, and cocci. The right panel images show the fluorescence observed when the excitation laser was used, the white points correspond to the cells which presented autofluorescence.

Discussion

In this experiment, we tried to have a rough determination of the fraction of active methanogenic microorganisms by measuring them through the autofluorescence of the protein F_{420}, which is a protein involved in the methanogenic process by CO_2 reduction. We took some micrographs in a fluorescent microscope and tried to have an estimation of the methanogens to propose a realistic fraction of methanogens to be used in the mathematical model.

The fluorescence approach has been already reported as a useful way for the determination of methanogenic *Archaea* (Lambrecht et al., 2017). Nevertheless, in that study, the fluorescence microscopy was combined with a more quantitative analysis such as flow cytometry. We also tried that method; however, because of the lack of a proper emission filter in the flow cytometer, we were not able to excite the F_{420} protein. So we relied just upon the determination done by the fluorescence microscope.

The F_{420} fluorescence technique could have some drawbacks. For example, methanogens which follow the acetoclastic pathway could bypass the F_{420} dependent steps (Lambrecht et al. 2017), implying that the value determined for the methanogenic population would be biased. Furthermore, the F_{420} could be sensible to oxic environments, yielding more oxidized $F_{420,}$ which is the fluorescent protein.

For the model approach, these results should be carefully considered. As at it has been stated, the main population that is being quantified is the hydrogenotrophic methanogens, while in the proposed mathematical model in this thesis methane generation is considered to be done just by the acetoclastic population. However, it has been reported that acetoclastic methanogenesis accounts for approximately 70% of the methane produced (van Lier et al. 2002), and a recent study of our group with an AnMBR under similar conditions as the one that are reported in this thesis showed a higher relative abundance of acetoclastic methanogens over the hydrogenotrophic ones. Also, we could not have a quantitative

approach due that the non-auto fluorescence microorganisms were not possible to count. For the next experiments, we suggest to implement a fixation method; although, it could damage or quench the F_{420} autofluorescence. That is why we consider that the best approach would be through flow cytometry. Although, with this experiment, we could observe that methanogens are not the major population of the AnMBR microorganisms.

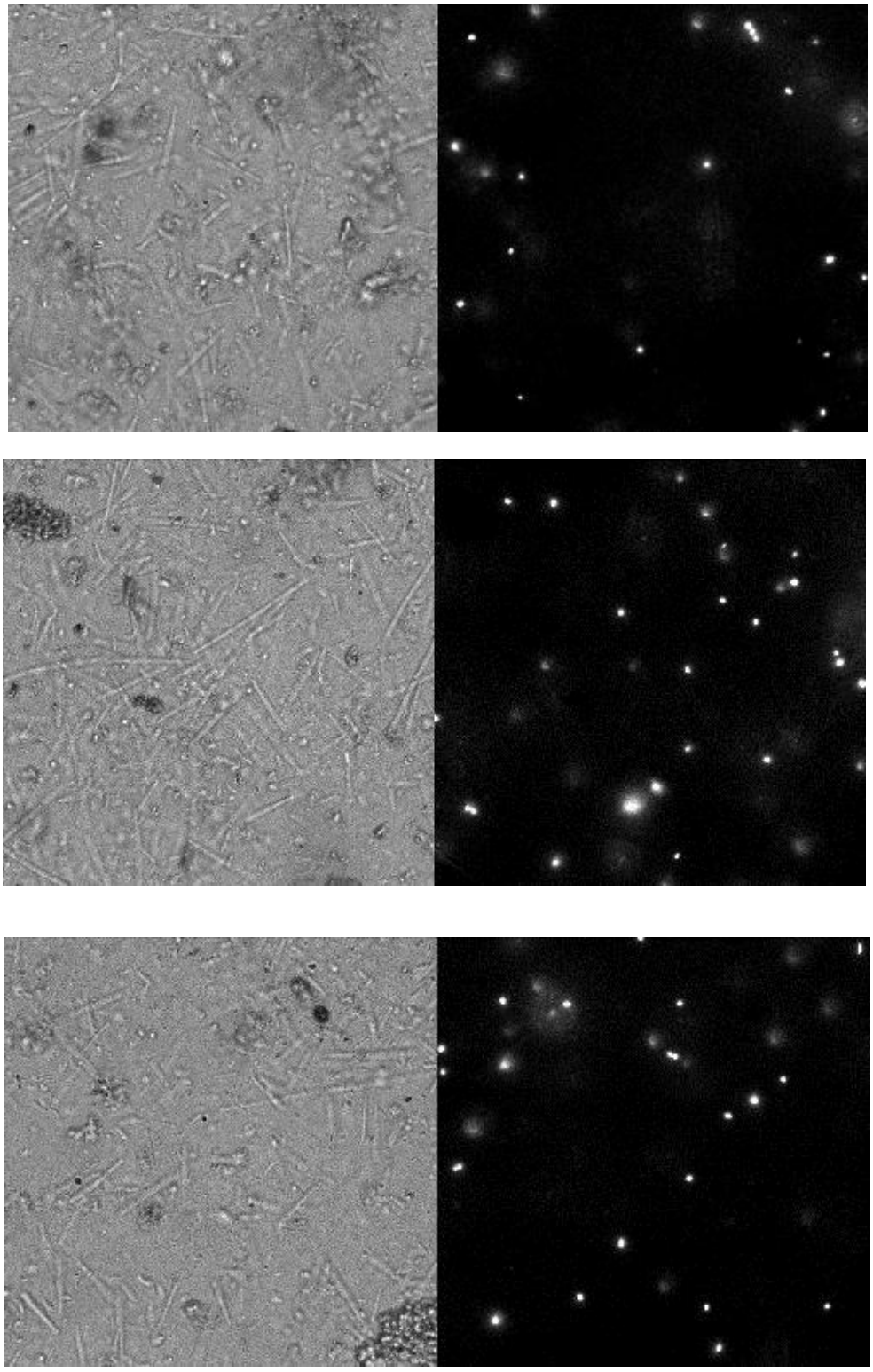

Appendix 4.4.1. Micrographs obtained by the fluorescent microscope. Three different areas of the crystal

microscope slide are shown. The left images show the micrograph when no UV excitation laser was used, it is possible to see the different morphologies (rod, long rod, and cocci) of the microorganisms. The right images show the micrographs when the 424 – 444 nm excitation filter was used. The white dots represent the microorganisms with autofluorescence, corresponding to the F_{420} positive microorganisms, mainly CO_2 reducer methanogens.

Conclusions and further suggestions

As conclusions, we state that it was possible to observe the F_{420} positive microorganisms in the AnMBR biomass. However, we could not get a qualitative determination of the fraction due that the microscopy did not allow us to count the other microorganisms present in the sample; nevertheless, we observed that F_{420} positive microorganism, which we could relate to hydrogenotrophic methanogens, are not the bigger population in the AnMBR biomass. As a recommendation, we would propose the use of flow cytometry. Or if the microscope would be used again, to have a combination of the autofluorescence with general dies such as SYBR-green, as well as considering the fixation of the sample with a technique that does not disrupt the F_{420} autofluorescence.

Acknowledgments

We want to acknowledge Dr. Ir. Jeremie Capoulade from the Kavli Institue of Nanosciences (TU Delft) for the help and support given to conduct this experiment.

Appendix 4.5 Effect of initial acetate concentration on acetate degradation

To determine if there was an inhibition by the acetate concentration of 2g Ac^-/L on the acetate conversion, we studied the acetate degradation of high initial acetate concentration [2g Ac-COD/L] and lower initial acetate concentration [1g Ac-COD/L]. The effect of initial acetate concentration on acetate degradation and methane production were shown in the Appendix 4.5.1.

With lower initial acetate concentration, the lag phase of methane production was reduced to about 27h. This might suggest that lower initial acetate concentration could have less inhibition on the acetate conversion. Moreover, it could also be observed that the specific methane production rate with initial acetate concentration of 1g AC-COD/L was higher than that of 2g Ac-COD/L, which might indicate that the methanogens were inhibited by the higher initial acetate concentration. However, as this supplementary experiment (1g AC-COD/L) was carried out 5 months later than the experiment with initial acetate concentration of 2g AC-COD/L, the adaptation of the biomass might also contribute to this difference.

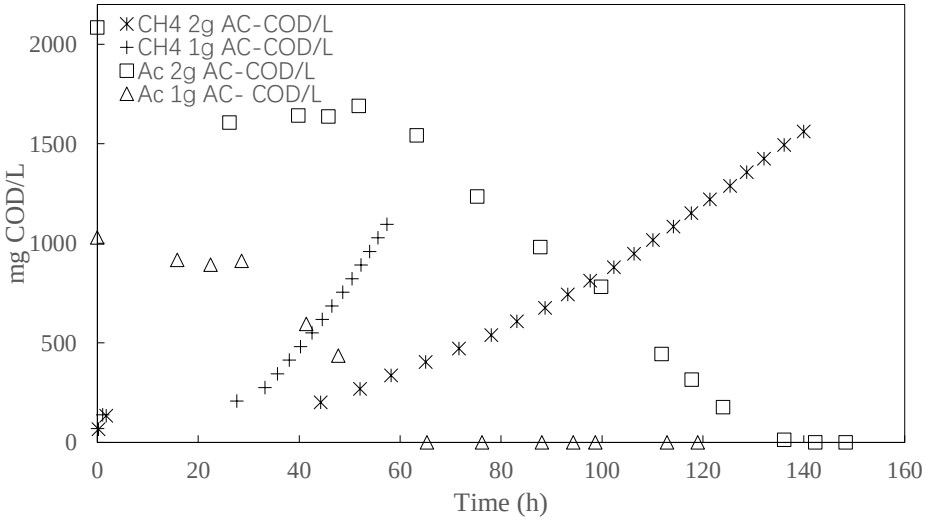

Appendix 4.5.1 Acetate degradation and methane production at initial acetate concentration of 1g Ac-COD/L and 2g Ac-COD/L with the biomass of AnMBR2. The SMA values for the initial acetate concentration of 1g Ac-COD/L and 2g Ac-COD/L were 0.156±0.007 g CH_4-COD/g VSS · d and 0.067± 0.003 g CH_4-COD/g VSS · d, respectively.

Appendix 4.6 Effect of specific biomass loading rate on acetate degradation

This experiment was carried out duplicated by motor mixing with the biomass of AnMBR1 and acetate concentration of 2g AC-COD/L. Biomass A was taken out from AnMBR1 before the acetate concentration in the influent was decreased (acetate concentration of 9.7 g Ac-COD/L, corresponding to an acetate load of 0.56 gAc-COD/gVSS·d) while biomass B was taken out, also from AnMBR1, but after the acetate concentration in the influent was decreased (at a concentration of 2 g AC-COD/L, and an acetate loading rate of 0.11 gAc-COD/gVSS·d). The effect of biomass loading rate on acetate degradation and methane production is shown in the Appendix 4.6.1.

The acetate degradation rate with biomass A was 32.7% faster than the rate of biomass B, indicating that the biomass under higher acetate loading rate had a better ability to degrade acetate when the same initial acetate concentration was applied during batch tests. The result of this experiment could well explain the result of 4.5.2, where the SMA was higher for the group of higher sodium group [18.6 g Na^+/L].

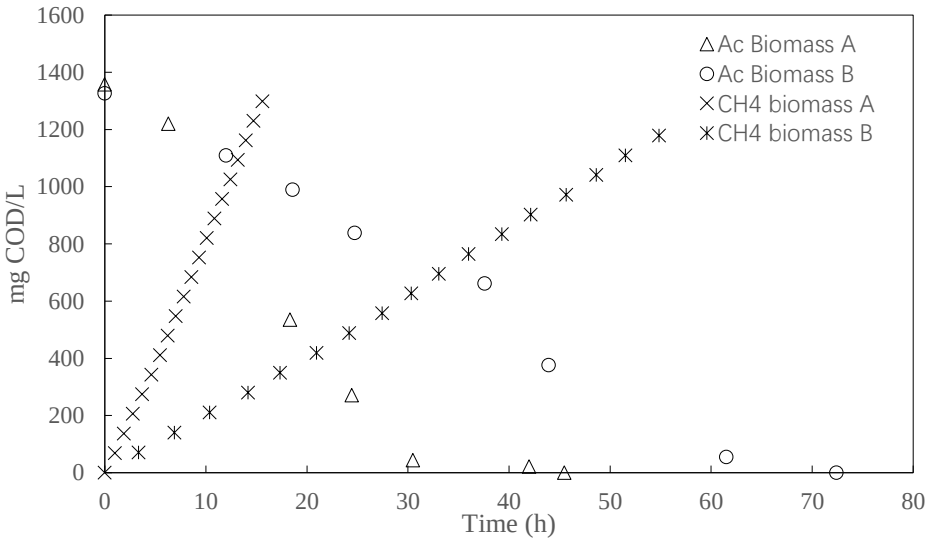

Appendix 4.6.1 Effect of AnMBR specific biomass acetate loading rate on the acetate degradation and methane production. Biomass A: AnMBR acetate loading rate of 0.56 g Ac-COD/gVSS.d; Biomass B: acetate loading rate of 0.11 g Ac-COD/gVSS·d. The SMA for the group of biomass A and biomass B were 0.156±0.007 gCH_4-COD/gVSS·d and 0.105 g CH_4-COD/gVSS·d (only one group of result available), respectively.

Appendix 4.7 Codes for robustness analysis

```
### Noise analysis2 -removal lag phase

xT = np.linspace(0, 50, 501)
m = len(xT)
v = np.zeros(m)

def fitcurve5(xT, KS_AC, KI_AC, km_AC, I2):
    for i in range (m):
        v[i] = Model_2(xT[i], KS_AC, KI_AC, km_AC, I2)
    return v

yT0 = fitcurve5(xT, 2.99999998e+02, 8.06420493e+02, 4.73658321e-01, 4.98545711e-01)
yT = yT0 + yT0 * 0.02 * np.random.normal(size = len(xT))

plt.plot(xT, yT, 'r--')
popt, pcov = curve_fit(fitcurve5, xT, yT, p0=(0, 2000, 0.01, 0.5), bounds=([0, 300, 0, 0], [300, 50000, 1, 1]), method='trf')
print(popt)

plt.xlabel('Time (hours)')
plt.ylabel('CH4-COD mg/L')
plt.title('Noise analysis for the model')
```